

# UC Santa Barbara

## UC Santa Barbara Electronic Theses and Dissertations

### Title

Extreme Winds in Association with Wildfire Spread and Risk in Coastal Santa Barbara, CA

### Permalink

<https://escholarship.org/uc/item/8gr654s9>

### Author

Zigner, Katelyn

### Publication Date

2021

Peer reviewed|Thesis/dissertation

UNIVERSITY OF CALIFORNIA

Santa Barbara

Extreme Winds in Association with Wildfire Spread and Risk in Coastal Santa Barbara, CA

A dissertation submitted in partial satisfaction of the  
requirements for the degree Doctor of Philosophy  
in Geography

by

Katelyn Marie Zigner

Committee in charge:

Professor Leila M.V. Carvalho, Chair

Professor Charles Jones

Professor Dar Roberts

September 2021

The dissertation of Katelyn Marie Zigner is approved.

---

Dar Roberts

---

Charles Jones

---

Leila M.V. Carvalho, Committee Chair

September 2021

Extreme Winds in Association with Wildfire Spread and Risk in Coastal Santa Barbara, CA

Copyright © 2021

by

Katelyn Marie Zigner

## ACKNOWLEDGEMENTS

I would like to express my deepest appreciation to my committee chair, Professor Leila M.V. Carvalho, for her tireless effort in making myself, and many others, more skillful researchers, and better people in general. Her continuous guidance through graduate school and through life has gotten me through many hardships and challenges. I am grateful for her persistence, patience, dedication, mentorship, and friendship through these years.

I would like to thank my committee members, Professor Charles Jones and Professor Dar Roberts for their advice, comments, and time to help improve this work. Their feedback is invaluable and greatly appreciated.

I would like to thank the past and present members of the CLIVAC lab and multiple other Geography friends for their support, assistance, and friendship through these years. Lasting memories were made with multiple members, and I will look back on the adventures fondly. I would also like to thank the UCSB Department of Geography and Earth Research Institute for their support.

I am undoubtedly grateful to my parents, Gerald and Leanne, who always pushed me to work toward the highest goals. Their constant assurance and love encouraged me to keep pursuing my dreams and ambitions.

Finally, I am thankful for Joe, who helped me gain confidence in my work and myself, and made me grow in ways I didn't know possible.

**Curriculum Vitae: Katelyn Marie Zigner**  
**August 2021**

**EDUCATION**

2021	Ph.D. Geography, University of California, Santa Barbara Santa Barbara, CA	GPA: 4.00/4.00
2016	B.S. Meteorology, Valparaiso University Valparaiso, IN	GPA: 3.69/4.00
2016	B.A. Geography, Valparaiso University Minor: Mathematics Valparaiso, IN	GPA: 3.69/4.00

**RESEARCH INTERESTS**

Climatology, Extreme wind events, Mountain meteorology, Fire weather, Wildfire modeling

**RELEVANT EMPLOYMENT, RESEARCH, AND FIELD WORK EXPERIENCE**

2020-Present	Pathways Student Intern. Decision Support Division, Meteorological Development Laboratory, OSTI, NWS, NOAA. Silver Spring, MD.
2018	Sundowner Winds Experiment-Pilot (SWEX-P). UC Santa Barbara, Goleta, CA
2017	GIS for Mars Mission Planning. NASA Langley Research Center, Hampton, VA
2016	GIS for Forestry Mapping. City of Kenosha, Kenosha, WI
2015	Oceanic Data Collection. NASA Student Airborne Research Program, Irvine, CA
2015-2016	Director of the Valparaiso University Storm Intercept Team (VUSIT). Valparaiso University, Valparaiso, IN
2013-2016	Severe Convective Storm Chases. Valparaiso University, Great Plains

**PUBLICATIONS AND PRESENTATIONS**

*Publications:*

**Zigner, K.**, Carvalho, L.M.V., Jones, C., Duine, G.J. (2021) Extreme winds and fire weather in coastal Santa Barbara, CA: An observational analysis. *International Journal of Climatology*. DOI: 10.1002/joc.7262

Duine, G.J., Carvalho, L.M.V., Jones, C., **Zigner, K.** (2021) The influence of topography on the diurnal cycle of sundowner winds in Coastal Santa Barbara, California. *JGR-Atmospheres* 126(8). DOI: 10.1029/2020JD033791

Jones, C., Carvalho, L.M.V., Duine, G.J., **Zigner, K.** (2020) Climatology of Sundowner winds in coastal Santa Barbara, California, based on 30-yr high resolution WRF downscaling. *Atmospheric Research* 249. DOI: 10.1016/j.atmosres.2020.10530

**Zigner, K.**, Carvalho, L.M.V., Peterson, S.H., Fujioka, F., Duine, G.J., Jones, C., Roberts, D.A., Moritz, M. (2020) Evaluating the ability of FARSITE to simulate wildfires

- influenced by extreme, downslope winds in Santa Barbara, California. *Fire* 3(3): 29. DOI: 10.3390/fire3030029
- Murray, A., Carvalho, L.M.V., Church R.L., Jones, C., Roberts, D., Xu, J., **Zigner, K.**, Nash, D. Coastal vulnerability under extreme weather (2020) *Applied Spatial Analysis and Policy*. DOI: 10.1007/s12061-020-09357-0
- Clark, C.A., Goebbert, K.H., Ganesh-Babu, B., Young, A.M., Heinlein, K.N., Casas, E.G., VanDe Guchte, A.P., Krull, A.J., Sefcovic, Z.P., Connelly, R.J., Caruthers, A.L., Haynes, M., **Zigner, K.**, Fingerle, S.L., Cade, E.P., Derolf, T.M., Schletz, S.M. (2020). Classification of Lake Michigan Snow Days for Estimation of the Lake-Effect Contribution to the Downward Trend in November Snowfall. *International Journal of Climatology* 40(3): 5656-5670. DOI: 10.1002/joc.6542
- Carvalho, L.M.V., Duine, G.J., Jones, C., **Zigner, K.**, Clements, C., Kane, H., Gore, C., Bell, G., Gamelin, B., Gomberg, D., Hall, T., Johnson, M., Dumas, J., Boldt, E., Hazard, R., Enos, W. (2020). The Sundowner Winds Experiment (SWEX) Pilot Study: Understanding Downslope Windstorms in the Santa Ynez Mountains, Santa Barbara, CA. *Monthly Weather Review* 148(4): 1519-1539. DOI: 10.1175/MWR-D-19-0207.1

*In progress:*

- Zigner, K.**, Carvalho, L.M.V., Jones, C., Benoit, J., Peterson, S.H., Duine, G.J., Roberts, D.A., Fujioka, F., Moritz, M. Wildfire risk in complex terrain and in the coastal Santa Barbara wildland-urban interface during extreme winds.

*Oral presentations:*

- 2021 “Unraveling principal mechanisms controlling downslope windstorms in coastal mountainous terrain using novel instrumental strategies.” Earth Science Information Partners Summer Meeting. July 19.
- 2021 “Risk and Resilience: Identifying regions of high wildfire threat.” Final Round of UCSB Grad Slam. March 8. Virtual.
- 2019 “Identifying Worst-Case-Scenario Extreme Wind Events for Advances in Fire Weather and Wildfire Modeling.” American Geophysical Union Fall Meeting. December 9-13, San Francisco, CA (Invited).
- 2019 “The Science and Art of Fire Spread Modeling.” Understanding Extreme Fire Weather Hazards and Improving Resilience in Coastal Santa Barbara (EXFHIRE-Workshop). October 24, Santa Barbara, CA.
- 2019 “Investigating the Connection between Extreme Wind Events and Wildfires.” Valparaiso University Professional Perspectives Guest Presentation. October 7, Valparaiso, IN.
- 2019 “Fired Up: How Advancements in Wildfire Modeling Will Help Society.” Semifinal Round of UCSB Grad Slam. April 15, Santa Barbara, CA.
- 2018 “Sundowner Winds and Fire Weather Conditions in Santa Barbara, CA: Observation and Modeling.” American Geophysical Union Fall Meeting. December 10-14, Washington D.C.
- 2017 “Spatiotemporal Analysis of Regional Wind Patterns in Coastal Santa Barbara County.” Earth Research Institute Monthly Meeting. October 12, Santa Barbara, CA.

*Poster presentations:*

- 2019 “Effects of Extreme Wind Variability on Modeled Wildfire Spread.” American Geophysical Union Fall Meeting. December 9-13, San Francisco, CA.
- 2018 “Spatiotemporal Analysis of Wind Extremes in Santa Barbara County, CA.” American Geophysical Union Fall Meeting. December 10-14, Washington D.C.
- 2015 “The Impact of Climatological Variables on Kelp Canopy Area in the Santa Barbara Channel.” American Geophysical Union Annual Conference. December 14-18, San Francisco, CA.

*Oral presentations by mentees:*

- 2019 Ginsburg, A., Zigner, K. “Evaluating the Relationship between Two Extreme Wind Events in Southern California for Advancements in Forecasting.” Research Mentorship Program Research Symposium. August 2, Santa Barbara, CA.
- 2019 Banerjee, R., Zigner, K. “Analysis of WRF Prediction Model Performance and its Spatiotemporal Characterization of Sundowners through PCA.” Research Mentorship Program Research Symposium. August 2, Santa Barbara, CA.
- 2019 Torres, C.V., Zigner, K. “Burnin’ Up the Breeze: Evaluating Sundowner Winds Effect on Aerosols during the Thomas Fire.” UCSB Environmental Science Senior Thesis Presentations. May 30, Santa Barbara, CA.

AWARDS & HONORS

- 2021 UC Santa Barbara Dept. of Geography Excellence in Research Award
- 2021 UCSB Grad Slam Runner-Up
- 2018, 2019 Earth Research Institute Travel Grant
- 2018, 2019 UC Santa Barbara Dept. of Geography Travel Grant
- 2018 Outstanding Student Presentation Award, AGU 2018 Annual Meeting
- 2016 Alfred H. Meyer Award for Excellence in Geography, Valparaiso University Department of Geography
- 2015 Gamma Theta Upsilon International Geographical Honor Society Annual Award for Excellence in Geography
- 2012-2016 Valparaiso University Presidential Scholarship

SKILLS

- Programming IDL (advanced), Bash (intermediate), Python (intermediate), R (beginner)
- Software ArcGIS, Fire Area Simulator, FlamMap, ENVI, Microsoft Suite
- Data formats Raster, shapefile, NetCDF, ASCII, grib2
- OS Windows, Linux
- Personal Time management, self-motivation, communication, organization

MENTORING EXPERIENCE



- Fall 2019 Geography Department Internship. Student: Oster, C. Project title: Comparisons between Observed Sundowner Events and the WRF Model.
- Summer 2019 Research Mentorship Program for Outstanding High School Students. Student: Ginsburg, A. Project title: Evaluating the Relationship between Two Extreme Wind Events in Southern California for Advancements in Forecasting
- Summer 2019 Research Mentorship Program for Outstanding High School Students. Student: Banerjee, R. Project title: Analysis of WRF Prediction Model Performance and its Spatiotemporal Characterization of Sundowners through PCA
- Fall 2018 - Senior Thesis Project in Environmental Science. Student: Torres, C.V.  
Spring 2019 Project title: Burnin' Up the Breeze: Evaluating Sundowner Winds Effect on Aerosols during the Thomas Fire

## TEACHING EXPERIENCE

- 2016 - 2018 Teaching Assistant, University of California, Santa Barbara
- |             |                                     |
|-------------|-------------------------------------|
| Fall 2016   | GEOG 3B: Land, Water, & Life        |
| Winter 2017 | GEOG 3A: Ocean / Atmosphere         |
| Spring 2017 | GEOG 12: Maps and Spatial Reasoning |
| Fall 2017   | GEOG 131: Mountain Weather          |
| Spring 2018 | GEOG 117: Polar Environments        |
- 2015 - 2016 Meteorology and Geography Lab Aide, Valparaiso University

## SERVICE AND OUTREACH

- 2018-2020 Faculty Representative Committee, UC Santa Barbara
- 2016-2020 Geography Awareness Week Volunteer, UC Santa Barbara
- 2016-2020 Space for Dinner Food Shelter Volunteer, UC Santa Barbara
- 2017-2018 Geography Outreach Committee, UC Santa Barbara
- 2016-2018 Women in STEM Mentorship Program, UC Santa Barbara
- 2012-2016 Valparaiso University Day of Caring Volunteer, Valparaiso University
- 2013 College Mentors for Kids, Valparaiso University

## PROFESSIONAL ASSOCIATIONS & HONOR SOCIETIES

- 2016 Phi Beta Kappa Honor Society
- 2015 American Geophysical Union
- 2015 Chi Epsilon Pi Meteorology Honor Society
- 2015 Gamma Theta Upsilon Geography Honor Society
- 2014 Mortar Board National Senior Honor Society
- 2012 American Meteorological Honor Society

## ABSTRACT

Extreme Winds in Association with Wildfire Spread and Risk in Coastal Santa Barbara, CA

by

Katelyn Marie Zigner

Coastal Santa Barbara County, California is characterized by extreme downslope wind events on the southern side of the Santa Ynez Mountains known as Sundowner winds (or Sundowners) that can rapidly spread wildfires toward highly populated regions. This research investigates these strong winds and the risk of wildfire spread in this region. The second chapter of this research explores the seasonal and diurnal patterns of wind, temperature, dew point, and a fire weather index, as well as their spatiotemporal variability, from an observational perspective. Utilizing station and buoy data, distinct differences were found between stations on the mountain slopes and stations on the foothills and on the coastal plain. Additionally, correlations revealed relationships between stations and buoys, and analysis of a vertical wind profiler at the Santa Barbara airport provided evidence of differences during Sundowners in the east and west parts of coastal Santa Barbara. Due to the dependence on winds in its calculation, fire weather indices were highest at stations on the mountain slopes, though all stations had recorded at least one time with critical fire weather. In the third chapter, the ability of an operationally-used uncoupled wildfire model called FARSITE (Fire Area Simulator) in reconstructing two wildfires that rapidly spread by Sundowner winds was tested. One wildfire was simulated relatively well, though some

differences in spread direction were evident. The perimeter and burn area of the second wildfire was underestimated in the simulations due to limitations built into the spotting algorithm. It was determined that the elevation of the launch site of an ember must be lower than the landing site. In the simulations for the Santa Barbara case studies, fire spread was predominantly downslope, thus the launch sites were commonly higher in elevation and spotting did not occur. This finding has ramifications for wildfires that are rapidly spread by spotting ahead of the fire front. In the fourth chapter, I created wildfire risk maps for this high-risk region. Three ignition modeling methods were employed using distances from previous ignitions and roads and trails, and these were input into the wildfire model with three varying wind scenarios: climatological winds, a composite of Sundowners, and a case study of an extreme Sundowner event. Simulations commonly hit areas on the mountain slopes overlooking downtown Santa Barbara and Montecito, and also near a major north-south running evacuation route, in part due to clustering of ignitions in this region. The simulations using climatological winds spread generally outward from the ignition locations and in contrast simulations run using extreme winds spread further south into the wildland-urban interface and toward more urban areas. These three chapters advance knowledge of typical versus extreme winds in this region, demonstrate how simulations align with previous influential wildfires, provide insight into wildfire model limitations, and identify potentially high-risk regions for wildfires, increasing wildfire resilience and preparedness.

## TABLE OF CONTENTS

1. Introduction.....	1
2. Extreme Winds and Fire Weather in Coastal Santa Barbara County, CA: An Observational Analysis .....	19
2.1 Abstract.....	20
2.2 Introduction.....	20
2.3 Data and Methods .....	25
2.4 Observed Wind Patterns and Extremes .....	31
2.4.1 <i>Seasonal</i> .....	31
2.4.2 <i>Diurnal</i> .....	33
2.4.3 <i>Extremes in winds using percentiles</i> .....	38
2.4.4 <i>Sundowner wind criteria</i> .....	39
2.4.5 <i>Correlations between buoy and land stations</i> .....	44
2.4.6 <i>Seasonal cycles, diurnal cycles, and Sundowner winds observed at the NOAA wind profiler</i> .....	49
2.5 Variability in temperature and dew point during extreme winds .....	53
2.5.1 <i>Temperature</i> .....	53
2.5.2 <i>Dew Point Temperature</i> .....	56
2.6 Spatiotemporal variability of the Fosberg Fire Weather Index.....	58
2.7 Discussion and Conclusions .....	60
2.8 Acknowledgements.....	64
2.9 Appendix.....	64

2.10 References.....	71
3. Evaluating the Ability of FARSITE to Simulate Wildfires Influenced by Extreme, Downslope Winds in Santa Barbara, California.....	78
3.1 Abstract.....	79
3.2 Introduction.....	79
3.3 Materials and Methods .....	84
3.3.1 Case studies .....	84
3.3.2 Wildland fire models .....	85
3.3.3 Fuel and topography data .....	86
3.3.4 Weather Data .....	89
3.3.5 Gust factor .....	93
3.3.6 Perimeter data .....	95
3.4 Results and Discussion .....	95
3.4.1 Sherpa Fire .....	95
3.4.2 Painted Cave Fire.....	98
3.4.3 Spotting limitations .....	104
3.4. 4 FlamMap comparisons .....	105
3.5 Conclusions.....	109
3.6 Acknowledgements.....	111
3.7 Appendix.....	111
3.8 References.....	115
4. Wildfire Risk in Complex Terrain and in the Coastal Santa Barbara Wildland-Urban Interface during Extreme Winds.....	126
4.1 Abstract.....	126

4.2 Introduction.....	127
4.3 Data and Methods .....	132
4.3.1 <i>Study area</i> .....	132
4.3.2 <i>Road and Trail, Ignition, and Historical Wildfire Data</i> .....	132
4.3.3 <i>Ignition Modeling Methods</i> .....	133
4.3.4 <i>FARSITE and Model Input</i> .....	136
4.4 Impacts of Varied Ignition Modeling Methods on Wildfire Spread..	139
4.4.1 <i>Ignitions in the WUI: Observations and Modeling</i> .....	139
4.4.2 <i>Wildfire spread risk in the WUI using varied ignition methods and wind scenarios</i> .....	142
4.5 Discussion and Conclusions .....	155
4.6 Acknowledgements.....	159
4.7 Appendix.....	160
4.8 References.....	160
5. Conclusion .....	167

## 1. Introduction

Santa Barbara, California is located next to the Pacific Ocean between the major cities of Los Angeles and San Francisco. In the southern part of the county, the coastal cities of Goleta, Santa Barbara, and Montecito are bordered by the Santa Barbara Channel to the south and by the Santa Ynez Mountains (SYM) to the north (Fig. 1.1). Few roads lead into and out of this region, with HWY 101 as the major east-west road and HWY 154 as the major north-south road. While most inhabitants live near the coast, the wildland-urban interface (WUI), the region where humans and nature coincide, is expanding into the SYM foothills as humans venture into areas further north.

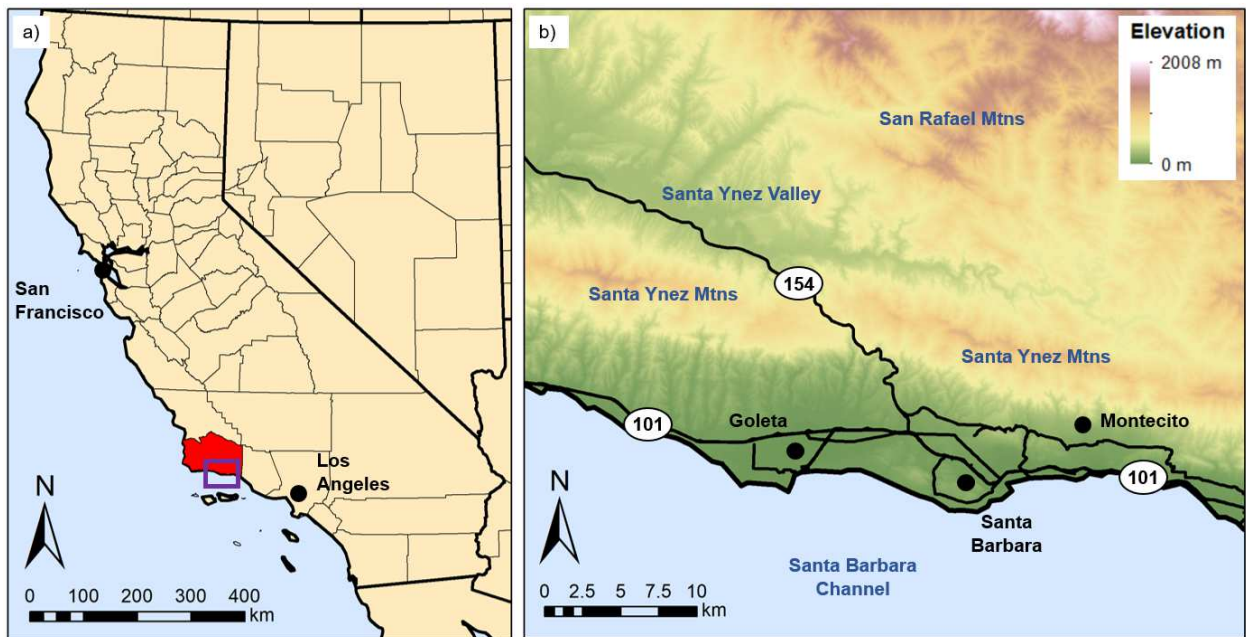


**Figure 1.1** – (a) State and county borders, with Santa Barbara County colored red. (b) Topography in southern Santa Barbara County (see purple box in (a) for subset). Cities are in black text and geographic features are in blue text. The thick lines indicate major roads, and highways are labeled.

Both extreme downslope wind events and rapidly spreading wildfires are common phenomena in the southern part of Santa Barbara County, significantly impacting the communities (Ryan 1996; Blier 1998; Cannon et al. 2017; Carvalho et al. 2020). In fact, all major wildfires in this region have been spread by strong winds. Given that maximum wind speeds occur on the southern slopes of the SYM during strong wind events (Jones et al. 2020; Duine et al. 2021), the growing WUI increases the threat of ignitions and the overall wildfire risk throughout this area. In some areas of the WUI in Santa Barbara, there is only one road leading to and from the homes, potentially creating issues in the case of mandatory evacuations. This dissertation analyzes the spatiotemporal characteristics of meteorological variables and a fire weather index, simulates two impactful wildfires, and suggests locations of highest wildfire risk in this region of complex topography.

### *Extreme Wind Events in Southern California*

Two extreme wind events are common in Southern California. To the east of Santa Barbara, Santa Ana winds effect an expansive area from San Diego County in the south to Ventura County in the north. Santa Ana winds (henceforth SAWs) are strong, offshore foehn winds that occur in the lee of the Transverse and Peninsular Mountains and commonly exhibit intensified winds via channeling in valleys (Raphael 2003; Conil and Hall 2006). Forced by horizontal pressure gradients between the desert high and coastal low, these events frequently occur in the cool season (Raphael 2003; Hughes and Hall 2010; Jones et al. 2010; Abatzoglou et al. 2013). Adiabatic processes may decrease humidity and increase temperatures during SAWs and create critical fire weather conditions (Abatzoglou et al. 2013; Jones et al. 2010; Jin et al. 2014). This has led to the rapid spread of destructive



wildfires in Southern California (Raphael 2003; Westerling et al. 2004; Hughes and Hall 2010; Moritz et al. 2010; Guzman-Morales et al. 2019).

While extensive research has identified the spatiotemporal characteristics and mechanisms of SAWs, less is known about the distinct Sundowner winds observed in Santa Barbara. Sundowner winds (or Sundowners) are strong cross-mountain (northerly) winds specific to coastal Santa Barbara County, named after the onset near sunset (Ryan 1996; Blier 1998). SAWs and Sundowners exhibit differing spatial extents, synoptic setups, and forcing mechanisms (Hatchett et al. 2018; Carvalho et al. 2020; Sukup 2013; Jones et al. 2020; Duine et al. 2021; Smith et al. 2018). One key difference is that Sundowners are not always associated with low relative humidity ( $< 15\%$ ) or temperature ramps (Blier 1998; Carvalho et al. 2020), however the presence of these help create critical fire weather conditions (Ryan 1996; Cannon et al. 2017).

Climatologically, Sundowners are most common in spring, though they do occur year-round (Jones et al. 2020; Smith et al. 2018). The National Weather Service Lox Angeles/ Oxnard defines a Sundowner as cross-mountain (northerly) winds that reach sustained winds of at least 13.4m/s (30 mph) or wind gusts at least 15.6 m/s (35 mph) (NWS-LOX, personal communication), albeit large spatial variability in wind speed exists on the southern SYM slopes. One of the variables examined to forecast Sundowners are pressure differences between the Santa Barbara Airport and nearby stations (Fig. 1.2). When pressure differences are forecasted between Santa Barbara and Santa Maria (to the northwest), strong winds may be expected in the western portions of the SYM mountains. However, when pressure differences are forecasted between Santa Barbara and Bakersfield (to the northeast), strong winds may occur on the eastern SYM slopes (Ryan 1996; Sukup 2013; Jones et al. 2020).

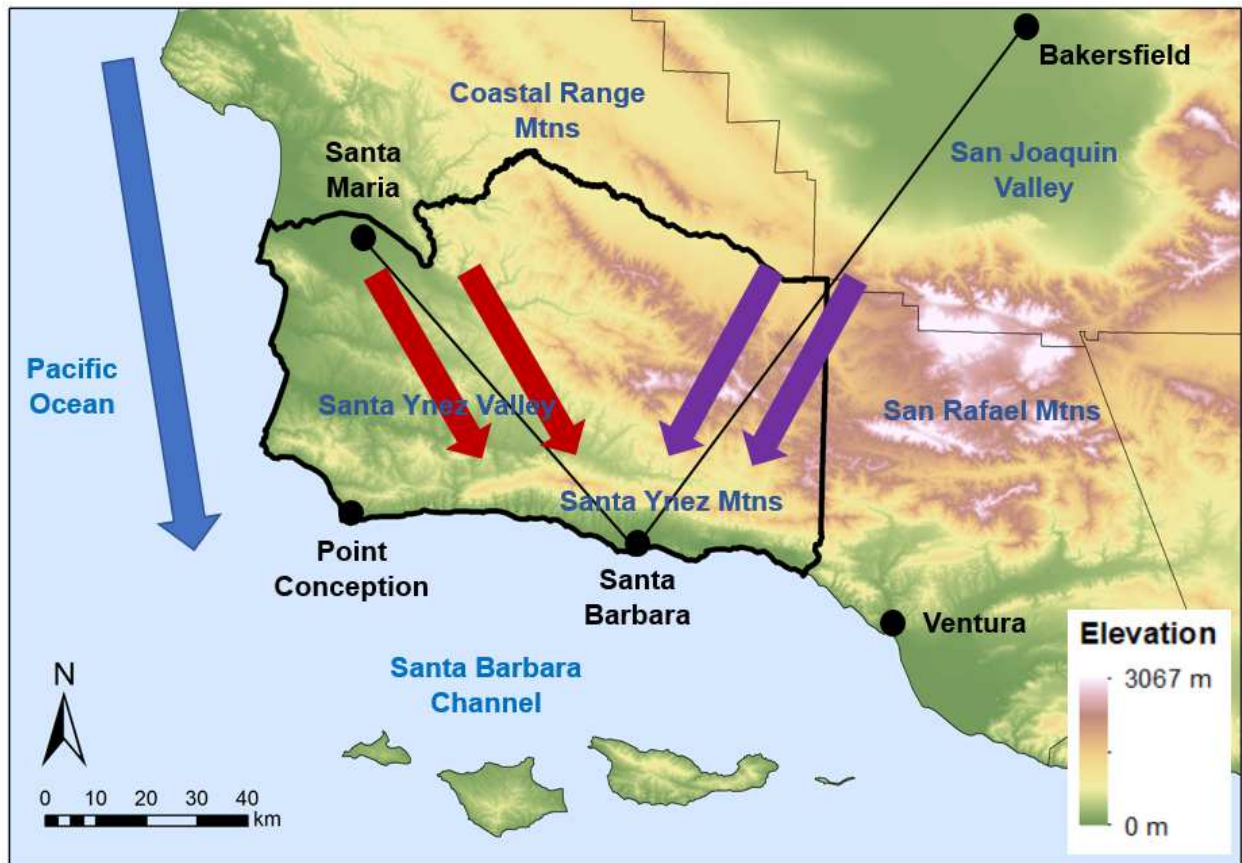


**Figure 1.2** – Topography in and around Santa Barbara County (outlined) and major cities in southern California (black dots and text). Geographic features are in blue text. The two black lines indicate the distance from the stations used when considering pressure differences in Sundowner forecasting. The red and purple arrows represent the northwesterly and northeasterly flow associated with western and eastern Sundowners, respectively. The blue arrow indicates the typical location of the coastal jet off the west coast of California.

Utilizing a combined empirical orthogonal function analysis on meridional and zonal winds from a 30-year Weather Research and Forecasting (WRF) model, Jones et al. (2020) found evidence of three Sundowner regimes: Western, Eastern, and Santa Barbara (a combination of Western and Eastern). Their study found that the coastal jet, typically running along the western coast of California (see Fig. 1.2), extends into the Santa Barbara Channel with strong winds during the western regime, although it is much weaker during the

eastern regime. Additionally, the western and Santa Barbara regime Sundowners are most common from March to May, and the eastern regime Sundowners are most common in January and February. Finally, the timing of onset and demise varies between regimes; the onset of winds in the western regime is around 1600-1700 PST, whereas the onset in the eastern regime is around 1800-1900 PST. The demise is around 2300 PST for western Sundowners and 0200 PST for eastern Sundowners (Jones et al. 2020).

The majority of Santa Barbara inhabitants live where strong Sundowner winds would spread fires south during the Eastern and Santa Barbara regimes. Recall that the most impactful wildfires in this region have been spread by Sundowner winds. Furthermore, the WUI is mainly comprised of houses rather than businesses, thus an ignition on the SYM slopes and Sundowner winds at night could be devastating as the few roads in and out of this region could be deadlocked during an evacuation, since most people would be home. Differentiation between these regimes will assist in improving forecasts of Sundowners and fire weather, ultimately increasing wildfire resource planning and preparedness.

### *Wildfires and Climate Change*

Wildfires are an ever-growing concern worldwide, and particularly in the western United States, due to the associated economic costs, injuries and casualties, and degraded air quality (Keeley et al. 2009; Wong et al. 2020; McWethy et al. 2019; Keeley et al. 2004; Calkin et al. 2014). Complex interactions between climate, vegetation, and human habitation makes the drivers of wildfire activity spatially heterogeneous (Keeley and Syphard 2018; Westerling and Bryant 2008; Parisien et al. 2012). In general, climate change is increasing fire activity. In California, both the wildfire frequency (Westerling et al. 2004; Westerling 2018) and the number of hectares burned (Westerling 2016; Williams and Abatzoglou 2016;

Westerling 2018) has increased. These trends are expected to continue to increase due to warmer temperatures and increased vapor pressure deficit affecting fuel flammability (Westerling et al. 2011; Westerling and Bryant 2008; Williams et al. 2019). In some areas, the increase in wildfire frequency will likely be related to the availability of fine fuels affected by reduced moisture availability from lower precipitation and higher temperatures (Westerling and Bryant 2008). In dry grasslands and shrublands, the impact of climate change on fine fuels outweighs the effect of temperature on fuel flammability (Westerling and Bryant 2008). The percentage of critical fire weather conditions has doubled since the early 1980s because of warmer fall temperatures and decreased fall precipitation (Goss et al. 2020; Swain 2021). Years with abnormally high precipitation totals can lead to increased fire burn area in the following years (Williams et al. 2019; Westerling 2018). While wildfires are natural occurrences and are necessary for the health of many ecosystems, communities have developed and/or are encroaching on wildfire-prone areas, greatly heightening wildfire risk and susceptibility (Calkin et al. 2014).

### *Wildfire Modeling, Resilience, and Planning*

Simulating wildfires using wildfire models can provide insight on the effectiveness of fuel treatments, utilization of different firefighting strategies, and the identification of high-risk regions. Multiple fire models exist and each is unique in its wildfire spread equations and algorithms. The more complex models are coupled, meaning the atmospheric feedback between the fire and microscale atmosphere is considered as the fire spreads. While this may provide more accurate reconstructions of fires by considering small-scale physics, these can be computationally expensive and require a long time to run. In contrast, many operationally-used fire models are relatively simple and uncoupled, meaning that the

feedback between the fire and atmosphere is not simulated in the fire spread. While these models may make more assumptions and not integrate complex physics observed in fire spread, many are much less computationally expensive and run faster than coupled models.

One frequently-used uncoupled fire model is the Fire Area Simulation (FARSITE) (Finney 1998), a two-dimensional semi-empirical wildfire model commonly used to determine wildfire size, location, and timing in operations for wildfire incidents (Stratton 2006; Scott 2006; Finney and Ryan 1995; Papadopoulos and Pavlidou 2011). This model uses Huygen's principle of wave propagation and the Rothermel fire spread equations to propagate fires using elliptical shapes at vertices on the fire front based on fuels, topography, and wind (Rothermel 1972). The advantage of this model is the relatively quick simulation run time and low computational expense. The limitation with uncoupled wildfire models is the lack of interaction between the simulated fire and the microscale weather, since the feedback can influence fire spread and intensity (Coen et al. 2013). More advantages and disadvantages of using a relatively simple wildfire model such as FARSITE can be found in (Papadopoulos and Pavlidou 2011).

Pre-fire planning is necessary for an effective response to fire and to mitigate potential future wildfires (Thompson et al. 2016). Ignition risk is high in public places, such as near roads and trails. The first couple hours after ignition are the most important in terms of evacuation planning and enforcement, particularly in the WUI and in urban areas. Multiple ideas have been proposed to increase resilience to wildfires, especially in the WUI. Land use planning and fuel treatments may be used to create a buffer zone around the WUI (Keeley et al. 2004). However, it is important to note that lower fuel loads resulting from fuel treatments will not stop wildfires during extreme fire weather, but the fire intensity would likely decrease and allow for methodical fire suppression techniques (Keeley et al.

2004; Keane et al. 2009). While wildfire suppression via fuel treatments are relatively effective (95-98%) (Calkin et al. 2014), this may lead to large and destructive wildfires that are difficult to suppress (Arno and Brown 1991; Cohen 2010). Furthermore, wildfire risk may be decreased by reducing the potential for building ignition, but this requires action by homeowners and private landowners rather than via an agency (Syphard et al. 2017; Syphard and Keeley 2019; Calkin et al. 2014). City planners may choose to create more compact housing and not restrict WUI expansion in fire-prone areas (Syphard et al. 2007; Syphard et al. 2012). Another method is to bury power lines (Kolden and Abatzoglou 2018), since many California wildfires are ignited by electrical above-ground powerline failures or the falling of powerlines. Finally, staged resources and additional staffing on critical weather days can increase fire resilience in the event of an ignition (Kolden and Abatzoglou 2018).

An example of how improvements in Sundowner forecasting, wildfire preparedness, and interagency communication stopped a potentially disastrous wildfire occurred when the Holiday Fire ignited in the foothills of Goleta in July 2018 (Fig. 1.3). The National Weather Service had communicated the high fire weather risk that day due to Sundowner conditions, and expressed concern that if a fire were to ignite, it would rapidly spread south toward populated areas. Resources had been strategically placed and additional staff were prepared. When an ignition occurred in the WUI, the fire was quickly contained and damages and costs were minimized on a critical weather day that could have ended in disaster (SBC Fire Department, per. comm.). This is one example of how incorporating effective firefighting strategies and communication can increase resilience toward these natural hazards.

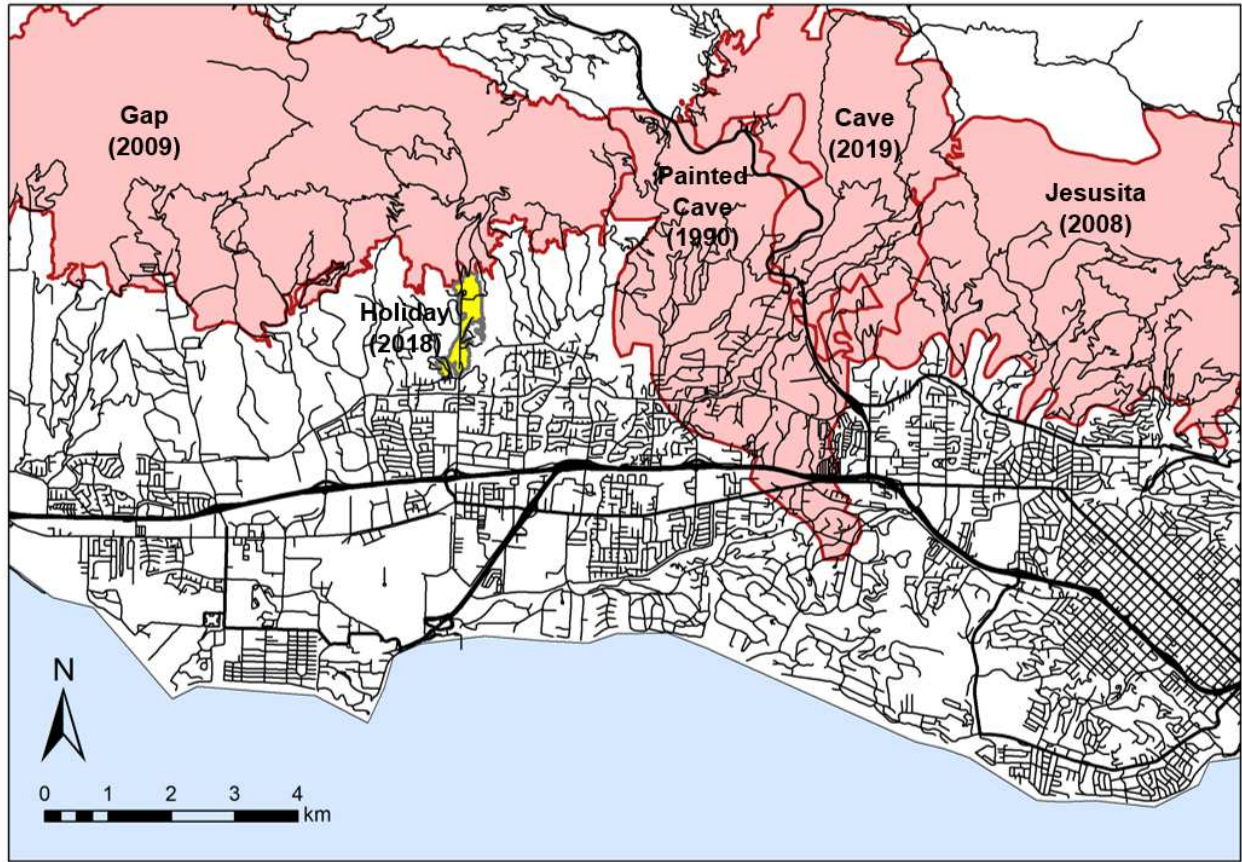


**Figure 1.3** – Major (thick lines) and minor (thin lines) roads in coastal Santa Barbara. Historical wildfire perimeters are shown in red, and the Holiday fire is shown in yellow.

### *Dissertation Objectives*

The research presented in this dissertation aims to provide novel insight into the observed seasonal cycles, diurnal cycles, and extremes of atmospheric variables in coastal Santa Barbara, and simulate impactful wildfires to identify areas at highest fire risk. **The objectives of this dissertation are:**

1. Analyze the observed seasonal cycles, diurnal cycles, and extremes of wind, temperature, dew point, and fire weather using regulated weather stations in coastal Santa Barbara (Chapter 2).
2. Investigate the ability of an operationally-used wildfire model to reconstruct two impactful wildfires rapidly spread by Sundowner winds (Chapter 3).

3. Utilize an uncoupled wildfire model to determine areas at highest wildfire risk in coastal Santa Barbara, with particular attention to areas in the WUI, using varied ignition locations and wind inputs (Chapter 4).

The second chapter of this dissertation uses observational data from eight Automated Service Observation Stations and Remote Automated Weather Stations in coastal Santa Barbara, in addition to a vertical wind profiler at the Santa Barbara Airport and four buoys to examine spatiotemporal variability and extreme conditions of weather in coastal Santa Barbara (Zigner et al. 2021). Distinctions were found between the timing of wind maxima and minima between stations located on the SYM slopes versus in the valley, in the foothills, and on the coastal plain, and correlations in wind were evident between land-based stations and buoys. Differences in wind direction during Sundowners were present at stations in the eastern and western parts of the SYM. During Sundowners, the temperature and dew point varied from typical conditions at two mountain stations, potentially indicating different processes and characteristics between Sundowner occurring on the eastern and western SYM slopes.

The third chapter determines whether FARSITE, an operationally-used wildfire model, can accurately reconstruct the perimeters of two fires that rapidly spread in Santa Barbara due to Sundowner winds (Zigner et al. 2020). The 2016 Sherpa fire ignited in the fairly uninhabited western part of coastal Santa Barbara, and the 1990 Painted Cave fire ignited on the mountain slopes overlooking Goleta and Santa Barbara. FARSITE successfully simulated the perimeters and burned area of the Sherpa fire when a gust factor was applied to the wind speeds. However, the burned area of the Painted Cave fire was largely underestimated by the simulations due to limitations in the spotting algorithm used in



FARSITE. This finding highlights the difficulties to realistically simulate wildfires driven by strong downslope winds, such as Sundowners or other similar types of wind events, present in uncoupled fire models which can't simulate three-dimensional processes that transport embers downstream of the fire front. Furthermore, changing the fuel map to include more flammable fuels increased the burned area for the Painted Cave fire, though large underestimations were still evident.

The fourth chapter uses FARSITE to produce multiple fire risk maps for coastal Santa Barbara with focus on ignition and wind input. Three ignition modeling methods were employed and examined using distances from previously ignitions and roads and trails, and three wind scenarios were input to the simulations: climatological, composite (mean) Sundowner, and an extreme Sundowner case study. The area hit by the most simulations regardless of wind input was near a major north-south evacuation route, which was hit by about 10% of the simulations. The high frequency of hits in this region can partially be explained by the large number of observed and modeled ignitions in this region. Furthermore, when Sundowner winds were input, the simulated fires reached an east-west evacuation route that is commonly used by homes in the WUI. While only 1 simulation reached this road when the Sundowner composite winds were used, approximately 7% of the simulations reached it using the extreme Sundowner case study winds. These findings have major implications for firefighting and evacuation planning.

## *References*

- Abatzoglou, J. T., Barbero, R., and Nauslar, N. J. (2013). Diagnosing Santa Ana winds in Southern California with synoptic-scale analysis. *Weather and Forecasting*, 28(3), 704-710.
- Arno S.F., and Brown J.K. (1991) Overcoming the paradox in managing wildland fire. *Western Wildlands*, Montana Forest and Conservation Experiment Station, Missoula, MT, USA, 40–46.
- Blier, W. (1998) The sundowner winds of Santa Barbara, California. *Weather and Forecasting*, 13, 702-716. Doi: 10.1175/1520-0434(1998)013<0702:TSWOSB>2.0.CO;2.
- Calkin, D. E., Cohen, J. D., Finney, M. A., Thompson, M. P. (2014) How risk management can prevent future wildfire disasters in the wildland-urban interface. *Proceedings of the National Academy of Sciences*, 111(2), 746-751.
- Cannon, F., Carvalho, L., Jones, C., Hall, T., Gomberg, D., Dumas, J., and Jackson, M. (2017) WRF Simulation of Downslope Wind Events in Coastal Santa Barbara County. *Atmospheric Research*, 191, 57–73. Doi: 10.1016/j.atmosres.2017.03.010.
- Carvalho, L., Duine, G.J., Jones, C., Zigner, K., Clements, C., Kane, H., Gore, G., Bell, G., Gamelin, B., Gomberg, D., Hall, T., Johnson, M., Dumas, J., Boldt, E., Hazard, R., and Enos, W. (2020) The Sundowner Winds Experiment (SWEX) Pilot Study: Understanding Downslope Windstorms in the Santa Ynez Mountains, Santa Barbara, CA. *Monthly Weather Review*, 148, 1519-1539. Doi: 10.1175/MWR-D-19-0207.1.
- Coen, J.L., Cameron, M., Michalakes, J., Patton, E.G., Riggan, P.J., Yedinak, K.M. (2013) WRF-Fire: Coupled Weather–Wildland Fire Modeling with the Weather Research and Forecasting Model. *J. Appl. Meteor. Climatol.* 52, 16–38.
- Cohen, J. (2010) The wildland-urban interface fire problem. *Fremontia* 38(2-3), 16–22.

- Conil, S., and Hall, A. (2006). Local regimes of atmospheric variability: A case study of Southern California. *Journal of Climate*, 19(17), 4308-4325.
- Duine, G.J., Carvalho L.M.V., Jones C., and Zigner K. (2021) The effect of upstream topography on the onset of Sundowner winds in coastal Santa Barbara, CA. *JGR-Atmospheres*, in press. Doi: 10.1029/2020JD033791.
- Finney, M.A., and Ryan, K.C. (1995) Use of the FARSITE Fire Growth Model for Fire Prediction in U.S. National Parks. In *Proceedings of the International Emergency Management and Engineering Conference*, San Diego, CA, USA, 9–12. pp. 183–189.
- Finney, M.A. (1998) FARSITE: Fire Area Simulator-Model Development and Evaluation; Research Paper RMRS-RP-4; U.S. Department of Agriculture, Forest Service, Rocky Mountain Research Station: Fort Collins, CO, USA.
- Goss, M., Swain, D. L., Abatzoglou, J. T., Sarhadi, A., Kolden, C. A., Williams, A. P., Diffenbaugh, N. S. (2020) Climate change is increasing the likelihood of extreme autumn wildfire conditions across California. *Environmental Research Letters*, 15(9), 094016.
- Guzman-Morales, J., and Gershunov, A. (2019) Climate change suppresses Santa Ana winds of Southern California and sharpens their seasonality. *Geophysical Research Letters*, 46(5), 2772-2780.
- Hatchett, B. J., Smith, C. M., Nauslar, N. J., and Kaplan, M. L. (2018) Brief communication: Synoptic-scale differences between Sundowner and Santa Ana wind regimes in the Santa Ynez mountains, California. *Natural Hazards and Earth System Sciences*, 18(2), 419-427.
- Hughes, M., and Hall, A. (2010) Local and synoptic mechanisms causing Southern California's Santa Ana winds. *Climate Dynamics*, 34(6), 847-857.

- Jin, Y., Randerson, J. T., Faivre, N., Capps, S., Hall, A., Goulden, M. L. (2014). Contrasting controls on wildland fires in Southern California during periods with and without Santa Ana winds. *Journal of Geophysical Research: Biogeosciences*, 119(3), 432-450.
- Jones, C., Fujioka, F., and Carvalho, L.M.V (2010) Forecast Skill of Synoptic conditions Associated with Santa Ana Winds in Southern California. *Monthly Weather Review*, 138, 4528-4541.
- Jones, C., Carvalho, L., Duine, G.J., Zigner, K. (2021) A New Climatology of Sundowner Winds in Coastal Santa Barbara, California, Based on 30-yr High Resolution WRF Downscaling. Submitted to *Atmospheric Research*. Doi: 10.1175/2010MWR3406.1.
- Keane, R. E., Agee, J. K., Fule, P., Keeley, J. E., Key, C., Kitchen, S. G., Schulte, L. A. (2009) Ecological effects of large fires on US landscapes: benefit or catastrophe? *A. International Journal of Wildland Fire*, 17(6), 696-712.
- Keeley, J.E., Fotheringham, C.J., Moritz, M.A. (2004) Lessons from the october 2003. Wildfires in Southern California. *Journal of Forestry*, 102(7), 26-31.
- Keeley, J.E., Safford, H., Fotheringham, C.J., Franklin, J., Moritz, M. (2009) The 2007 southern California wildfires: lessons in complexity. *Journal of Forestry*, 107(6), 287-296.
- Keeley, J. E., and Syphard, A. D. (2018) Historical patterns of wildfire ignition sources in California ecosystems. *International journal of wildland fire*, 27(12), 781-799.
- Kolden, C.A., and Abatzoglou, J.T. (2018) Spatial distribution of wildfires ignited under katabatic versus non-katabatic winds in mediterranean Southern California USA. *Fire*, 1(2), 19.

- McWethy, D.B., Schoennagel, T., Higuera, P.E., et al. (2019) Rethinking resilience to wildfire. *Nature Sustainability*, 2(9), 797-804.
- Moritz, M. A., Moody, T. J., Krawchuk, M. A., Hughes, M., Hall, A. (2010) Spatial variation in extreme winds predicts large wildfire locations in chaparral ecosystems. *Geophysical Research Letters*, 37(4).
- Papadopoulos, G.D., and Pavlidou, F.-N. (2011) A Comparative Review on Wildfire Simulators. *IEEE Syst. J.*, 5, 233–243.
- Parisien, M. A., Snetsinger, S., Greenberg, J. A., Nelson, C. R., Schoennagel, T., Dobrowski, S. Z., Moritz, M. A. (2012) Spatial variability in wildfire probability across the western United States. *Int. J. Wildland Fire*, 21(4), 313-327.
- Raphael, M. N. (2003). The santa ana winds of california. *Earth Interactions*, 7(8), 1-13.
- Rothermel, R.C. (1972) A Mathematical Model. for Predicting Fire Spread in Wildland Fuels; Research Paper INT-115; U.S. Department of Agriculture, Forest Service, Intermountain Forest and Range Experiment Station: Ogden, UT, USA, 40.
- Ryan, G. (1996) Downslope winds of Santa Barbara, California. National Oceanic and Atmospheric Administration Technical Memorandum NWS WR-240, Scientific Services Division, Western Region, Salt Lake City, Utah, USA.
- Scott, J.H. (2006) Comparison of Crown Fire Modeling Systems Used in Three Fire Management Applications; RMRS-RP-58; U.S. Department of Agriculture, Forest Service, Rocky Mountain Research Station: Ft. Collins, CO, USA.
- Smith, C.M., Hatchett, B.J., Kaplan, M.L. (2018) Characteristics of sundowner winds near Santa Barbara, California, from a dynamically downscaled climatology: environment and effects near the surface. *J. Appl. Meteorol. Clim.*, 57, 589–606. Doi: 10.1175/JAMC-D-17-0162.1.

- Stratton, R.D. (2006) Guidance on Spatial Wildland Fire Analysis: Models, Tools, and Techniques; General Technical Report RMRS-GTR-183; U.S. Department of Agriculture, Forest Service, Rocky Mountain Research Station: Ft. Collins, CO, USA.
- Sukup, S. (2013) Extreme northeasterly wind events in the hills above Montecito, California. Western Region Technical Attachment NWS WR-1302. National Weather Service Western Region, Salt Lake City, UT.
- Swain, D. L. (2021) A shorter, sharper rainy season amplifies California wildfire risk. *Geophysical Research Letters*, 48(5), e2021GL092843.
- Syphard, A. D., Radeloff, V. C., Keeley, J. E., Hawbaker, T. J., Clayton, M. K., Stewart, S. I., Hammer, R. B. (2007) Human influence on California fire regimes. *Ecological applications*, 17(5), 1388-1402.
- Syphard, A. D., Keeley, J. E., Massada, A. B., Brennan, T. J., Radeloff, V. C. (2012) Housing arrangement and location determine the likelihood of housing loss due to wildfire. *PloS one*, 7(3), e33954.
- Syphard, A. D., Brennan, T. J., Keeley, J. E. (2017) The importance of building construction materials relative to other factors affecting structure survival during wildfire. *International Journal of Disaster Risk Reduction*, 21, 140-147.
- Syphard, A. D., and Keeley, J. E. (2019) Factors associated with structure loss in the 2013–2018 California wildfires. *Fire*, 2(3), 49.
- Thompson, M. P., Bowden, P., Brough, A., Scott, J. H., Gilbertson-Day, J., Taylor, A., Anderson, J., Haas, J. R. (2016) Application of wildfire risk assessment results to wildfire response planning in the southern Sierra Nevada, California, USA. *Forests*, 7(3), 64.

- Westerling, A. L., Cayan, D. R., Brown, T. J., Hall, B. L., Riddle, L. G. (2004). Climate, Santa Ana winds and autumn wildfires in southern California. *Eos, Transactions American Geophysical Union*, 85(31), 289-296.
- Westerling, A. L., and Bryant, B. P. (2008) Climate change and wildfire in California. *Climatic Change*, 87(1), 231-249.
- Westerling, A. L., Bryant, B. P., Preisler, H. K., Holmes, T. P., Hidalgo, H. G., Das, T., Shrestha, S. R. (2011) Climate change and growth scenarios for California wildfire. *Climatic Change*, 109(1), 445-463.
- Westerling, A. L. (2016) Increasing western US forest wildfire activity: sensitivity to changes in the timing of spring. *Philosophical Transactions of the Royal Society B: Biological Sciences*, 371(1696), 20150178.
- Westerling, A. L. (2018) Wildfire Simulations for California's Fourth Climate Change Assessment: Projecting Changes in Extreme Wildfire Events with a Warming Climate: a Report for California's Fourth Climate Change Assessment. Sacramento, CA: California Energy Commission.
- Williams, A. P., and Abatzoglou, J. T. (2016) Recent advances and remaining uncertainties in resolving past and future climate effects on global fire activity. *Current Climate Change Reports*, 2(1), 1-14.
- Williams, A. P., Abatzoglou, J. T., Gershunov, A., Guzman-Morales, J., Bishop, D. A., Balch, J. K., Lettenmaier, D. P. (2019) Observed impacts of anthropogenic climate change on wildfire in California. *Earth's Future*, 7(8), 892-910.
- Wong, S.D., Broader, J.C., Shaheen, S.A. (2020) Review of California Wildfire Evacuations from 2017 to 2019. University of California, Institute of Transportation Studies. Doi: 10.7922/G29G5K2R

- Zigner, K., Carvalho, L.M.V., Peterson, S.H., Fujioka, F., Duine, G.J., Jones, C., Roberts, D.A., Moritz, M. (2020) Evaluating the ability of FARSITE to simulate wildfires influenced by extreme, downslope winds in Santa Barbara, California. *Fire* 3(3): 29.
- Zigner, K., Carvalho, L.M.V., Jones, C., Duine, G.J. (2021) Extreme winds and fire weather in coastal Santa Barbara, CA: An observational analysis. In press for the *International Journal of Climatology*.



## **2. Extreme Winds and Fire Weather in Coastal Santa Barbara County, CA: An Observational Analysis**

Katelyn Zigner<sup>1</sup>, Leila M.V. Carvalho<sup>1,2</sup>, Charles Jones<sup>1,2</sup>, Gert-Jan Duine<sup>2</sup>

<sup>1</sup> Department of Geography, University of California, Santa Barbara, CA, USA

<sup>2</sup> Earth Research Institute, University of California, Santa Barbara, CA, USA

This work has been published in the International Journal of Climatology:

Zigner, K., Carvalho, L.M.V., Jones, C., Duine, G.J. (2021) Extreme winds and fire weather in coastal Santa Barbara, CA: An observational analysis. International Journal of Climatology. DOI: 10.1002/joc.7262

## **2.1 Abstract**

Coastal Santa Barbara (SB) County in Southern California, characterized by a Mediterranean climate and complex topography, is a region prone to downslope windstorms that create exceptional fire weather conditions and rapidly spread wildfires. The Santa Ynez Mountains, oriented from east to west, rise abruptly from the coast, separating air masses from the ocean and the Santa Ynez Valley. The juxtaposition of these geographic features generates spatiotemporally variable wind regimes. This study analyzes diurnal-to-seasonal wind cycles and extremes in this region using hourly data from eight weather stations and four buoys for the period 1998-2019. Data from a vertical wind profiler was extracted from Aug. 2016 – Sept. 2020. Temperature, dew point, and the Fosberg fire weather index are examined at land stations. We show that cycles in wind speed vary spatiotemporally; mountain (valley and coastal) stations exhibit a pronounced semiannual (annual) cycle, and wind maxima are observed during the evening (afternoon) at mountain (valley and coastal) stations. Differences in wind speed percentiles exceeding 14 m/s were evident among stations, and strong winds recorded at buoys were significantly correlated (between 0.3 and 0.5) to land stations. However, cross-correlational analysis did not reveal any temporal lags between mountain stations and buoys. Distributions of temperature and dew point during extreme winds differed between east and west mountain stations. Significant fire weather conditions were most frequent, exceeding 5% occurrence, at mountain stations.

## **2.2 Introduction**

Southern California is characterized by a Mediterranean climate, with dry summers and wet winters. Nonetheless, regional differences in climate are attributed to the complex

terrain spanning the U.S. West Coast. Santa Barbara (SB) County, situated in Southern California, provides an example of a region where topography and proximity to the ocean creates remarkable spatiotemporal variability in atmospheric variables. With a 100 km length, 10 km width, and peaks over 1.2 km above sea level, the Santa Ynez Mountains (SYM) exhibit a distinctive east-west orientation and separate the cool Pacific Ocean from the Santa Ynez Valley (SYV). The San Rafael Mountains, north of the SYM with peak elevations exceeding 2 km, help create the ‘v-shape’ of the SYV (Fig. 2.1). The complex terrain and oceanic influence generate interacting thermally-driven wind circulations along the coast (Dorman and Winant 2000), on the slopes of the SYM, and along the SYV to the north (Jones et al. 2020).

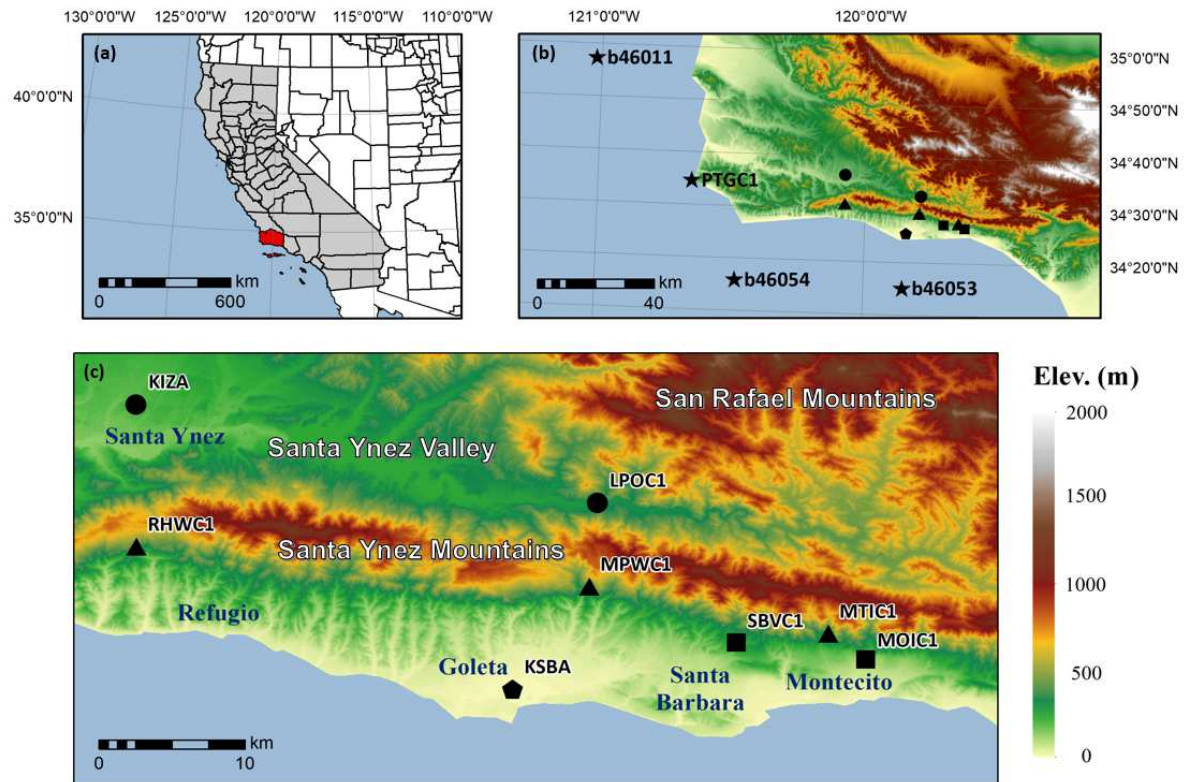


**Figure 2.1** - (a) California counties (grey) and Santa Barbara County (red). (b) Digital elevation model of Santa Barbara County with land stations and buoys. Shapes identify station categorization used throughout the paper: Valley (circle), mountain (triangle), foothill (square), coast (pentagon), and buoy (star). Station details are provided in Table 2.1. (c)

Further detail of land stations, showing multiple ridges and valleys on the south side of the Santa Ynez Mountains. Cities are shown in blue text.

Another unique feature of the region is the downslope windstorm frequently observed on the southern SYM slopes. These cross-mountain (northerly) winds are known as ‘Sundowners’ due to their typical onset near sunset (Blier 1998; Ryan 1996; Cannon et al. 2017; Smith et al. 2018; Duine et al. 2019; Carvalho et al. 2020; Jones et al. 2020). Sundowners are infamous for their role in rapidly spreading wildfires that often disrupt the community of ~130,000 inhabitants living in coastal SB (Zigner et al. 2020). The National Weather Service Oxnard/ Los Angeles (henceforth NWS-LOX) is particularly concerned about these cross-mountain (northerly) winds when sustained speeds reach 13.4 m/s (30 mph) or gusts reach 15.6 m/s (35 mph) (NWS-LOX, personal communication). Sundowners may produce gale-force winds and critically low relative humidity ( $< 15\%$ ) (Sukup 2013; Cannon et al. 2017; Carvalho et al. 2020; Jones et al. 2020). Although temperature ramps do not occur during all Sundowners (Blier 1998; Carvalho et al. 2020), a handful of past events have reported atypically hot temperatures after sunset, exceeding 30°C during some summer Sundowners (Ryan 1996; Blier 1998; Zigner et al. 2020).

Wildfire behavior is driven by fuels, topography, and weather (Countryman 1972). However, weather is the leading factor in wildfire spread and intensity during extreme winds (Rothermel 1983; Keeley et al. 2009; Moritz et al. 2010). Locally, the NWS-LOX defines ‘Red Flag Criteria’ in most of southern California as dry fuels with any one of: 1) relative humidity (RH)  $< 15\%$  with sustained winds  $> 25$  mph or gusts  $> 35$  mph for 6 hours, 2) RH  $< 10\%$  with sustained winds  $> 15$  mph or gusts  $> 25$  mph for 6 hours, 3) widespread and/or significant dry lightning, or 4) forecaster discretion (typically used with RH close to the

criteria in 1) or 2) and very strong winds) (National Weather Service Los Angeles/ Oxnard). Thus, Sundowners may create significant fire weather conditions. With expansion into the wildland-urban interface served by a few narrow and winding roads (Fig. A2.1 for imagery of this area), understanding the spatiotemporal variability of strong winds and fire weather is critical to identify particularly at-risk regions.

The bulk of knowledge regarding winds in SB is based on regional models focusing on Sundowner winds (Cannon et al. 2017; Hatchet et al. 2018; Smith et al. 2018; Duine et al. 2019; Carvalho et al. 2020; Jones et al. 2020). These studies showed spatial and temporal variability in wind speed and direction on the SYM slopes during these events; The Sundowner Winds Pilot Experiment (Carvalho et al. 2020) examined radiosonde and station data from a Sundowner event in April 2019 and found spatial differences in wind speed and direction along the SYM. Radiosonde profiles indicated that Sundowners are associated with a lee slope jet and were associated with mountain waves, in agreement with model output examining Sundowners in Smith et al. (2018), Duine et al. (2019), and Jones et al. (2020). Using 30 years of hourly mesoscale simulations, Jones et al. (2020) identified three distinct Sundowner wind regimes (East, West, and Santa Barbara) that are differentiated by spatial and temporal characteristics, including the magnitude of winds on the southern SYM slopes and the strength and position of the coastal jet.

Nonetheless, no previous study to date has investigated diurnal and seasonal cycles of winds based on observations, including the relationships between winds in the SYV, on the SYM, and in coastal SB using station data. Dorman and Winant (2000) studied winds in the Santa Barbara Channel using primarily buoy data, but that study did not extensively analyze land-based weather stations nor examine relationships between winds in the Santa Barbara channel and Sundowners. Furthermore, although destructive wildfires have

undoubtedly impacted SB, no study has analyzed the spatial or temporal variability in extreme fire weather conditions in this region.

The primary objective of this study is to develop an in-depth analysis of surface winds and fire weather in coastal SB utilizing long-term observational station data and the National Oceanic and Atmospheric Administration (NOAA) wind profiler installed at the Santa Barbara airport. The main scientific questions investigated in this manuscript are as follows: 1) Are east and west Sundowner regimes distinct and evident from data collected at weather stations? 2) Are strong surface winds at buoys near Point Conception (to the west of SB) and in the Santa Barbara channel related to strong winds at land-based stations? and 3) Do extreme fire weather conditions vary between mountain locations? These issues will be examined by calculating various wind statistics, including diurnal-to-seasonal cycles, percentiles, and correlations. Additional meteorological variables such as temperature and dew point are analyzed during extreme winds, and a fire weather index is used to determine the frequency of significant fire weather conditions. Advancing knowledge of spatial and temporal wind and fire weather patterns in coastal SB using observations have practical applications in weather forecasting and climate investigations. Moreover, the statistical analyses provided here based on stations may enable improvements in resource allocation, including the placement of new stations and profilers, potentially contributing to strategic fuel management, minimizing risk around homes and other structures (McWethy et al. 2019; Miller et al. 2020). These results can be useful for the creation of in situ fire management strategies, as proposed in Thompson et al. (2016), and contribute to evacuation planning in a region highly vulnerable to wildfires (Li et al. 2019). Finally, the proposed methods can potentially contribute to understanding wind regimes in other coastal regions dominated by Mediterranean climate and exhibiting complex topography.

The paper is organized as follows. Section 2.2 explains the data and processing methods. Section 2.3 explores diurnal-to-seasonal wind cycles, wind percentiles, the application of the NWS-LOX Sundowner criteria at each station, correlations between land and buoy stations, and utilization of data from the wind profiler. Section 2.4 analyzes diurnal and seasonal cycles of temperature, relative humidity, dew point, and examines variability during extreme winds. Section 2.5 examines variability in fire weather through the use of a fire weather index, and Section 2.6 provides a discussion and summary of the main findings.

## **2.3 Data and Methods**

Data were obtained from eight land-based stations through the MesoWest network (Horel et al. 2002) in coastal SB and the SYV (Table 2.1). Stations were categorized into four classes based on location and elevation: valley, mountain, foothill, and coastal (Figs. 2.1 and A2.1). Mountain stations are located on the southern SYM slopes above foothill stations. Few stations were available closer to the SYM crest (within 250 m), and these stations were not selected for analysis because of the short time periods for data collection at the time of manuscript submission (less than 3 years of data). Furthermore, the majority of these stations have not followed standard protocols for sensor installation, as implemented by the NWS and U.S. Forest Service, unlike the other stations selected in this study. Therefore, all stations analyzed in this study maintain the standards set among government-owned stations. The single coastal station (KSBA) has the lowest elevation and is situated less than 1.5 km from the coast. This station was separated from other groups because of the potential influence of the marine boundary layer, shown more subtly at all other stations. Additional data were collected from three National Data Buoy Center (NDBC) buoys in the

Santa Barbara Channel and near Point Conception to the west (see Fig. 2.1b for location); a land station available from the NDBC was added since it represents a key location in the western part of the analysis domain.

**Table 2.1** - Information on weather stations including location, elevation, operating agency (NWS: National Weather Service, USFS: US Forest Service, NDBC: National Data Buoy Center), and temporal data collection details. Stations LPOC1 and MTIC1 changed reporting times in their history, hence the multiple reporting times. All NDBC-owned stations recorded hourly data until the mid-2010's when all began collecting data every 10-minutes.

STATION ID	STATION NAME	LATITUDE	LONGITUDE	ELEVATION (m)	AGENCY	REPORTING TIME (min.s)	STATION INSTALLATION
KIZA	Santa Ynez Airport	34.607	-120.076	205	NWS	Varied over time	April 2005
KSBA	Santa Barbara Airport	34.426	-119.844	3	NWS	Varied over time	Nov. 1998
LPOC1	Los Prietos	34.544	-119.791	299	USFS	10, 14, 35	Dec. 1999
MOIC1	Montecito #2	34.445	-119.626	87	USFS	07	April 2011
MPWC1	San Marcos Pass	34.491	-119.796	454	USFS	06	July 2015
MTIC1	Montecito	34.461	-119.649	493	USFS	10, 14, 47	Jan. 2000
RHWC1	Refugio	34.517	-120.075	447	USFS	06	July 2015
SBVC1	Santa Barbara Botanic Garden	34.456	-119.706	230	USFS	24	June 2011
b46011	Santa Maria	34.956	-121.019	0	NDBC	00, 10, 20, 30, 40, 50	Jan. 1998
B46053	East Santa Barbara	34.252	-119.853	0	NDBC	00, 10, 20, 30, 40, 50	Jan. 1998
b46054	West Santa Barbara	34.265	-120.477	0	NDBC	00, 10, 20, 30, 40, 50	Jan. 1998
PTGC1	Point Arguello	34.577	-120.648	0	NDBC	00, 10, 20, 30, 40, 50	Jan. 1998

Data were downloaded from the installation date to August 2019. The variable installation dates (Table 2.1) affected the number of observations available at stations. Initial quality control was undergone by the MesoWest data network and the NDBC. Additional quality control data analysis was performed by evaluating the existence of discontinuities or abrupt shifts in means, upper and lower percentiles, caused by changes in instrument sensor. We extracted and examined sample outliers in wind speed, temperature, and dew point, and



found no evidence of erroneous data. Hence, all data provided by the data networks were utilized.

The land-based stations are comprised of both NWS Automated Service Observation Stations (ASOS) and U.S. Forest Service Remote Automated Weather Stations (RAWS) (National Wildfire Coordinating Group). Inherent differences exist between ASOS and RAWS; Wind instruments on ASOS are installed 10 m above ground level and calculate sustained wind speed as the average wind over a 2 min period from a 5 sec sampling frequency. RAWS wind instruments are installed 6.1 m above ground level and calculate sustained wind speed as the average wind over a 10 min period from a 3 sec sampling frequency. Temperature and humidity sensors are placed at 2 m above ground level for ASOS and 1.2-2.4 m above ground level for RAWS (National Wildfire Coordinating Group).

Reporting times for observations vary between the agencies; ASOS report sub-hourly data, RAWS report hourly data, and NDBC report hourly and sub-hourly data depending on the buoy or station. To compare among stations, data were processed to create one representative data point per hour. This was completed using different techniques depending on the number of observations per hour and the time of the observations. At stations with one reported observation per hour recorded 15 minutes prior to or 15 minutes after the hour (LPOC1, MOIC1, MPWC1, MTIC1, and RHWC1), the recorded observation was used. For example, the processed data at 0600 PST at RHWC1 was the observation recorded at 0606 PST. At stations with one observation per hour recorded between 15 minutes to 45 minutes after the hour (LPOC1 and SBVC1), the observations in the aforementioned 30-min period before and after each hour were averaged. For example, the processed data point 0600 PST at SBVC1 was calculated by averaging the observations at 0524 and 0624 PST. At stations

with sub-hourly observations (KIZA, KSBA, and all NDBC stations), we averaged all observations 15 minutes prior to and 15 minutes after the hour. For example, the processed data point 0600 PST at KSBA was calculated by averaging all observations between 0545 and 0615 PST.

In addition to data from land stations, hourly vertical wind data were obtained from a NOAA Physical Sciences Laboratory 449 MHz wind profiler (Ecklund et al., 1988) located at the Santa Barbara airport from Aug. 2016 to Sept. 2020. Wind profilers transmit electromagnetic pulses vertically in at least two slightly different directions (~75 degrees), which allow for the analyzation of winds in three dimensions. A signal-to-noise ratio is used to differentiate atmospheric phenomena (i.e. clouds, precipitation) from non-meteorological obstructions (i.e. birds, planes). In particular, the type of wind profiler at the Santa Barbara airport is a coaxial-colinear phased array antenna with a peak transmit power of 2000 W. Hourly data were obtained, typically ranging from 200 m to 8 km AGL with a vertical resolution of approximately 100 m. These data provided a complementary analysis into the vertical wind profile of seasonal and diurnal cycles, and during Sundowner events.

Fire weather indices can identify critical fire weather conditions that may facilitate rapid wildfire spread. One widely-used fire weather index is the Fosberg Fire Weather Index (FFWI; Fosberg 1978). The FFWI calculates the small-scale and short-term (e.g. hourly) fire weather conditions using wind speed, temperature, and relative humidity (Goodrick 2002). The FFWI and the National Fire Danger Rating System are used operationally to forecast areas of enhanced fire threat. We used the FFWI to examine areas at high risk of wildfire spread due to extreme winds in coastal SB.

The FFWI is defined as:

$$FFWI = \frac{\eta * \sqrt{1 + U^2}}{0.3002}$$

where U is wind speed in mph, and  $\eta$  is the moisture damping coefficient, defined as:

$$\eta = 1 - 2\left(\frac{m}{30}\right) + 1.5\left(\frac{m}{30}\right)^2 - 0.5\left(\frac{m}{30}\right)^3$$

The equilibrium moisture content (m) is a function of temperature in degrees Fahrenheit (t) and relative humidity in percent (h), given by:

$$m = \begin{cases} \text{for } h \leq 10\%: \\ 0.03229 + 0.281073h - 0.000578ht \\ \text{for } 10\% < h \leq 50\%: \\ 2.22749 + 0.160107h - 0.01478t \\ \text{for } h > 50\%: \\ 21.0606 + 0.005565h^2 - 0.00035ht - 0.483199h \end{cases}$$

To account for precipitation,  $m=30$  when precipitation reaches 0.25 mm in the previous 24 hours, as applied to Santa Ana Winds in Jones et al. (2010). The FFWI ranges between 0 and 100, reaching 100 when RH is 0% and wind speed is 30 mph. FFWI values exceeding 50 are considered significant for fire weather on a national scale (Goodrick 2002; Hazra et al. 2018).

Seasonal (diurnal) cycles of wind speed, temperature, dew point, and FFWI were created by calculating the daily (hourly) mean and fitting the first two harmonics. For the correlations amongst and between land and buoy stations, significance was assessed by applying a non-parametric test based on Monte Carlo resampling. The test was constructed by randomly resampling the time series for each pair of stations 10,000 times (using the number of matching data points) and calculating the linear Pearson's correlation coefficient between the pair. The  $H_0$  hypothesis (no correlation) was rejected if the absolute value of the

correlation was greater than the 95th or 99th percentile of the absolute value of the respective random distribution. When we compared Sundowner versus non-Sundowner days using the vertical wind profiler, statistical significance was determined using a Student's t-statistic for  $u$  and  $v$  wind components. In this case, we reject  $H_0$  if either  $u$  or  $v$  are statistically significant at the 5% significance level.

To analyze variations in temperature and dew point during Sundowners (as defined by the NWS-LOX wind criteria), we calculated hourly medians of temperature and dew point during hours not reaching Sundowner criteria for each season and compared with temperature and dew point data during Sundowners. The number of hours that reached Sundowner criteria in each season ranged between 0 to 216 at MTIC1 and 3 to 134 at RHWC1 (length of records is different for each station). Thus, given the large difference in sample sizes between non-Sundowner and Sundowner hours and the unknown distributions of these differences, we assessed the statistical significance in the differences in medians based on a non-parametric test. For this test, we constructed a distribution of 10,000 random samples extracted from non-Sundowner data separated by hour and season. Each one of these sampled of non-Sundowner hours have the same number of records as the Sundowner hours. Then, the median of the Sundowner data for the matching season/ hour was compared to the resulting distribution of the non-Sundowner medians. The null hypothesis is that the Sundowner medians do not differ from randomly obtained medians of the non-Sundowner cases. We reject the null hypothesis at the 95th confidence interval if the Sundowner median was less than the 2.5th percentile or greater than the 97.5th percentile (considering a two-tail test) of the respective distribution of non-Sundowner medians.

## 2.4 Observed Wind Patterns and Extremes

### 2.4.1 Seasonal

We start by first presenting the seasonal variability of mean winds at ASOS and RAWS. Valley, foothill, and coastal (henceforth “non-mountain”) stations exhibit a distinct wind pattern compared to mountain stations, with non-mountain stations reporting a smaller seasonal wind speed range ( $< 1$  m/s) and no bimodal pattern in mean wind speed (Fig. 2.2). Mountain stations record the highest wind speeds, largest range in wind speeds, and exhibit a bimodal pattern throughout the year; wind speeds are strongest in spring, then decrease in summer, and increase again in fall. Additionally, RHCW1 in the west SYM typically records the strongest winds, followed by MPWC1 in the central SYM, and finally MTIC1 in the east SYM. Located on the western SYM (Fig. A2.1b), RHCW1 seems to be strongly influenced by the dominant coastal NW flow and coastal jet (Rahn et al. 2014; Smith et al. 2018b). MPWC1 (central SYM) is near San Marcos Pass, a prominent gap in the central SYM oriented northwest-to-southeast that may contribute to channeling northwesterly winds. MTIC1 (east SYM) is located on a prominent peak on a ridge in the eastern SYM above Montecito with the surrounding canyons oriented northeast-to-southwest (Fig. A2.1c).

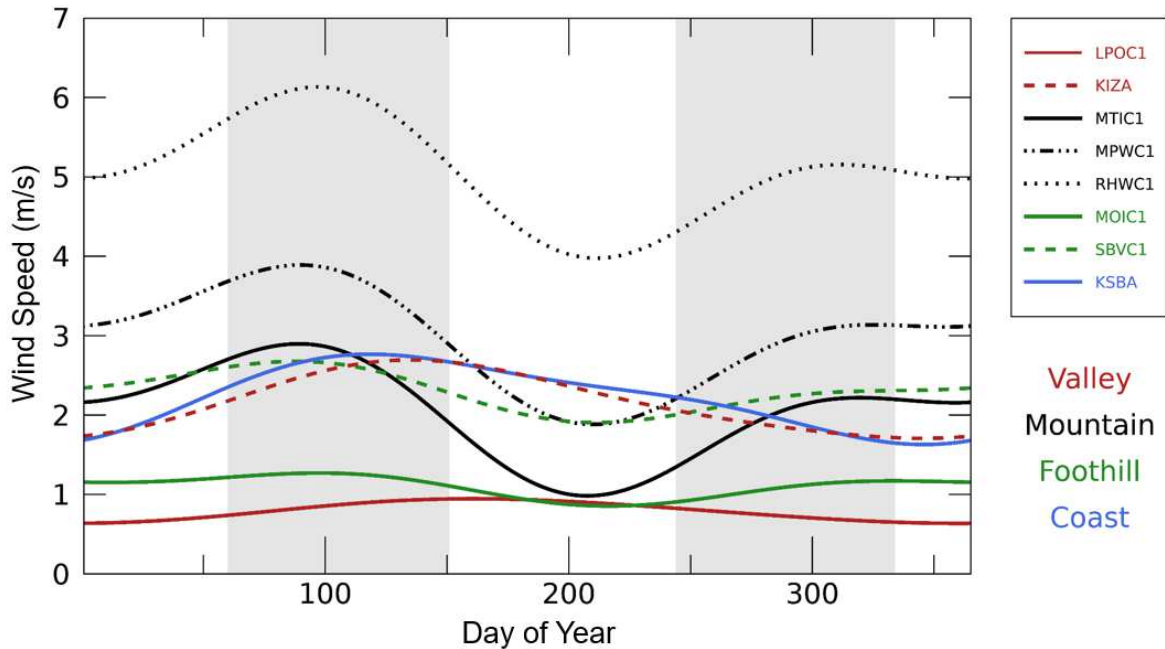


**Figure 2.2** - Seasonal cycles of wind speed by station. Grey shading indicates spring and fall.

Most stations record maximum wind speeds in spring (Mar – May), consistent with the highest frequency of Sundowner winds (e.g., Hatchett et al. 2018; Smith et al. 2018a; Jones et al. 2020). Mean wind speeds range between 2-6 m/s at mountain stations and 0.5-3 m/s at non-mountain stations. In summer (Jun - Aug), wind speed decreases at all stations except LPOC1, ranging between 1-5 m/s at mountain stations and 1-3 m/s at non-mountain stations. It should be noted that in summer and early fall, the mean wind speed is commonly larger at KSBA (coast), KIZA (valley), and SBVC1 (east SYM) than at mountain stations MPWC1 (central SYM) and MTIC1 (west SYM). In fall (Sept - Nov), wind speed decreases at valley stations and the coastal station, and increases at foothill and mountain stations. Mean wind speed at all stations remains fairly constant until the end of winter when it increases into spring.

#### *2.4.2 Diurnal*

Similar to the seasonal cycle, the diurnal cycle differs between mountain and non-mountain stations (Fig. 2.3). At mountain stations, the strongest winds occur during the night (between 2000 and 2200 PST). RHC1, located in the western SYM, records the highest mean magnitude (greater than 6 m/s) and greatest amplitude of the diurnal cycle compared to other stations. Notably, the mean wind speed and amplitudes of the diurnal cycle progressively decrease eastward at mountain stations. Foothill, valley, and coastal stations exhibit a very different diurnal cycle, with the strongest winds observed in the afternoon (between 1200 and 1600 PST) created by horizontal pressure gradients creating valley and land-sea circulations. During the day, winds are driven up valley as the inner parts of the valley heat more than the plain (Giovannini et al 2017). Similarly, the formation of a sea breeze occurs as the land heats more than the ocean, driving onshore daytime winds (Markowski and Richardson 2011). In the SYV, the sea breeze may reach KIZA and interact with the up-valley circulation (Bastin et al. 2005). Westerly winds are recorded most frequently at valley stations in the summer and least frequently in the winter (not shown). KSBA (coastal) and KIZA (valley) record mean wind speeds in the afternoon that are greater than stations on the slopes of the SYM (Fig. 2.3).

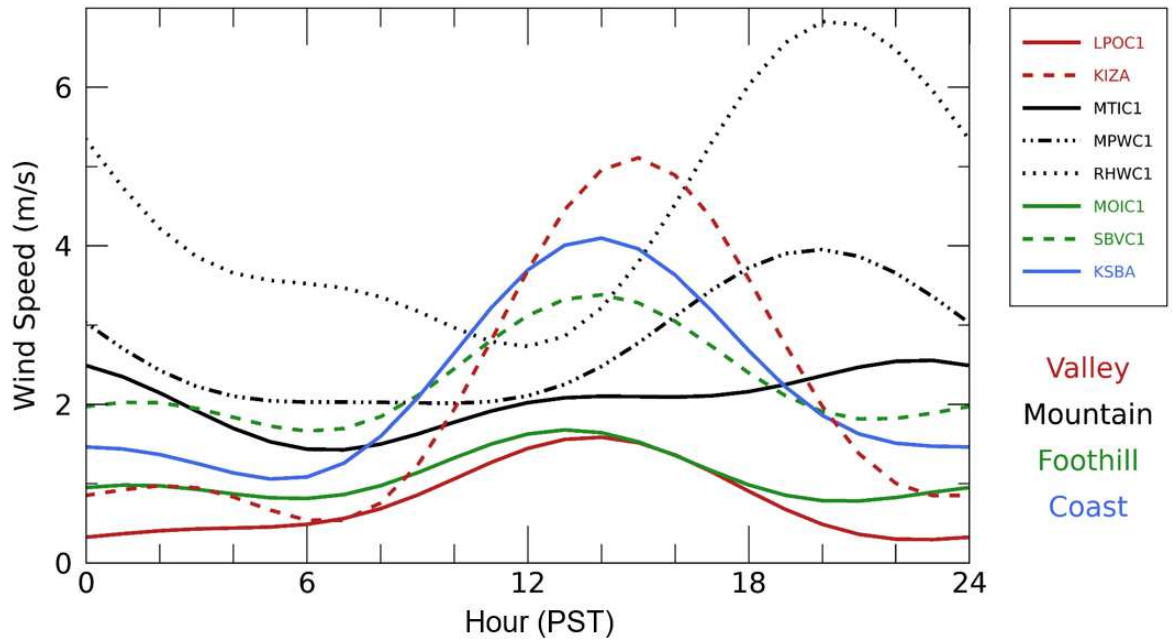


**Figure 2.3** - Diurnal cycles of wind speed at each station. All months were considered.

The combined frequency of wind speed and direction at each station separated according to the time of the day are assessed based on wind roses (Figs. 2.4,2.5). Only winds at or exceeding 0.5 m/s are shown, since weak winds ( $< 0.5$  m/s) are ill-defined for analysis of wind direction. Additionally, the quality control analysis indicated that changes in sensors at some stations have affected the frequency of very light winds (less than 0.5 m/s). Differences in dominant frequency of wind direction are observed among stations, illustrating the complexity of wind systems in the region. Between 1500 and 1700 PST, most mountain and foothill stations record weak-to-moderate upslope (southerly) winds. The daytime upslope, thermally driven winds are more frequently observed with southeast direction at western station RHWC1, while other mountain stations record weak ( $< 4$  m/s), southwesterly winds (Fig. 2.4). These predominant wind orientations could result from the placement of the station in relation to local topographic features (Fig. A2.1). Approximately



25% of the winds in this time period recorded at RHWC1 are comparatively northwesterly and strong, commonly exceeding 8 m/s. This can be explained by the persistent northwesterly flow in this region (Dorman and Winant 2000). Additionally, the strong winds ( $> 8$  m/s) recorded between 1500 to 1700 PST at RHWC1 (Fig. 2.4) may reflect contributions from the early onset of Sundowners on the western SYM slopes (Jones et al. 2020; Carvalho et al. 2020; Duine et al. 2021).

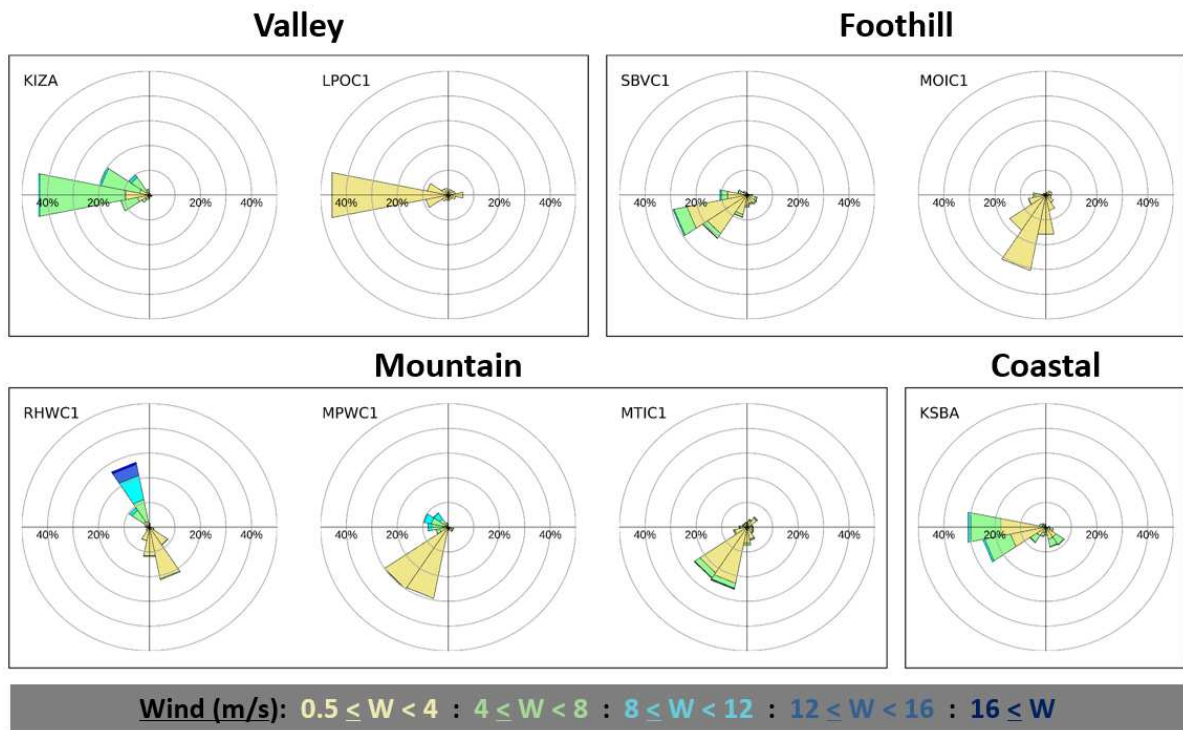


**Figure 2.4.** Wind roses created using data between 1500 and 1700 PST. Spokes are broken into  $22.5^\circ$  increments, where the length of the spoke indicates wind direction frequency and the coloring indicates wind speed at each direction. Only winds  $\geq 0.5$  m/s wind speed threshold were included.

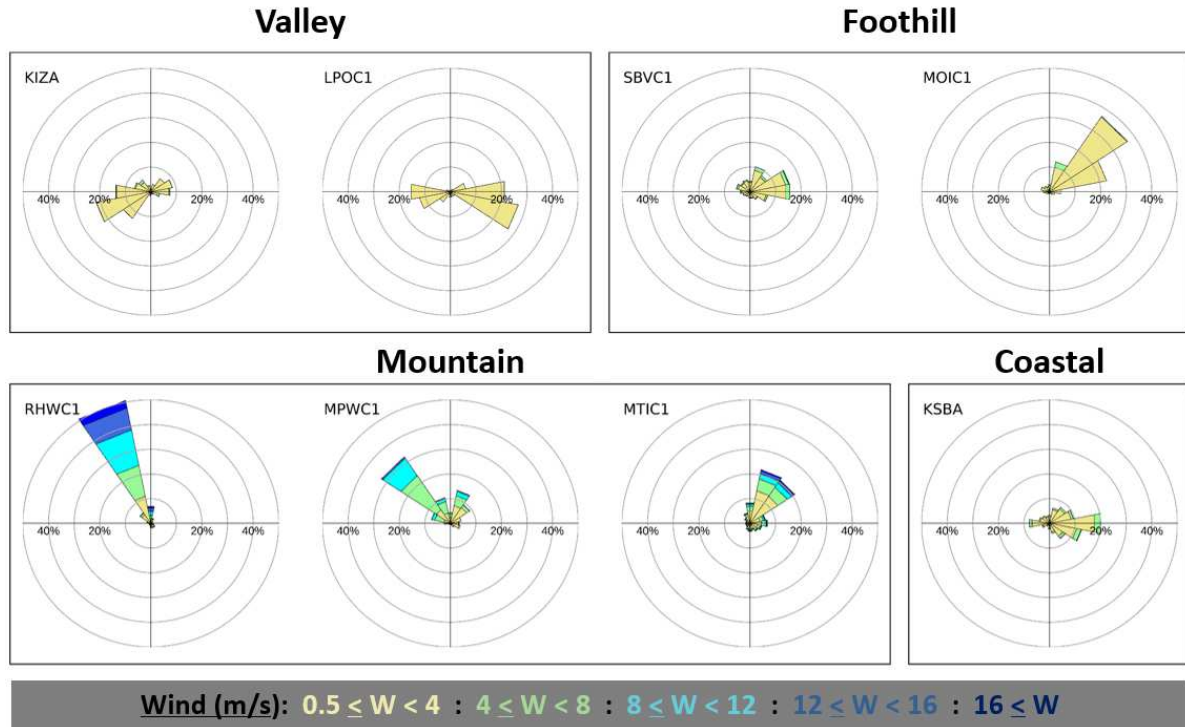


**Figure 2.5.** Similar to Figure 2.4 created using data between 2100 and 2300 PST.

We notice a transition from upslope (southerly) to downslope (northerly) winds at most stations on the southern-facing slopes of the SYM in the late afternoon and early evening, as indicated by wind roses from 1800 to 2000 PST (Fig. A2.2) and from 2100 to 2300 PST (Fig. 2.5). Generally, the strongest winds are at mountain stations around 2000 PST (Fig. 2.3) and have northerly components (Figs. 2.4,2.5), continuing through the evening. Radiative surface cooling on the mountain slopes creates downslope (northerly) flow (Markowski and Richardson 2000; Skillingstad et al. 2001). The timing and strength of these circulations depend on many factors including slope angle (Nadeau et al. 2013), mountain range orientation with respect to azimuth angle of the sunset, and valley geometric scales (Duine et al. 2017).

Downslope (northerly) wind direction systematically varies along the slopes of the SYM in the evening; downslope winds at RHCW1 (west SYM) and MPWC1 (central SYM)

are dominantly northwesterly, whereas eastern SYM stations in the foothills (MOIC1, SBVC1) and on the slopes (MTIC1) exhibit mostly northeasterly winds (Fig. 2.5). The variation in wind directions observed in the west and east regions of the south-facing SYM have been shown in climatological simulations with WRF (Jones et al. 2020). Although more studies are necessary to evaluate all mechanisms explaining the behavior of wind direction along the slopes of the SYM, sensitivity tests and simulations have shown that the upstream (north) San Rafael Mountains play a critical role in the timing of the onset of the northeasterly winds, and this effect is particularly important in the eastern SYM (Duine et al. 2021).

The coastal station KSBA records a diurnal wind regime consistent with findings regarding flow in the Santa Barbara channel (Dorman and Winant 2000). This station typically records southeasterly winds around 0900 PST and westerly winds around 1200 PST (not shown) and 1500-1700 PST (Fig. 2.4), transitioning to easterly (onshore) winds around 2100 PST (Fig. 2.5). Dorman and Winant (2000) determined that winds in the western, central, and eastern Santa Barbara Channel exhibit different regimes, and the coastal station KSBA shares similarities with their termed “eastern regime,” which is characterized by fairly weak and reversing winds compared to flow within the channel.

Similar to the coastal station, valley stations (KIZA and LPOC1) record maximum wind speeds from 1300 to 1500 PST (Fig. 2.3) and exhibit dominant westerly wind direction between 1500 and 1700 PST (Fig. 2.4). LPOC1 (located up valley; see Fig. 2.1) is relatively far from the coast, and its location in a narrow portion of the SYV results in stronger mountain-valley and up-valley circulations (Rampanelli et al. 2004; Stull 2012; DeWecker et al. 1998). The up-valley circulation appears as a relevant mechanism explaining the westerly wind direction at LPOC1 in the late afternoon and the relatively weaker average

peak wind speed ( $\sim 1$  m/s). The most remarkable changes in wind direction at both valley stations are observed in late evening, contrasting with stations in the mountain and foothills where wind changes direction early in the evening. During the night, when a stratified stable boundary layer is well established near the surface, down-valley circulations driven by the rapid cooling of the mountain slopes and upper valley (Fig. 2.1) (Stull 2012; DeWekker et al. 1998) may explain the eastward shift in wind direction observed at LPOC1 (Fig. 2.5). Notice that the down-valley circulation seems to be less important at KIZA due to its geographic location in a wider part of the valley (Fig. 2.1), corroborating with simulations in DeWekker et al. (1998).

#### *2.4.3 Extremes in winds using percentiles*

This section investigates the statistics of extreme surface winds on a station-by-station basis using percentiles. Station analysis indicates that the strongest winds in coastal SB are recorded primarily at mountain stations in the early evening and from a northerly direction (Figs. 2.3-2.5). When examining wind speed percentiles that consider all wind directions (Fig. 2.6), the highest values are recorded at RHWC1, an expected result given that this station typically records the highest wind speeds seasonally and diurnally (Figs. 2.2,2.3). Until approximately the 75th percentile, wind speed percentile values are below 5 m/s except for RHWC1. At the 75<sup>th</sup> percentile MPWC1 records the second-highest wind speed values ( $\sim 5$  m/s), followed by KIZA, KSBA, SBVC1, and MTIC1, respectively. The values at MTIC1 surpass all non-mountain stations at the 92<sup>nd</sup> percentile and surpass MPWC1 at the 97<sup>th</sup> percentile (Fig. 2.6a). The rapid increase in values at MTIC1 indicates that this station typically records weak-to-moderate-strength winds (between 2 to 5 m/s) and occasionally records strong winds, exceeding 10 m/s with approximately 4% occurrence.

The NWS-LOX Sundowner wind criteria ( $\geq 13.4$  m/s) is reached at RHWC1 at the 95<sup>th</sup> percentile and at MTIC1 at the 99<sup>th</sup> percentile (Fig. 2.6a). With the exceptions of MOIC1 and LPOC1, all other stations have reached these criteria for at least one observation (Fig. 2.6b). Because gust data were not available at all stations, they were not included in this analysis.

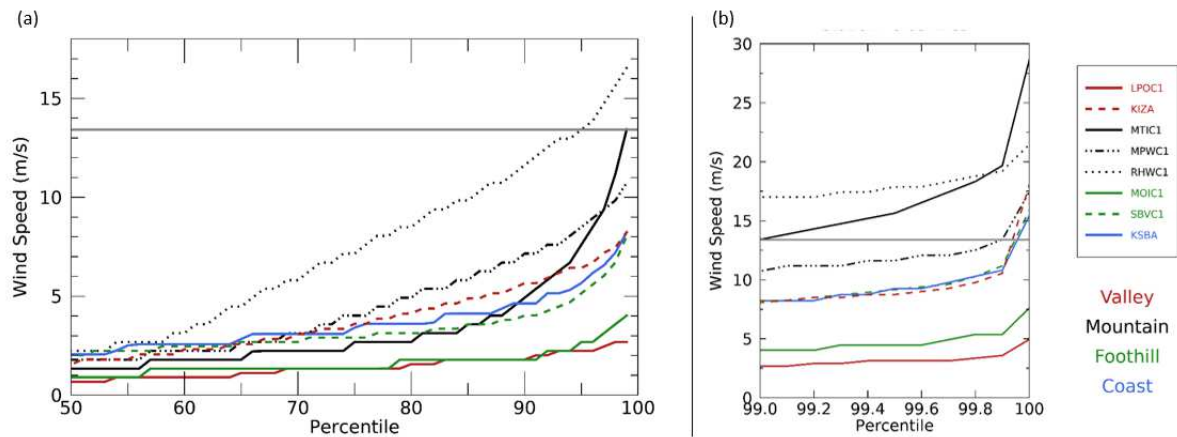


**Figure 2.6** - Wind speed percentiles by station from the (a) 50<sup>th</sup> to 99<sup>th</sup> percentiles and (b) 99<sup>th</sup> to 100<sup>th</sup> percentiles using data from the entire year. The maximum value is recorded as the value at the 100<sup>th</sup> percentile. The horizontal gray line indicates the NWS-LOX Sundowner criteria for sustained winds (13.41 m/s, or 30 mph).

#### 2.4.4 Sundowner wind criteria

When we consider hours with northerly (between 315° and 45°) winds exceeding 13.4 m/s (30 mph) or gusts exceeding 16.4 m/s (35 mph), all stations south of the SYM ridgeline have reached the NWS-LOX Sundowner wind criteria. Table 2.2 shows statistics for the percent of evening-to-morning hours (1800 to 0600 PST) that reached Sundowner wind criteria for the entire year and for each season individually. Focus in this section will be given for the entire year and for spring, which is the season with the peak of Sundowner

events (Jones et al. 2020; Smith et al. 2018a) and the strongest winds (Fig. 2.3). While there are no stations representative of conditions on the mountain ridge, simulations have shown that the strongest winds are observed in upper-to-mid slopes of the SYM in association with the lee-slope jet that characterizes Sundowner winds (Smith et al. 2018a; Duine et al. 2019, 2021; Carvalho et al. 2020; Jones et al. 2020). The mountain stations are placed where Sundowners are generally the strongest.

**Table 2.2** - Statistics by-station on the total sample size (number of available hours for the entire time span), sundowner occurrences (the total number of hours reaching NWS-LOX Sundowner criteria), and the percentage of hours reaching Sundowner criteria. Recall that the NWS-LOX Sundowner criteria is northerly winds with either sustained speeds at least 13.4 m/s (30 mph) or gusts at least 15.6 m/s (35 mph). Statistics were calculated for the entire year (top 3 rows) and by season. Only the evening and early morning hours (1800 to 0600 PST) were considered in this analysis.

	MTIC1	MPWC1	RHWC1	MOIC1	SBVC1	KSBA
<b>ALL DATA</b>						
Total Sample Size	85994	17263	17264	39194	38602	97377
Sundowner Occurrences	4213	351	2705	45	344	25
% Reaching Sundowner Criteria	4.90	2.03	15.67	0.11	0.89	0.03
<b>BY SEASON</b>						
<b>Winter (DJF)</b>						
Total Sample Size	21159	4603	4605	9338	9324	24136
Sundowner Occurrences	1126	55	440	17	108	10
% Reaching Sundowner Criteria	5.32	1.19	9.55	0.18	1.16	0.04
<b>Spring (MAM)</b>						
Total Sample Size	21614	4749	4747	9991	9531	24718
Sundowner Occurrences	1904	170	1104	22	152	9
% Reaching Sundowner Criteria	8.81	3.58	23.26	0.22	1.59	0.04
<b>Summer (JJA)</b>						
Total Sample Size	21556	4371	4373	10423	10306	24408
Sundowner Occurrences	266	92	748	2	31	1
% Reaching Sundowner Criteria	1.23	2.10	17.10	0.02	0.30	0.00
<b>Fall (SON)</b>						
Total Sample Size	21665	3540	3539	9442	9441	24115
Sundowner Occurrences	917	34	413	4	53	5
% Reaching Sundowner Criteria	4.23	0.96	11.67	0.04	0.56	0.02

RHWC1 (west SYM) has the highest percentage of hours meeting Sundowner criteria, reaching 15.7% frequency considering overnight hours during all months and 23.3% frequency in overnight hours during only spring (Table 2.2). The station with the second-highest percentage of hours meeting the criteria is MTIC1 (east SYM) with 4.9% frequency in overnight hours considering all months and 8.8% frequency in overnight hours during spring. MPWC1 (central SYM) records frequencies of 2.0% and 3.6% for overnight hours considering all months and in spring only, respectively. All non-mountain stations record Sundowner wind criteria frequencies less than 1% for the entire year and less than 2% for spring only. SBVC1 on the foothills records the highest frequencies of non-mountain

stations (0.9% considering all seasons and 1.6% in spring), whereas KSBA records the lowest (0.03% considering all seasons and 0.04% in spring) (Table 2.2).

Next, we investigate the wind direction at each station when Sundowner wind criteria was met. Figure 2.7 displays the  $u$  (horizontal axis) and  $v$  (vertical axis) wind components in spring that reached Sundowner wind criteria, using both sustained wind and wind gust thresholds (reported at RAWS stations only; see Table 2.1 for the list of these stations). Sustained winds below 13.4 m/s are present when wind gusts exceeded 15.6 m/s at the time. To investigate systematic variations during the evening, the colored dots indicate two four-hour subsets: 1700-2000 PST and 2100-0000 PST. It is important to acknowledge that the station installation date (Table 2.1) affects the data presented in Fig. 2.7. RHWC1 and MTIC1 recorded the highest number of hours reaching Sundowner wind criteria, even though there is a considerable difference in the total sample size of observations; RHWC was installed in July 2015, whereas MTIC1 was installed in January 2000 (Table 2.2). Contrastingly, KSBA recorded the fewest hours reaching these criteria despite having the longest observational record, indicating that only the strongest Sundowners, or Sundowners that occur with a retreated (further offshore) marine boundary layer, reach the coastal plain.



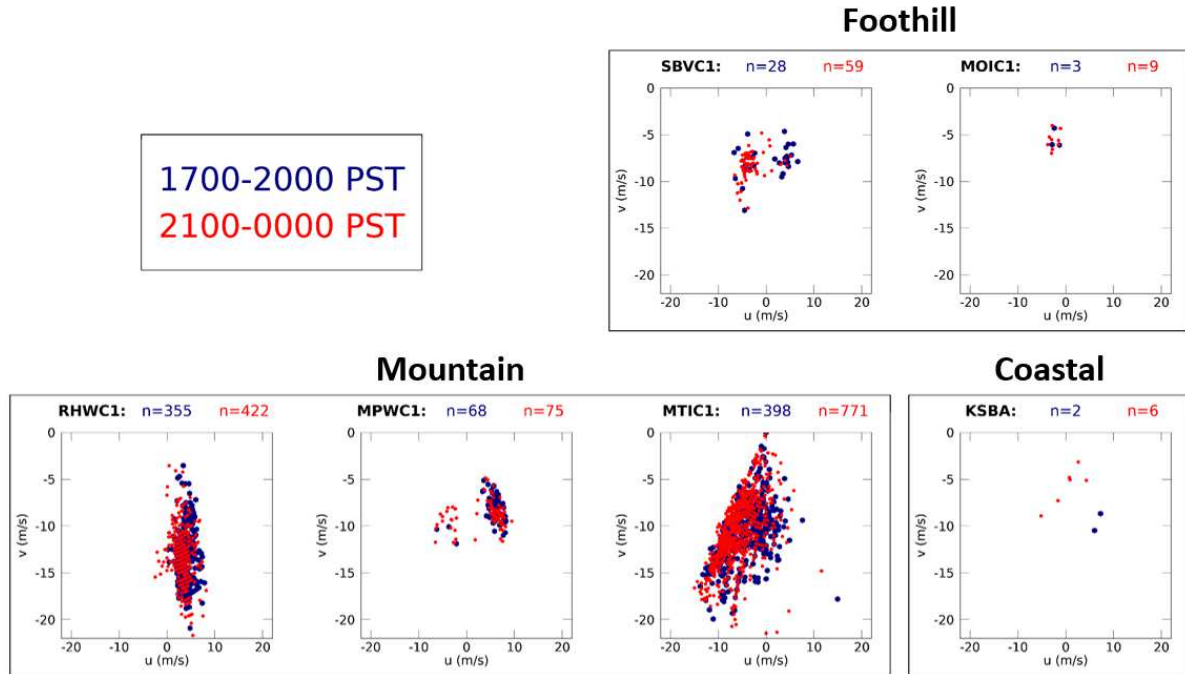


**Figure 2.7** - Scatterplots of  $u$  and  $v$  wind components (in m/s) during springtime hours reaching the NWS-LOX Sundowner criteria. Colors indicate time of day, broken into two 4-hour increments. Note that the period of installation differs among stations (Table 2.1) and thus affects the potential number of hours that may reach Sundowner wind criteria.

Wind direction during hours that reached Sundowner wind criteria is variable amongst mountain stations (Fig. 2.7); RHWC1 records north-northwesterly winds, MPWC1 records northwesterly and northeasterly winds, and MTIC primarily records northeasterly winds. Foothill station MOIC1 records northeasterly winds and SBVC1 records both northeasterly and northwesterly winds. Therefore, patterns of wind direction during Sundowners are similar to those obtained in the climatology (Figs. 2.4,2.5). These spatial differences in wind direction have been identified in the climatological simulations of Sundowners in Jones et al. (2020). The few hours during which Sundowner wind criteria was satisfied at KSBA (coastal) indicate predominantly northwesterly winds (Fig. 2.7). Strong, offshore winds are rarely recorded at stations closer to the ocean. Duine et al. (2019)

indicated that during Sundowners the wind speed maxima on mountain slopes quickly decreases in magnitude toward the coastal plain. Moreover, due to the proximity of the coast, cool and stably stratified marine air can be horizontally advected onto land during these events, preventing the lee jet from reaching ground level (Carvalho et al. 2020). Winds generally become more westerly in the later evening, from 2100 to 0000 PST (red dots in Fig. 2.7) compared to earlier where the easterly component is usually stronger (blue dots in Fig. 2.7). This pattern is most evident at RHC1, MTIC1, and SBVC1.

#### *2.4.5 Correlations between buoy and land stations*

The spatial and temporal variability in winds around Point Conception and in the Santa Barbara Channel are primarily controlled by a coastal jet. However, opposing winds associated with eddies may create a more complex three-layer system in some atmospheric conditions (Rahn et al. 2014). Typically, the SYM act as a barrier to the persistent northwesterly flow along the western California coastline, creating an expansion fan into the western SBC (Skylingstad et al. 2001; Dorman and Koracin 2008). In the presence of strong pressure gradients and a deep marine boundary layer, supercritical flow in the channel creates regions of wind acceleration and turning, or wind stress curl (Koracin et al. 2004). A shallow MBL creates subcritical flow, and the jet accelerates around Point Conception quickly decelerates further into the channel.

Using an 11-year climatology from the WRF model at 2 km spatial resolution, Smith et al. (2018a, b) postulated that Sundowners are in part caused by the inland propagation of the alongshore coastal California jet. That study indicated that the jet ranged between 600 and 1200 m above sea level in SYV during Sundowners, and was closer to the surface at locations further west. In the Sundowner regimes proposed in Jones et al. (2020), a strong

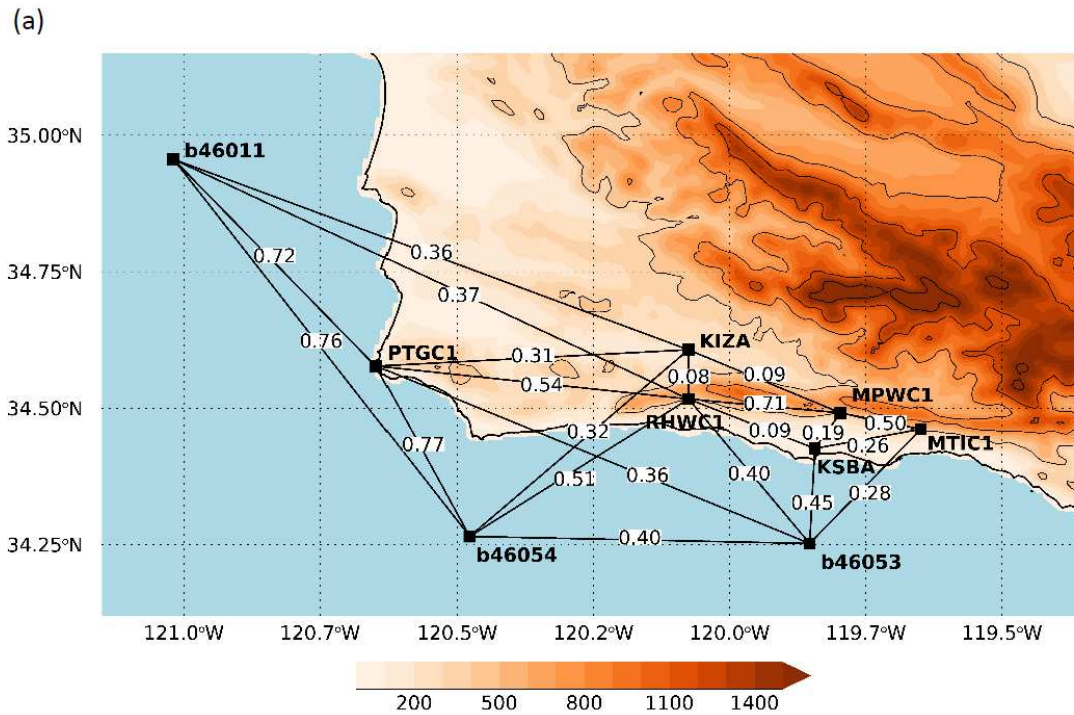
coastal jet (greater than 12 m/s) is present around Point Conception in the western regime, with northwesterly winds in the Santa Barbara Channel. However, during the eastern Sundowner regime, the coastal jet is weaker and does not extend into the Santa Barbara Channel.

To evaluate the relationship between observed winds during Sundowners and the coastal jet, we correlate winds at buoys and land stations. First, the seasonal and diurnal cycles of wind speed were calculated at the NDBC stations (Fig. A2.3a). The strongest winds occur around and just south of Point Conception at PTGC1 (Point Arguello, CA) and b46054 (west SB channel) with means maximizing around 8.5 m/s in late spring and early summer, consistent with Dorman and Winant (2000). Maximum median wind speeds at b46011 (offshore to the west) and b46053 (east SB channel) are recorded in mid-spring around 6.5 m/s and 5.5 m/s, respectively. The minimum mean wind speed at b46011 is 5 m/s in late summer, whereas at b46053, it reduces to 4 m/s in early winter.

Diurnally, maximum mean wind speeds at both PTGC1 (Point Arguello, CA) and b46054 (west SB channel) are around 8.5 m/s at 1900 PST, whereas b46053 (east SB channel) records maximum speeds (6 m/s) at 1700 PST, and b46011 (offshore, west) records maximum speeds (7 m/s) at 1600 PST (Fig. A2.3b). Minimum values are recorded between 0800 and 1000 PST at all stations, with mean wind speeds ranging between 3.5 m/s at b46053 to 6.5 m/s at PTGC1 and b46054.

To examine relationships between the coastal jet and surface winds at land stations, we correlated winds at RHWC1 and MTIC1 with all four NDBC stations. Data were subset to include only spring (season with the highest frequency of Sundowners) at 2000 PST. This time was chosen since it marks the typical onset of strong winds on the slopes of the SYM during spring according to models and observations (Jones et al. 2020; Carvalho et al. 2020).

Figure 2.8a shows linear correlations between NDBC stations and five land stations (RHWC1, MTIC1, MPWC1, KIZA, KSBA). Correlations between all of these stations are shown in Fig. 2.8b. No lag was applied in these figures. All data that had matching times between stations were used, and results were maintained if only days or hours with Sundowners (i.e. NWS Sundowner criteria was met at RHWC1 or MTIC1) were investigated (not shown).



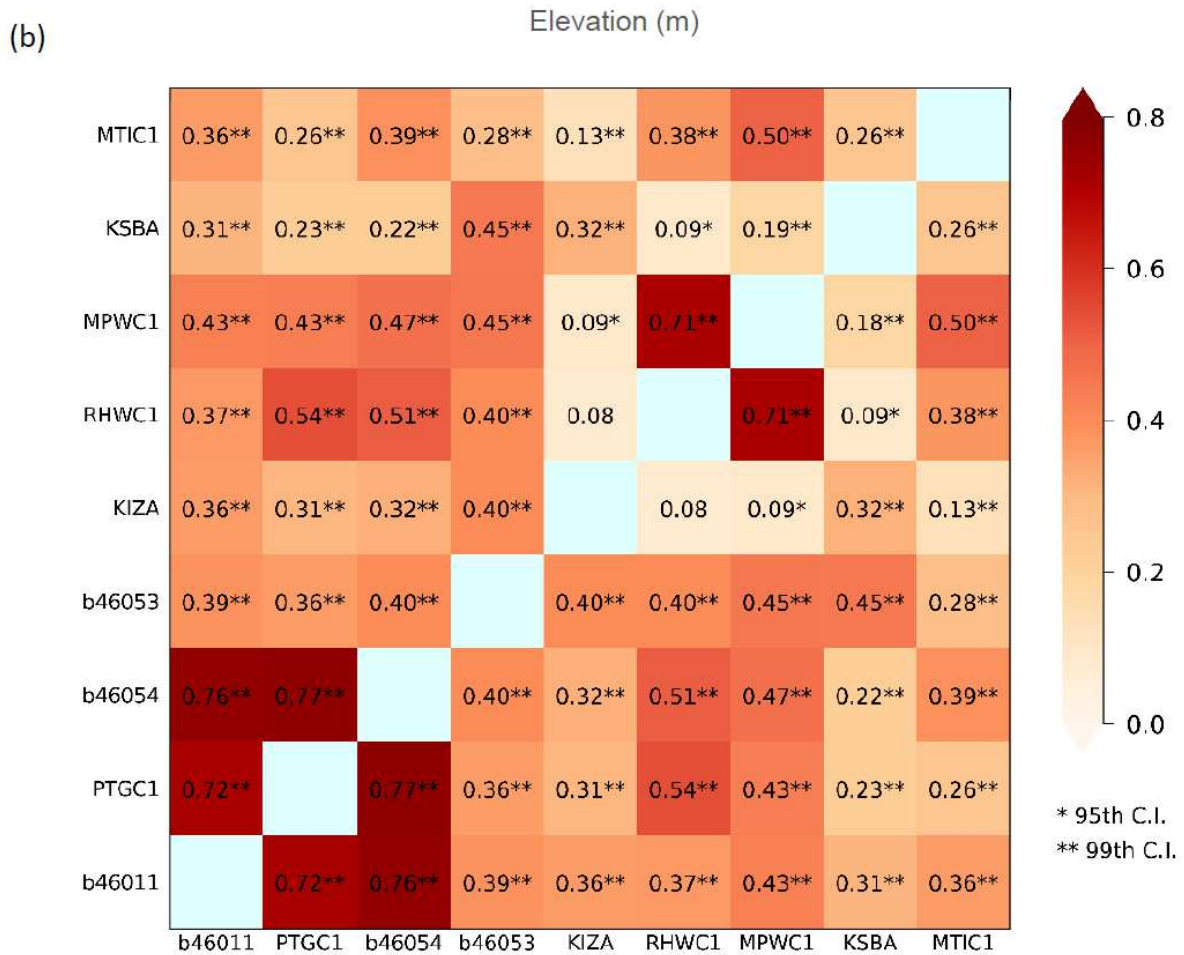


**Figure 2.8** - Correlations of wind speed in spring at 2000 PST. (a) Map of selected correlations between and amongst select land station and buoys. (b) Grid of all possible correlations, where values are repeated across the 1:1 axis. \* indicates significance at the 95<sup>th</sup> confidence interval, and \*\* indicates significance at the 99<sup>th</sup> confidence interval.

Correlations (R-values) calculated in this study are similar to the correlations of summer mean surface winds in Dorman and Winant (2000), which correlated wind speed along the wind direction principal axis in summer. Western buoys b46011, PTGC1, and b46054 are moderate-to-highly correlated amongst each other (0.72-0.77). The eastern buoy (b46053) is typically decoupled from other buoys, demonstrated by the lower correlations with western buoys (0.36-0.40). Instead, b46053 has slightly higher correlations with land

stations KSBA and MPWC1 (0.45 for both), due to the various regimes that commonly dominate wind flow in the SB Channel (Dorman and Winant 2000).

The coastal station (KSBA) has low correlations with all stations, ranging between 0.09 to 0.26 at other land stations analyzed and 0.22 to 0.45 at buoy stations. In particular, the correlations are very low between KSBA and RHWC1 (0.09) and KSBA and MTIC1 (0.26), and the correlation between RHWC1 and MTIC1 is low-to-moderate (0.38). While relatively far in distance compared to distance between other stations, RHWC1 and MPWC1 record a moderate-to-high wind speed correlation (0.70), which is likely related to strong winds recorded from the north-northwesterly wind direction at both stations. The valley station KIZA has the lowest correlations with RHWC1 and MPWC1, which can be explained by the influence of the up-valley circulation discussed before, which contrasts with the mechanisms driving winds at higher elevations on the mountain slopes.

Lag correlations were calculated using buoy data in the six hours prior to 2000 PST to determine whether strong winds at a buoy preceded strong winds recorded at RHWC1 and MTIC1 (Fig. A2.4). Correlations between buoys and the two land stations varied little with a lag applied (ranged less than 0.1). This indicates that there is no difference in phase observed at the surface between the peak of Sundowners and the intensification of winds in the Santa Barbara Channel or near Point Conception. Moreover, these findings show that there are moderate correlations between buoys and land stations RHWC1 (0.32-0.54) and MTIC1 (0.26-0.41), even when lags are applied (Fig. A2.4). This process was repeated using the six hours prior to 1800 and 2200 PST, and similar results were found.

Despite the close proximity, circulation off the coast near Point Conception and in the SYV differs from circulation south of the SYM. This analysis indicated that strong near-surface winds on the SYM are positively correlated (at the 5% significance level) with each

other and with buoy stations (Fig. 2.8). In the western SYM, correlations between RHWC1 and buoys b46054 and PTGC1 are 0.51 and 0.54, respectively, while the correlation between RHWC1 and MPWC1 is 0.71 (which indicates a much stronger linear relationship). In the central and eastern SYM, the correlation between MPWC1 and MTIC1 is 0.50. However, in some cases, the correlation is very weak (i.e. 0.09 between KSBA and RHWC1). Similar correlation analysis was performed for conditions classified as ‘Sundowners’ at RHWC1 (western SYM) and MTIC1 (eastern SYM) and results were very similar to those obtained for all days and conditions (not shown). While this observational analysis cannot provide complete evidence of the relationship between the coastal jet and Sundowners, this work highlights that even though these correlations are positive, they are not strongly linear ( $r^2$  less than 50%). This indicates the need for more observational and modeling studies investigating the complex interactions between the marine boundary layer, the coastal jet, the lee-slope jet, and local circulations to explain the spatial variability of winds in this region.

#### *2.4.6 Seasonal cycles, diurnal cycles, and Sundowner winds observed at the NOAA wind profiler*

To understand local wind flow in the boundary layer, we investigated winds from the vertical wind profiler at the Santa Barbara airport from the surface to 2600 m. Days with the strongest winds within the boundary layer (typically less than 1000 m AGL) and above are generally in winter and the weakest winds are in summer (Fig. A2.5a). Patterns of wind direction vary diurnally and throughout the year at lower elevations, possibly linked to the diurnal circulations and the behavior of the marine boundary layer as explained next.

Diurnally, close to the surface, wind speeds and wind directions are similar to the land-based KSBA station (Fig. A2.5b). Nonetheless, the profiler shows some interesting

aspects of the diurnal cycle within the boundary layer. For instance, on average, there is a transition between the nighttime easterlies and daytime westerlies in the mid-morning (between 0800 and 1000 PST) within the lowest 600 m AGL. The transition is characterized by the weakest winds (less than 2 m/s). At 12 PST, winds strengthen and become southwesterly-to-westerly until 20 PST, when they transition back to easterlies. Above the boundary layer, winds rapidly accelerate. Another observation is that the mean wind direction at and above 1200 m AGL is commonly from the northwest for most of the day, intensifying and turning into a northerly direction at approximately above 500 m AGL (possibly indicating the top of the boundary layer, consistent with modeling studies – e.g. Duine et al. 2019, 2021). This occurs around sunset, indicating the formation of a low-level (super-geostrophic) nocturnal jet that lasts only a few hours (Stull 2000).

Of particular interest are the wind profiles on days with Sundowners. Figure 2.9 shows the profiler composite of wind speed and direction on days that did and did not record at least 1 hour reaching the NWS-LOX Sundowner criteria (see Section 2.4.4) between 18 and 06 PST at MTIC1 (a-c) and RHWC1 (d-f). All seasons were used. In the difference plots (c, e), only vectors that are statistically significant at the 95<sup>th</sup> confidence interval are plotted.



### KSBA Wind Profiler - Composite Wind Speeds

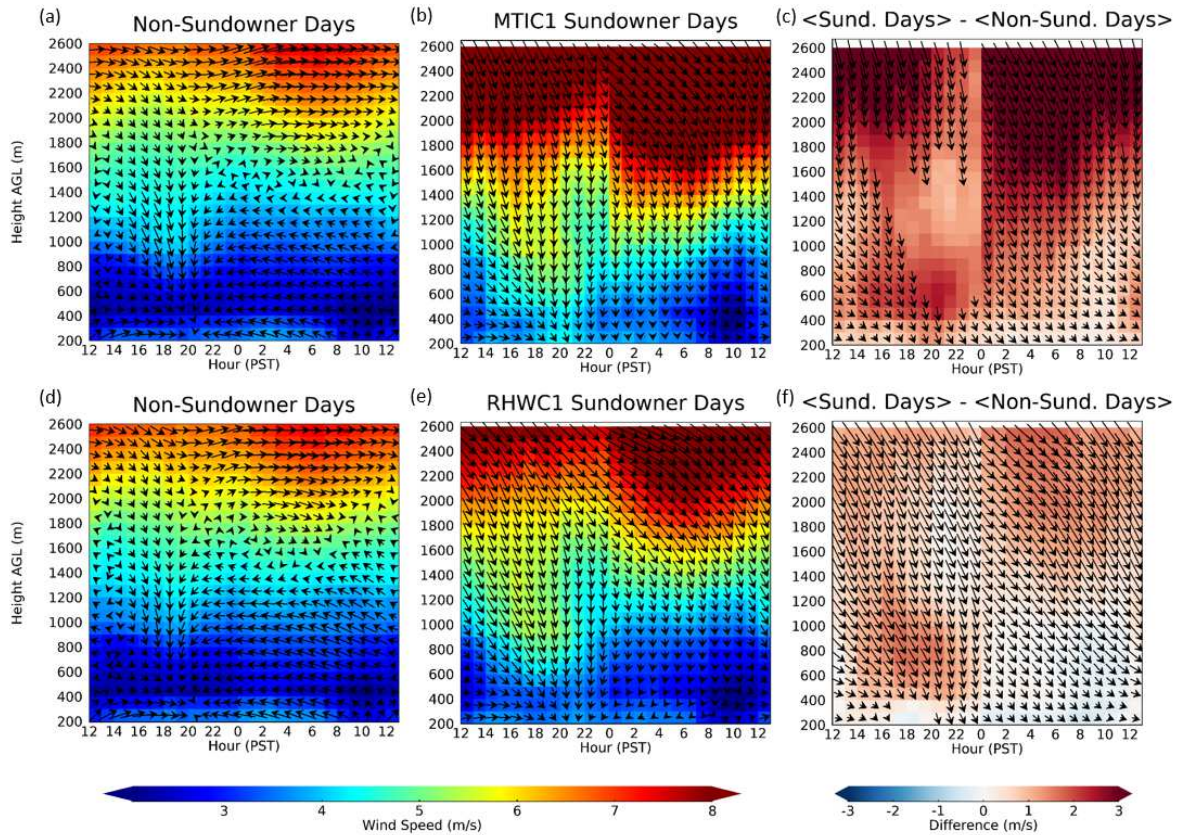


**Figure 2.9** – Wind speed and direction composites at the Santa Barbara Airport vertical profiler for days when the NWX-LOX Sundowner criteria between 18 to 06 PST (a) were not reached for at least 1 hour at MTIC1 and (b) were reached for at least one hour at MTIC1. (c) shows the difference between (a) and (b). Plots (d), ©, and (f) are the same as (a), (b), and (c) but at RHCW1. The u and v wind components were averaged to calculate composite wind directions in (a), (b), (d), and ©. The vectors were calculated for (c) and (f) by subtracting the u and v components for the Sundowner day composites (b, e) from the non-Sundowner composites (a, d). Only statistically significant vectors (determined by the Student’s t-test) are plotted.

During Sundowners recorded at MTIC1, wind speeds are up to 2 m/s stronger than non-Sundowner days from 14 to 22 PST typically between from 400 m to 800 m AGL. The peak of these winds occurs around 20 PST, which is consistent with the observed characteristics of Sundowners. This peak in winds is linked to the intensification of winds associated with the lee-slope jet around sunset (Fig. 2.9b). Notice that during this period,

winds tend to change from NW during the day to NNW around sunset. Up to 200 m AGL, winds are weaker during the day, intensifying around 20 PST and weakening late in the evening. Nonetheless, strong northerly winds are observed above 1600 m AGL (Figs. 2.9b,c), indicating the importance of synoptic forcing generating cross-mountain winds as a precursor of Sundowners (Cannon et al. 2017; Carvalho et al. 2020; Duine et al. 2021).

Relatively smaller differences are observed for wind profiler composites on Sundowner days at RHWC1 (Fig. 2.9f); Wind speed between 500 m to 1500 m is 1-2 m/s stronger than normal from 17 to 21 PST, and in the early morning hours, while below 400 m AGL there are less systematic changes in circulation. This is likely related due to the fact that even during Sundowners, a strong stably stratified marine boundary layer may maintain the lee-slope jet above 200 m AGL as indicated in simulations in Carvalho et al. (2020) and Duine et al. (2021). In the upper levels, winds above 1500 m are up to 2 m/s stronger with a stronger northwesterly component particularly from 0200 to 1200 PST. This may allude to the importance of upper-level dynamics producing Sundowners during the western regime (winds exhibit typically a NW direction), discussed in Jones et al. (2020) and Hatchett et al. (2018). Overall, analysis of data collected at the wind profiler demonstrates that both wind speed and direction differences are present when extreme, northerly winds are recorded at land-based stations. Mechanisms explaining the intensification of the jet have been investigated with radiosondes in Carvalho et al. (2020) and have been related to mountain wave activity and hydraulic jumps.

## 2.5 Variability in temperature and dew point during extreme winds

In Section 2.4, we highlighted the spatiotemporal variability of winds in coastal SB. Given the complex circulations in the SYV, SYM, and over the SB channel evident through the wind analysis, it is necessary to examine other meteorological variables such as temperature, relative humidity, and dew point to better understand atmospheric processes in this region. The seasonal and diurnal cycles for temperature, relative humidity, and dew point are shown in Fig. A2.6. The seasonal and diurnal cycles for these variables will not be discussed. The remainder of this section is devoted to evaluating the behavior of these variables during Sundowners.

### 2.5.1 Temperature

While some studies have suggested that a temperature increase is one of the main characteristics during Sundowner events (Hatchett et al. 2018; Smith et al. 2018a), other studies have shown no evidence of a systematic signature in temperature ramps everywhere in the domain (Blier 1998; Carvalho et al. 2020). Additionally, the spatiotemporal variability in temperature during Sundowners has not yet been examined based solely on observations. Figure 2.10 shows the diurnal median temperatures and the interquartile range (shaded) by season when NWS-LOX Sundowner criteria was not reached. Boxplots indicate the median, interquartile range, and minimum and maximum temperatures observed during hours reaching Sundowner criteria. All boxplots shown have medians that are statistically significantly different than temperature medians under non-Sundowner conditions. Hours without boxplots either had too few hours that reached Sundowner criteria (less than 10 instances) or the difference between median temperatures were not statistically significant.

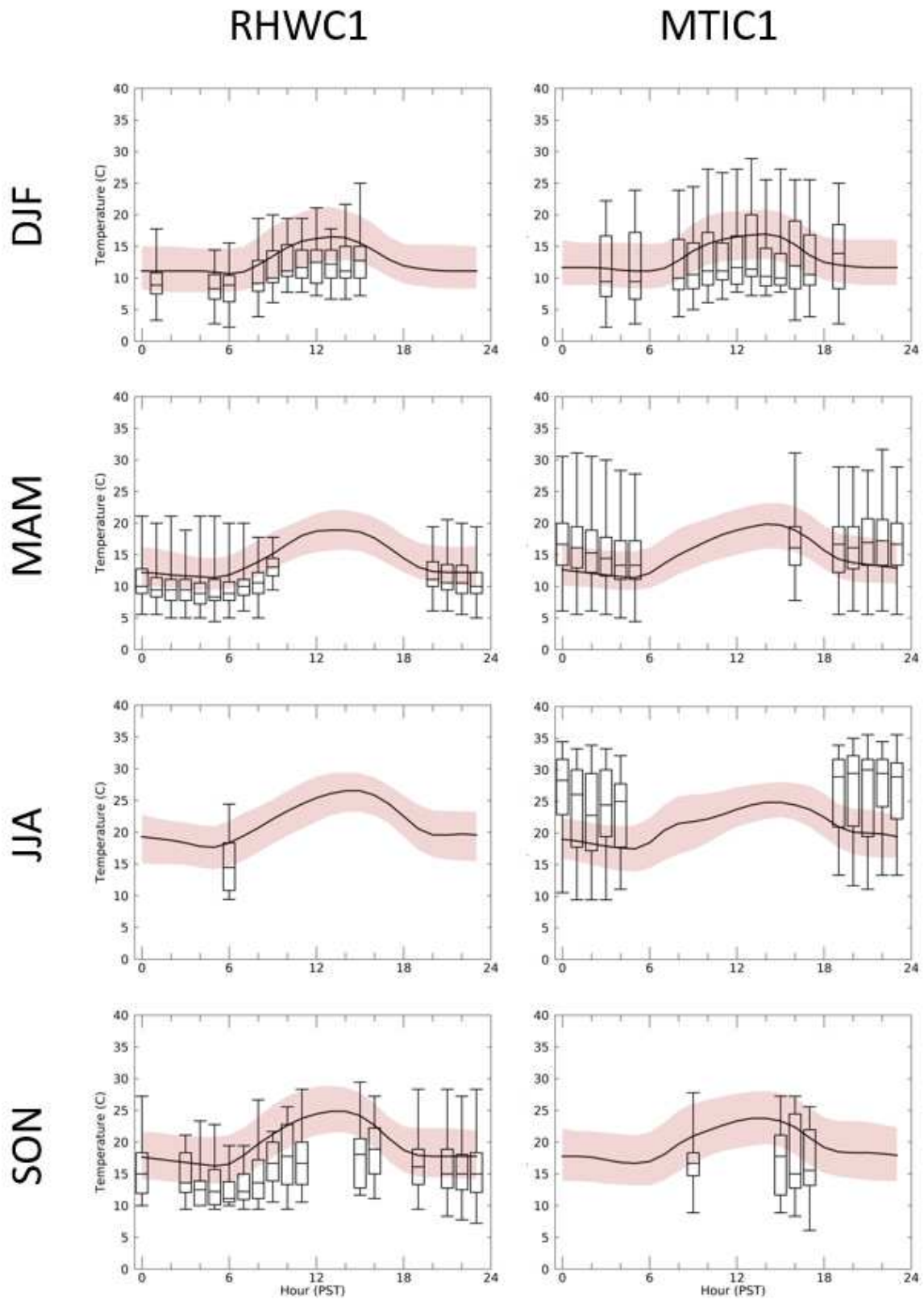


**Figure 2.10** – Diurnal cycles of median temperatures (thick black lines) and the interquartile range (red shading; 25<sup>th</sup> to 75<sup>th</sup> percentiles) of temperatures during non-Sundowner winds. Boxplots show the median, interquartile range, and minimum and maximum temperatures during Sundowner winds at MTIC1 (right) and RHWC1 (left) subset by season. The boxplots shown are statistically significant at the 95<sup>th</sup> confidence interval (when compared to the median temperature for that hour using all available data). See Section 2.2 for an explanation of the significance testing method.

At MTIC1 (east SYM), temperatures during strong winds vary depending on season and time of day (Fig. 2.10, right column). In fall and winter, temperatures during strong, northerly (typically NE) winds are, on average, cooler than the seasonal median. It is possible that these dates are typically occurring in association with frontal systems. In contrast, temperatures during extreme winds in spring and summer are warmer than the seasonal normal, and the hours with statistically significant differences are in the evening and early morning. This warming is from mountain wave processes and adiabatic compression related to Sundowners (Blier 1998; Cannon et al. 2017; Hatchett et al. 2018; Smith et al. 2018a; Carvalho et al. 2020).

At RHWC1, temperatures during extreme winds are frequently cooler than normal regardless of hour or season (Fig. 2.10, left column), although the hours that have statistically significant differences in the median between temperatures during Sundowners and without Sundowners vary between seasons; the lower temperatures during Sundowners in the morning and early afternoon are statistically significant in winter, whereas in spring the cooling is more evident in the evening and morning hours. This may also reflect the fewer cases during the other times. In summer, statistical significance is observed only at 06 PST, whereas lower temperatures seem to dominate throughout the day in fall. The lower temperatures during strong northerly winds at RHWC1 can be explained by the advection of

cool oceanic air (from the Pacific Ocean) by the northwesterly winds, possibly in association with the intensification of the coastal jet, as exemplified in simulations of back-trajectories in Duine et al. (2021). Furthermore, this station is close to the ridgeline (Fig. 2.1c,A2.1a,b) that partly diminishes the effect of adiabatic compression on temperatures (Carvalho et al. 2020).

### *2.5.2 Dew Point Temperature*

Similar to Figure 2.10, Figure 2.11 shows the diurnal median Td with the interquartile range during non-Sundowner conditions and boxplots for hours with statistically significant differences in the median Td during Sundowners. At MTIC1, the hours with statistically significant differences in the median vary between seasons, but commonly occur in the evening and/or morning. In spring, almost all hours (except 12 PST) have significant differences. During Sundowners, the median Td is typically lower than non-Sundowner conditions. This may be explained by the transport of dry air from levels above the mountain top to lower elevations, as indicated in the case study discussed in Carvalho et al. (2020) and shown through back trajectories in Duine et al. (2021). This is also suggested with results from the wind profiler (Fig. 2.9).



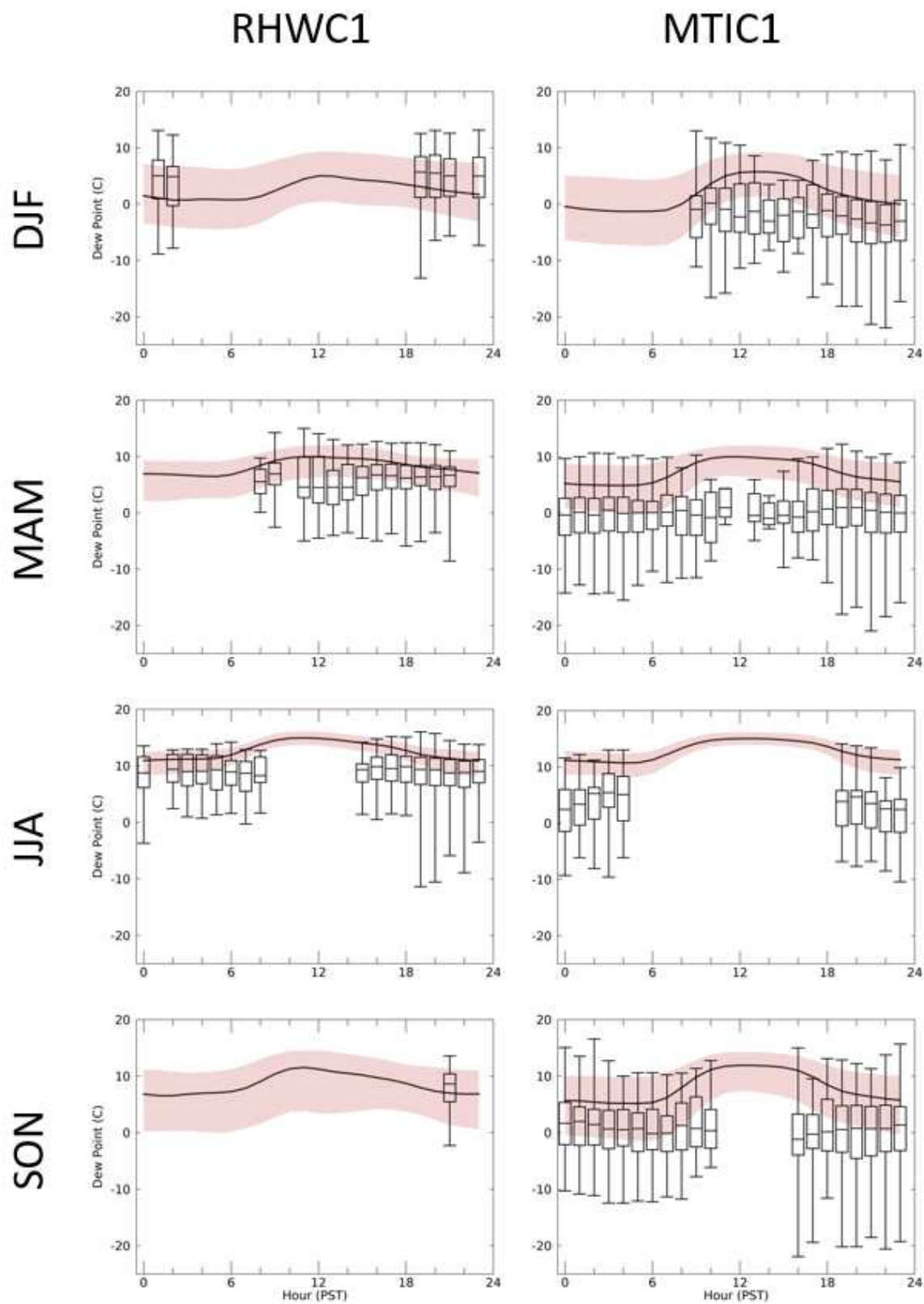


Figure 2.11 - Similar to Figure 2.10 using dew point.

At RHC1, the median Td during Sundowners is higher than average in the evening and early morning in fall and winter (Fig. 2.11). This is possibly from the influence of moist oceanic air advected by the northwesterly winds as discussed before. In spring, the Td during strong northerly winds decrease relative to the non-Sundowner Td in the afternoon and evening. During summer, when the lower troposphere is warmer and drier, lower Td values are frequently observed in the evening and morning during strong Sundowners. It is important to note that fewer events have been observed at RHC1 compared to MTIC1 due solely to differences in record length: approximately 4 years of data was examined at RHC1 whereas nearly 20 years of data was examined at MTIC1 (Table 2.1).

The spatiotemporal variability of temperature and Td during strong, northerly winds illustrates the complexity of meteorological processes in this region. Nonetheless, the influence of strong cross-mountain (northerly) winds on Td (and thus, specific humidity) is quite evident and relevant, and may be a dominant factor in the low relative humidity often observed during these events. Additional studies are necessary to determine the relative contributions of mountain waves in increasing adiabatic warming and subsequent drying, as well as horizontal advection. Evaluating patterns of temperature and Td during extreme cross-mountain winds has important implications in forecasting fire weather and improving wildfire preparedness.

## **2.6 Spatiotemporal variability of the Fosberg Fire Weather Index**

Due to the large influence of wind speed on FFWI calculations, the seasonal cycle of the FFWI (Fig. A2.6d) is unsurprisingly similar to wind speed (Fig. 2.2), although the



bimodal pattern is more pronounced with FFWI than wind speed. This is because maximum mean wind speeds are recorded in spring, but temperatures are higher in fall, increasing FFWI values for these two seasons. FFWI values peak at all stations except LPOC1 in spring, averaging between 16 to 20 at mountain stations and between 3 to 10 at non-mountain stations. Similar values are recorded in fall, separated by relative minima in summer at most stations. On a diurnal timescale, the FFWI cycle (Fig. A2.6h) resembles the wind speed cycle (Fig. 2.4); non-mountain stations record maximum FFWI values (between 5 and 24) in the early afternoon, whereas mountain stations record maximum values (between 12 and 26) in the evening. Seasonal variations in the diurnal cycles of FFWI were examined (not shown), and found that the timing of the minimum and maximum FFWI values is consistent in all seasons. The smallest (largest) values of FFWI were observed in winter (summer) due to a combination of colder (warmer) weather and wetter (drier) conditions.

To examine the frequency of significant fire weather ( $\text{FFWI} > 50$ ) at each station, we calculated percentiles of FFWI values (Fig. 2.12). Overall, the strong winds at mountain stations result in the highest FFWI percentile values; RHWC1 reaches the significant FFWI threshold in all seasons, MTIC1 reaches the threshold in all seasons except for summer, and MPWC1 reaches the threshold in summer. In winter, a combination of relatively low temperatures, higher precipitation, and weaker winds result in lower percentiles at nearly all stations. In spring, strong winds at MTIC1 greatly increase FFWI, and values above the 95th percentile are higher at MTIC1 than RHWC1; these values exceed 50, which is considered critical fire weather. In summer, high temperatures and reduced precipitation create higher percentile values, especially at RHWC1 which reaches the significant FFWI 50 threshold at the 90th percentile. Additionally, KIZA records percentile values comparable with those

found at mountain stations because of the similar wind speeds in summer (Fig. 2.2). In fall, the percentiles are similar to winter due to decreasing temperatures and the beginning of the rainy season. It is important to note that all stations have recorded at least one hour with significant fire weather (Fig. A2.7).

## **2.7 Discussion and Conclusions**

Coastal Santa Barbara experiences extreme weather phenomena including strong, downslope wind events called Sundowners and significant fire weather conditions. This observational analysis characterized the spatiotemporal variability of winds in this region. Although the relatively low density of weather stations in coastal SB is not enough to fully explain Sundowner characteristics and mechanisms, an examination of data recorded at stations can complement previous studies that used high-resolution atmospheric models to examine winds, temperatures, and moisture in this region, and specifically Sundowner events. Our observational examination of yearly and diurnal cycles of wind indicates that, from a climatological perspective, the maximum speeds are observed in spring. Diurnally, the timing of maximum wind speed varies between mountain and non-mountain stations; winds at mountain stations peak in the evening (2000 to 2200 PST), whereas winds at non-mountain stations peak in the afternoon (1300 to 1400 PST). These results are consistent with previous model-based studies including Jones et al. (2020) and Hatchett et al. (2018).

Smith et al. (2018a) evaluated an 11-year climatology using WRF with 2-km grid cell resolution and created a ‘Sundowner Index’ using the northerly wind component and temperatures differences between each grid cell and a peak (La Cumbre Peak) on the SYM ridgeline. Jones et al. (2020) examined 30 years of WRF at 1-km grid cell resolution and

used combined empirical orthogonal function analysis to identify three Sundowner regimes: Eastern, Western, and Santa Barbara. In contrast, Smith et al. (2018a) argues that there is a continuum of Sundowners determined by wind direction at the SYM ridgeline rather than separate types. Furthermore, these simulations and observational analyses agree that a lee-slope jet forms on the southern SYM slopes during Sundowners, creating maximum wind speeds on the mountain slopes rather than near the ridgeline (Smith et al. 2018a; Carvalho et al. 2020; Duine et al. 2021; Jones et al. 2020).

Similarly, we found that mountain stations consistently record the strongest winds out of all stations, and the frequency of Sundowners (defined using the NWS-LOX criteria) varies greatly among stations (Table 2.2). This finding is consistent with Blier (1998) and Smith et al. (2018a) who state that stations far from the mountains such as KSBA do not record all Sundowner events due to the limited downstream extent of Sundowners and the influence of the marine boundary layer. During strong, cross-mountain (northerly) winds, variability in wind direction is evident; RHCW1 (west SYM) and MPWC1 (central SYM) record primarily northwesterly winds, and MTIC1 (east SYM) records northeasterly winds (Figs. 2.5,2.7,2.9). Using 4 years of hourly wind data from the NOAA wind profiler, we showed differences existing in winds within the marine boundary layer and aloft. The profiler characterized the nocturnal jet and showed differences in wind speed and direction when the NWS-LOX Sundowner criteria was reached at RHCW1 (western SYM) and MTIC1 (eastern SYM) (Fig. 2.9). These results reinforce the idea of eastern and western Sundowner regimes proposed in Jones et al. (2020). Moreover, weak-to-moderate wind speed correlations between RHCW1 and MTIC1 (0.38), and MPWC1 and MTIC1 (0.50) (Fig. 2.8), indicate linear relationships between strong winds on the eastern, central, and western SYM slopes are often not observed. The relationship between Sundowners and the

coastal jet is noted in Smith et al. (2018a) and Jones et al. (2020) during the ‘western regime’ only. In our study, correlations among and between land and buoy stations indicates that strong winds offshore are moderately correlated with western station RHCW1 and central station MPWC1, with correlations ranging between 0.37-0.54 and 0.43-0.47 respectively. However, there is no evidence of phase differences between the peaks of winds over land and in the Santa Barbara Channel based on lag-correlations between buoys and land stations MTIC1 and RHCW1, which may be expected in case of an eastward progression of winds as postulated in Smith et al. (2018a).

Temperature,  $T_d$ , and the FFWI were additionally examined. During Sundowner winds, temperature variability may respond to a combination of effects, including temperature advection from upstream sources (Blair 1998; Carvalho et al. 2020; Duine et al. 2021) and subsidence related to mountain wave development and the transport of air from above the mountain top (Carvalho et al. 2020; Jones et al. 2020; Blair 1998). Additionally, warming was found in some, but not all, Sundowner case studies examined using observations and/or models (Ryan 1996; Blair 1998; Cannon et al. 2017; Hatchett et al. 2018; Carvalho et al. 2020). During strong northerly winds in spring and summer, MTIC1 (west SYM) records temperature increases and dew point decreases in the evening and early morning hours (Figs. 2.10,2.11), potentially from adiabatic warming and/or upstream influences (Duine et al. 2021). In contrast, RHCW1 records cooler temperatures and lower dew points during extreme winds, which may be from an oceanic influence. Similar to methods employed in Duine et al (2021) and Carvalho et al. (2020), future work using back trajectory analysis could assist in determining the sources of air parcels, and may relate to or explain patterns observed in temperature and dew point during Sundowners.

Due to the large dependence on wind speed in the calculation, the seasonal and diurnal cycles of the FFWI are similar to wind speed; maximum values are typically recorded in spring and fall, and in the evening at mountain stations. Mountain stations record the highest frequency of critical fire weather conditions, although all stations have recorded significant fire weather. Some caveats are present when utilizing and interpreting this fire index. While temperatures are highest during summer and fuels are drier than winter and spring, relatively weaker winds decrease the FFWI values as a result of the large dependence on the index's reliance on wind speed. Additionally, it's important to note that the FFWI does not account for long-term trends in variables such as precipitation on seasonal and yearly scales (i.e. drought, excessive rainfall) and the respective role in fuel moisture, which are important factors concerning wildfire risk. Future work may be completed to create an operational product that incorporates the climatology of fire weather conditions with real-time data and fuel data to identify regions of high wildfire risk.

While the observational data investigated in this study have inherent caveats, including differences in station placement (i.e. ridge, valley) and different record lengths among stations, they provide valuable insight into actual surface conditions and allow for comparisons with Sundowner research that utilize atmospheric models. The addition of stations on the SYM ridgeline, in the Santa Ynez Valley, or in the San Rafael Mountains could benefit future studies, as collecting data from upstream sources may improve our understanding of conditions leading to Sundowners and extreme fire weather. Advancing knowledge on the variability and predictability of extreme winds and fire weather conditions with climatological studies can improve resource allocation (including the placement of new weather stations and other technical resources), and may contribute to wildfire mitigation, ultimately increasing resilience of the local community toward wildfires.

## 2.8 Acknowledgements

This work was funded by the NSF-PREEVENTS ICER -1664173. The authors acknowledge and appreciate collaborations with the National Weather Service - Los Angeles/ Oxnard Office. We appreciate the suggestions made by the anonymous reviewers. This work was made possible by the agencies participating in the MesoWest data network ([mesowest.utah.edu](http://mesowest.utah.edu)). Data for the wind profiler were provided by the NOAA/OAR/ESRL/PSL, Boulder Colorado, USA from their Web site at <http://psl.noaa.gov/>.

## 2.9 Appendix

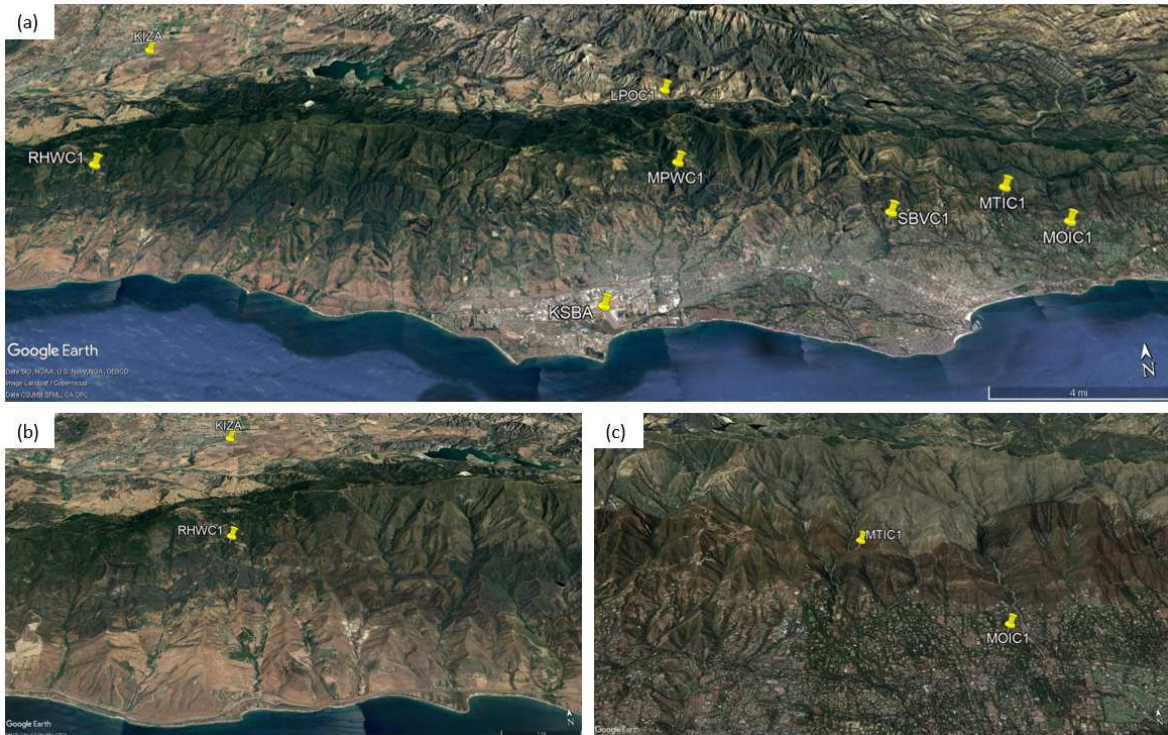


**Figure A2.1** - Images from Google Earth showing stations in relation to topography and urban areas. All stations are shown in (a), (b) focuses on the western SYM and the SYV plain, and (c) shows the eastern SYM, along with highly populated areas.

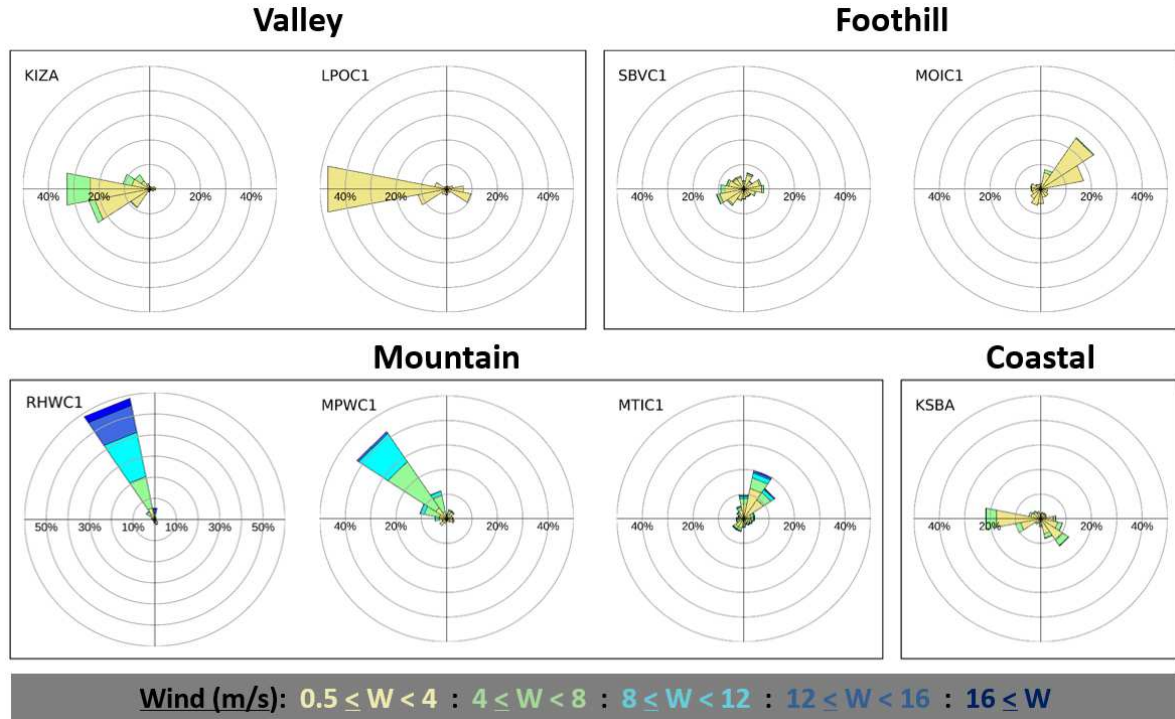


**Figure A2.2** - Similar to Figure 2.4 using data between 1800 and 2000 PST. Notice the axes on RHWC1 extend to 60% to capture the high frequency of NNW winds, while all other wind roses extend to 50%.

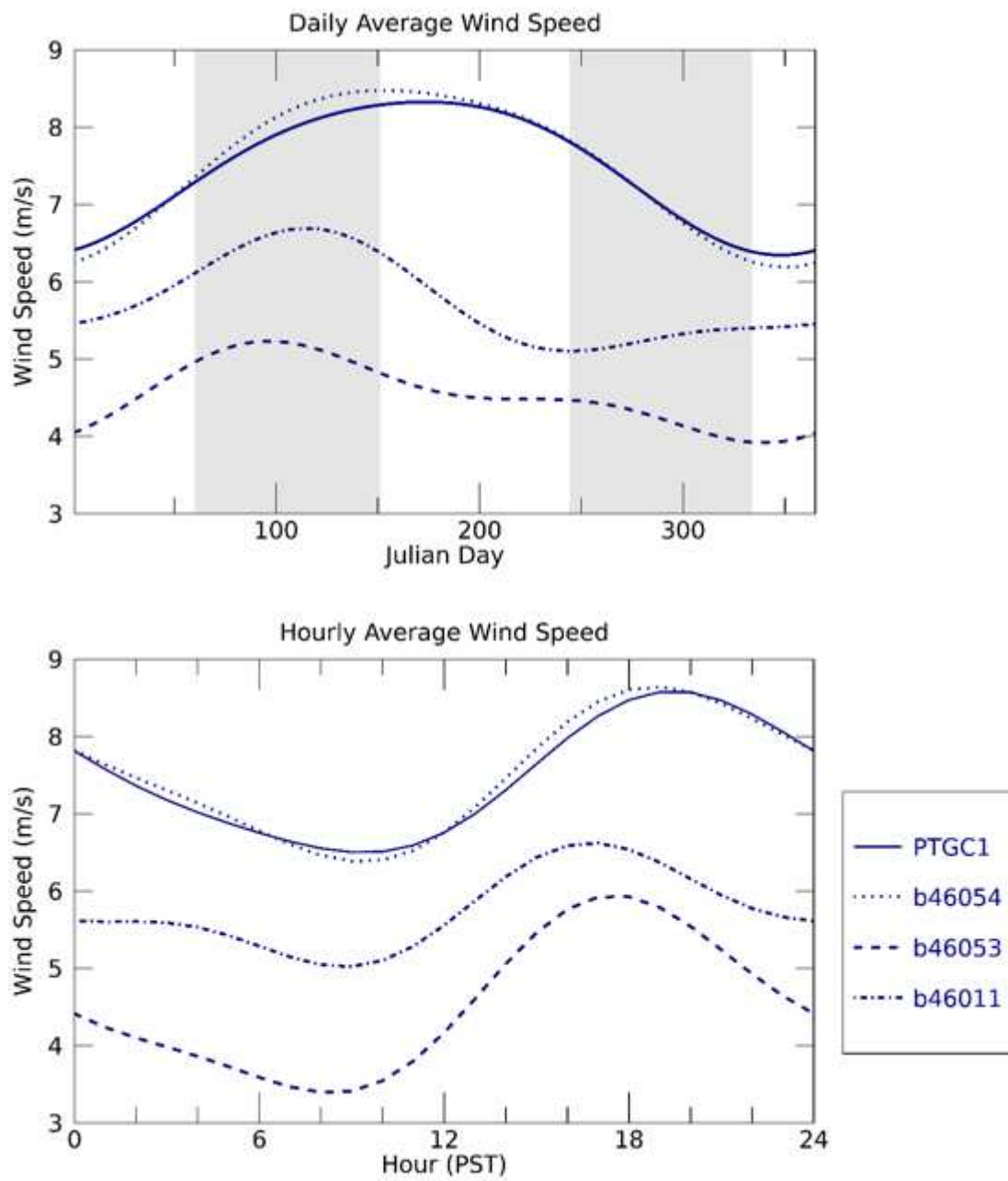


**Figure A2.3** - Seasonal and diurnal cycles of wind speed for buoy stations. Grey shading indicates spring and fall.



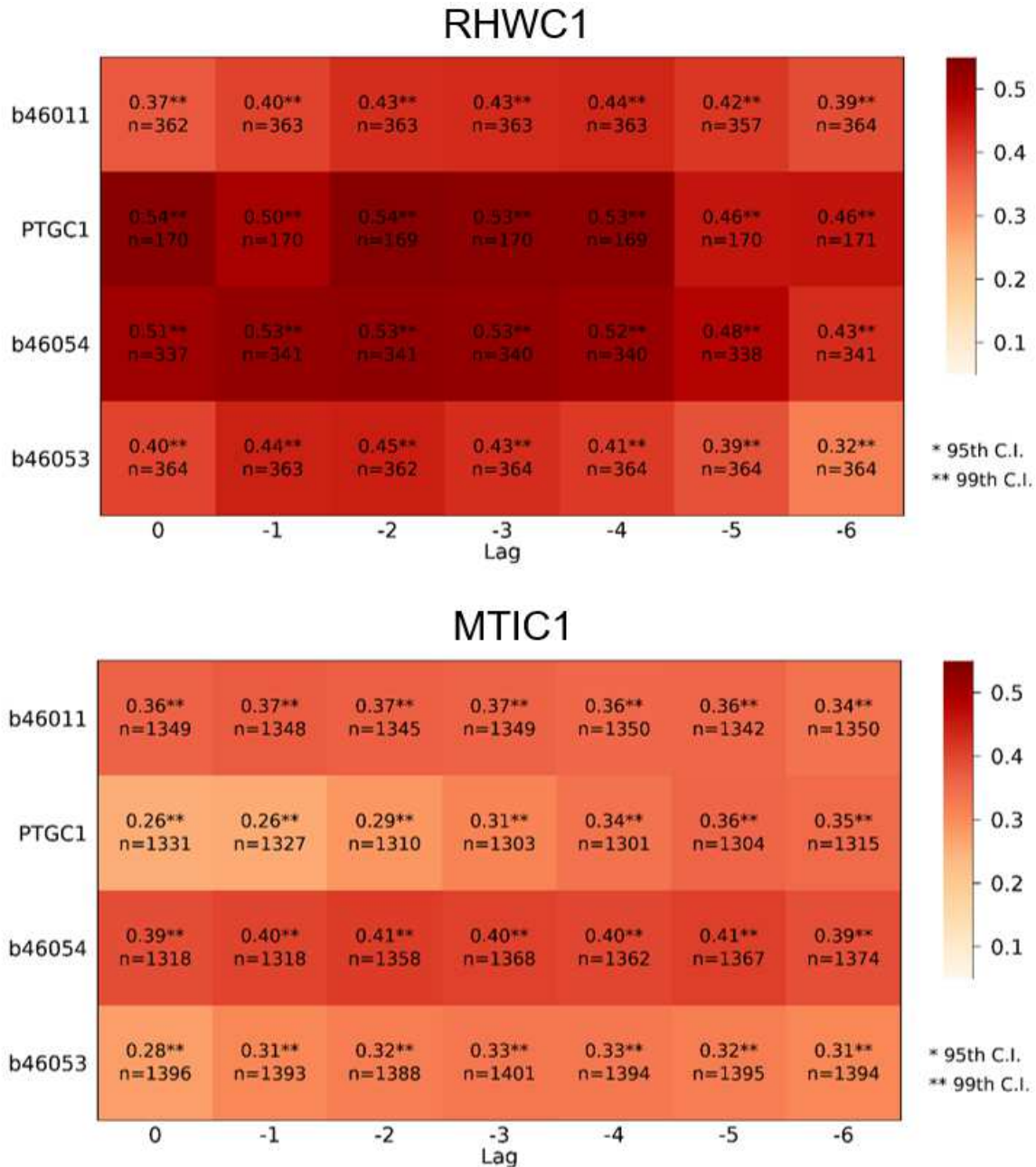


**Figure A2.4** - Correlations and the number of observations for wind speed lags in spring at 2000 PST (at land stations) at RHWC1 (top) and MTIC1 (bottom). The lag is the wind speed in the 6 hours prior to 2000 PST at buoys. \* indicates significance at the 95th confidence interval, and \*\* indicates significance at the 99th confidence interval. Due to a large number of observations, statistical significance was determined using Monte Carlo resampling.

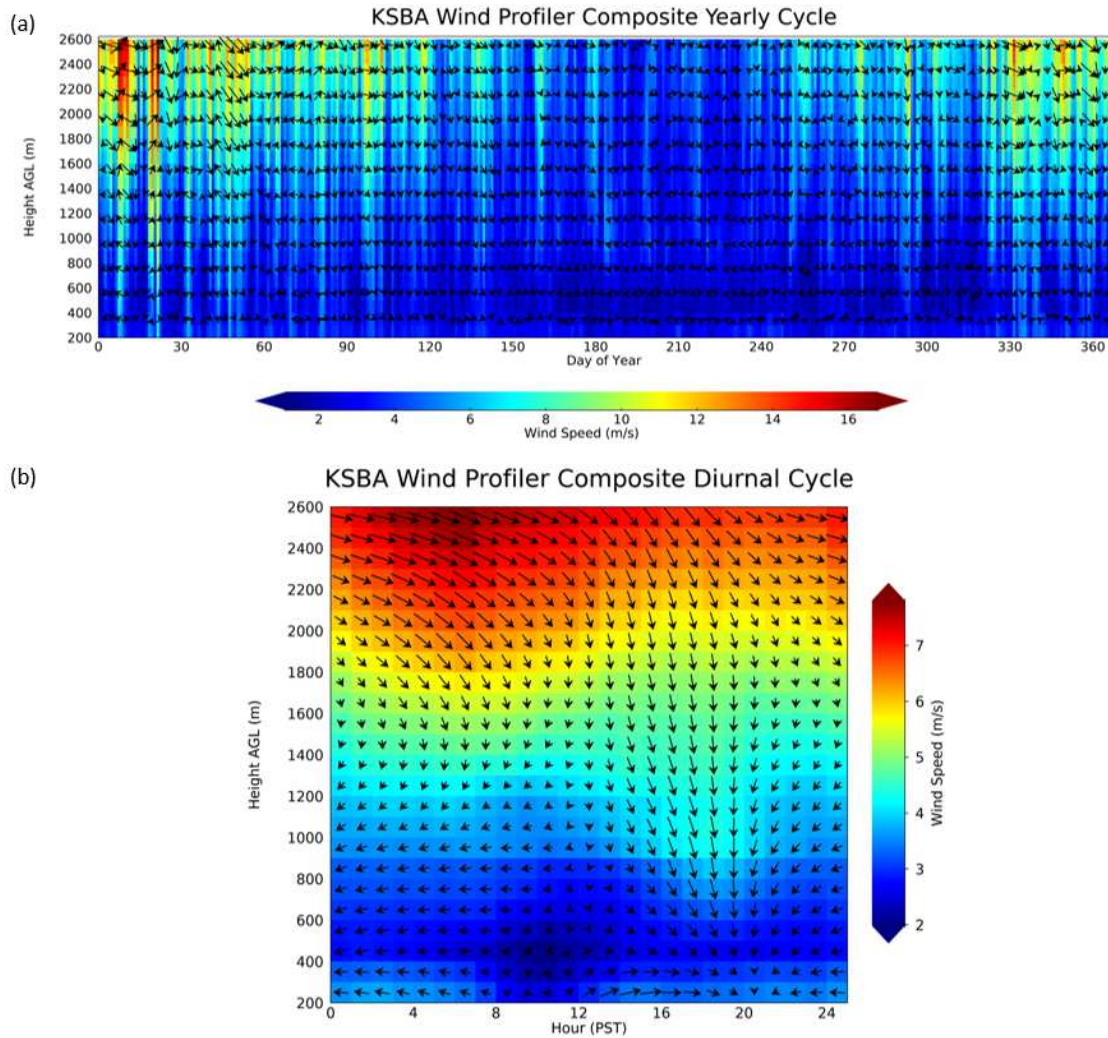


**Figure A2.5** - Yearly (a) and diurnal (b) cycles of wind speed and direction (calculated using the u and v wind components) at the Santa Barbara airport vertical wind profiler.

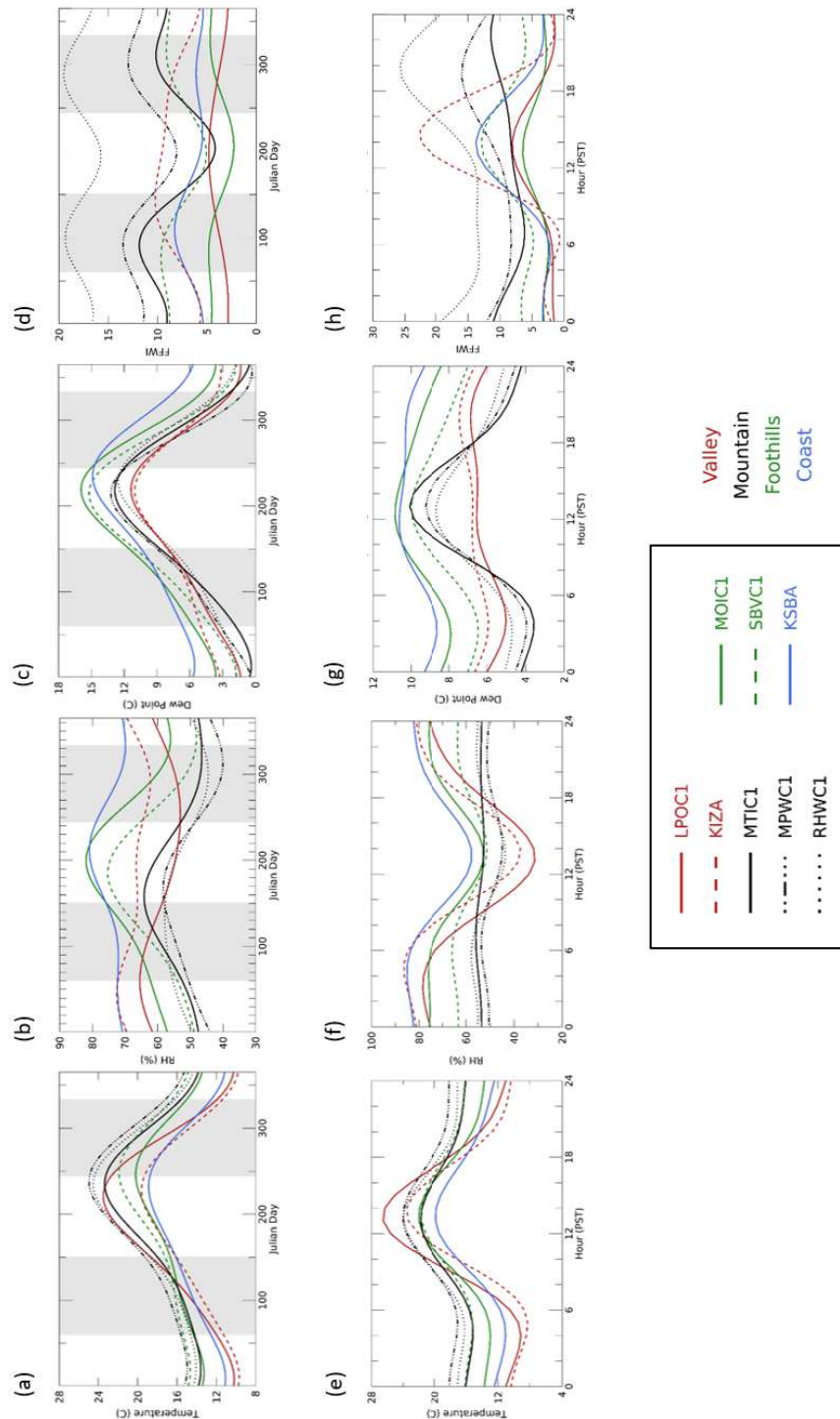


**Figure A2.6** - Seasonal and diurnal cycles of temperature (a, e), relative humidity (b, f), dew point temperature (c, g), and Fosberg Fire Weather Index values (d, h). Diurnal cycles were calculated using all seasons. Grey shading indicates spring and fall.

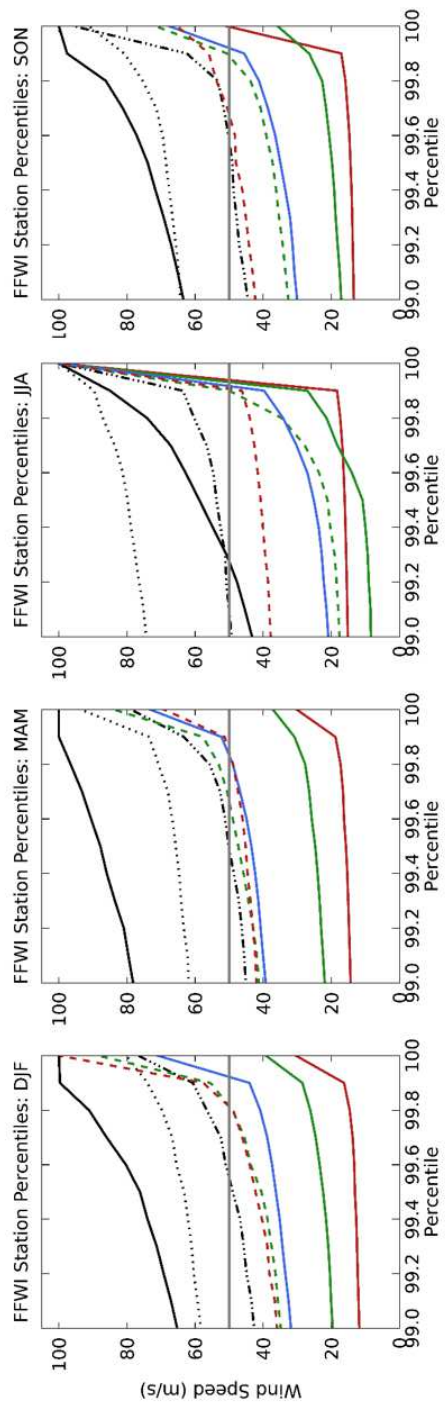


**Figure A2.7** - FFWI percentiles from the 99th to 100th percentiles during each season. The maximum value is recorded as the value at the 100th percentile. The horizontal gray line indicates the threshold for significant fire weather conditions (FFWI > 50).

## 2.10 References

- Bastin, S., Drobinski, P., Dabas, A., Delville, P., Reitebuch, O., and Werner, C. (2005) Impact of the Rhône and Durance valleys on sea-breeze circulation in the Marseille area. *Atmospheric research*, 74, 303-328. Doi: 10.1016/j.atmosres.2004.04.014.
- Blier, W. (1998) The sundowner winds of Santa Barbara, California. *Weather and Forecasting*, 13, 702-716. Doi: 10.1175/1520-0434(1998)013<0702:TSWOSB>2.0.CO;2.
- Cannon, F., Carvalho, L., Jones, C., Hall, T., Gomberg, D., Dumas, J., and Jackson, M. (2017) WRF Simulation of Downslope Wind Events in Coastal Santa Barbara County. *Atmospheric Research*, 191, 57–73. Doi: 10.1016/j.atmosres.2017.03.010.
- Carvalho, L., Duine, G.J., Jones, C., Zigner, K., Clements, C., Kane, H., Gore, G., Bell, G., Gamelin, B., Gomberg, D., Hall, T., Johnson, M., Dumas, J., Boldt, E., Hazard, R., and Enos, W. (2020) The Sundowner Winds Experiment (SWEX) Pilot Study: Understanding Downslope Windstorms in the Santa Ynez Mountains, Santa Barbara, CA. *Monthly Weather Review*, 148, 1519-1539. Doi: 10.1175/MWR-D-19-0207.1.
- Countryman, C.M. (1972) *The Fire Environment Concept*. USDA Forest Service: Berkeley, CA, USA, 15.
- De Wekker, S.F., Zhong, S., Fast, J.D. and Whiteman, C.D. (1998) A numerical study of the thermally driven plain-to-basin wind over idealized basin topographies. *J. Applied Meteorology*, 37, 606-622. Doi: 10.1175/1520-0450(1998)037<0606:ANSOTT>2.0.CO;2.
- DiGiacomo, P.M. and Holt, B. (2001) Satellite observations of small coastal ocean eddies in the Southern California Bight. *J. Geophysical Research: Oceans*, 106, 22521-22543. Doi: 10.1029/2000JC000728.

- Dorman, C.E. and Winant C.D. (2000) The structure and variability of the marine atmosphere around the Santa Barbara Channel. *Monthly Weather Review*, 128, 261-282. Doi: 10.1175/1520-0493(2000)128<0261:TSAVOT>2.0.CO;2.
- Dorman, C.E., and Koračin, D. (2008). Response of the summer marine layer flow to an extreme California coastal bend. *Monthly weather review*, 136(8), 2894-2922. Doi: 10.1175/2007MWR2336.1.
- Duine, G.J., Hedde, T., Roubin, P., Durand, P., Lothon, M., Lohou, F., Augustin, P., and Fourmentin, M. (2017). Characterization of valley flows within two confluent valleys under stable conditions: observations from the KASCADE field experiment. *Quarterly J. of the Royal Meteorological Society*, 143, 1886-1902. Doi: 10.1002/qj.3049.
- Duine, G.J., Jones, C., Carvalho, L., and Fovell, R.G. (2019) Simulating sundowner winds in coastal Santa Barbara: Model Validation and Sensitivity, *Atmosphere*, 10, 155. Doi: 10.3390/atmos10030155.
- Duine, G.J., Carvalho L.M.V., Jones C., and Zigner K. (2021). The effect of upstream topography on the onset of Sundowner winds in coastal Santa Barbara, CA. *JGR-Atmospheres*, in press. Doi: 10.1029/2020JD033791.
- Ecklund, W. L., Carter, D. A., and Balsley, B. B. (1988). A UHF wind profiler for the boundary layer: Brief description and initial results. *Journal of Atmospheric and Oceanic Technology*, 5(3), 432-441.
- Faivre, N., Jin, Y., Goulden, M.L., and Randerson J.T. (2014) Controls on the spatial pattern of wildfire ignitions in Southern California. *Int. J. Wildland Fire*, 23, 799-811. Doi: 10.1071/WF13136.

- Fosberg, M.A. (1978) Weather in wildland fire management: the fire weather index. Proceedings of Conference on Sierra Nevada Meteorology, June 19-21, American Meteorological Society: Lake Tahoe, CA.
- Giovannini, L., Laiti, L., Serafin, S., and Zardi, D. (2017) The thermally driven diurnal wind system of the Adige Valley in the Italian Alps. Quarterly J. of the Royal Meteorological Society, 143, 2389-2402. Doi: 10.1002/qj.3092.
- Goodrick, S.L. (2002) Modification of the Fosberg fire weather index to include drought. Int. J. Wildland Fire, 11, 205-211. Doi: 10.1071/WF02005.
- Hatchett, B.J., Smith, C.M., Nauslar, N.J., and Kaplan, M.L. (2018) Brief Communication: Synoptic-scale differences between Sundowner and Santa Ana wind regimes in the Santa Ynez Mountains, California. Nat. Hazard. Earth Syst., 18. Doi: 10.5194/nhess-18-419-2018.
- Hazra, A., Reich, B.J., Shaby, B.A., and Staicu, A.M. (2018) A semiparametric spatiotemporal Bayesian model for the bulk and extremes of the Fosberg Fire Weather Index. arXiv preprint arXiv:1812.11699.
- Horel, J., Splitt, M., Dunn, L., Pechmann, J., White, B., Ciliberti, C., Lazarus, S., Slemmer, J., Zaff, D., and Burks, J. (2002) Mesowest: Cooperative mesonets in the western United States. Bulletin of the American Meteorological Society, 83, 211-226. Doi: 10.1175/1520-0477(2002)083<0211:MCMITW>2.3.CO;2.
- Jones, C., Fujioka, F., and Carvalho, L.M.V (2010) Forecast Skill of Synoptic conditions Associated with Santa Ana Winds in Southern California. Monthly Weather Review, 138, 4528-4541.
- Jones, C., Carvalho, L., Duine, G.J., and Zigner, K. (2021) A New Climatology of Sundowner Winds in Coastal Santa Barbara, California, Based on 30-yr High

- Resolution WRF Downscaling. Submitted to Atmospheric Research. Doi: 10.1175/2010MWR3406.1.
- Keeley, J.E.; Safford, H.; Fotheringham, C.J., Franklin, J., Moritz, M. (2009) The 2007 southern California wildfires: Lessons in complexity. *J. Forestry*, 106, 287-296.
- Koracin, D., Dorman, C.E., Dever, E.P. (2004) Coastal Perturbations of Marine-Layer Winds, Wind Stress, and Wind Stress Curl along California and Baja California in June 1999. *J. Physical Oceanography*, 35, 1152-1173. Doi: 10.1175/1520-0485(2004)034<1152:CPOMWW>2.0.CO;2.
- Li, D., Cova, T.J., and Dennison, P.E. (2019). Setting wildfire evacuation triggers by coupling fire and traffic simulation models: a spatiotemporal GIS approach. *Fire technology*, 55(2), 617-642. Doi: 10.1007/s10694-018-0771-6.
- Markowski, P., and Richardson, Y. (2011) *Mesoscale meteorology in midlatitudes* (Vol. 2). John Wiley & Sons.
- McWethy, D.B., Schoennagel, T., Higuera, P.E., Krawchuk, M., Harvey, B.J., Metcalf, E.C., Schultz, C., Miller, C., Metcalf, A.L., Buma, B., Virapongse, A., Kulig, J.C., Stedman, R.C., Ratajczak, Z., Nelson, C.R., Kolden, C. (2019). Rethinking resilience to wildfire. *Nature Sustainability*, 2(9), 797-804. Doi: 10.1038/s41893-019-0353-8.
- Miller, R.K., Field, C.B., Mach, K.J. (2020). Barriers and enablers for prescribed burns for wildfire management in California. *Nature Sustainability*, 3(2), 101-109. Doi: 10.1038/s41893-019-0451-7.
- Moritz, M.A., Moody, T.J., Krawchuk, M.A., Hughes, M., Hall, A. (2010) Spatial Variation in Extreme Winds Predicts Large Wildfire Locations in Chaparral Ecosystems: Extreme Winds and Large Wildfires. *Geophysical Research Letters*, 37. Doi: 10.1029/2009GL041735.



- Nadeau, D.F., Pardyjak, E.R., Higgins, C.W., Huwald, H., and Parlange, M.B. (2013) Flow during the evening transition over steep Alpine slopes. *Quarterly Journal of the Royal Meteorological Society*, 139, 607-624. Doi: 10.1002/qj.1985.
- National Weather Center Los Angeles/ Oxnard. 830 NWS LA, Oxnard. Available online: [https://www.wrh.noaa.gov/lox/fire\\_weather/redflag.pdf](https://www.wrh.noaa.gov/lox/fire_weather/redflag.pdf)
- National Wildfire Coordinating Group (2014) Interagency Wildland Fire Weather Station Standards & Guidelines. National Wildfire Coordinating Group: Boise, ID, USA, Vol. PMS 426-3, 55.
- Parish, T.R., Rahn, D.A., and Leon, D. (2014). Aircraft observations of the marine boundary layer adjustment near Point Arguello, California. *J. Applied Meteorology and Climatology*, 53(4), 970-989. Doi: 10.1175/JAMC-D-13-0164.1.
- Rahn, D.A., Parish, T.R., and Leon, D. (2014) Coastal jet adjustment near Point Conception, California, with opposing wind in the bight. *Monthly Weather Review*, 142, 1344-1360. Doi: 10.1175/MWR-D-13-00177.1.
- Rampanelli, G., Zardi, D., and Rotunno, R. (2004) Mechanisms of up-valley winds. *J. of the atmospheric sciences*, 61, 3097-3111. Doi: 10.1175/JAS-3354.1.
- Rothermel, R.C. (1983) How to Predict the Spread and Intensity of Forest and Range Fires; Research Paper INT-GTR-143; U.S. Department of Agriculture, Forest Service, Intermountain Forest and Range Experiment Station: Ogden UT, USA. Doi: 10.2737/int-gtr-143.
- Ryan, G. (1991) Sundowner winds. Weather Service Office: Santa Maria, CA, USA, 18.
- Ryan, G. (1996) Downslope winds of Santa Barbara, California. National Oceanic and Atmospheric Administration Technical Memorandum NWS WR-240, Scientific Services Division, Western Region, Salt Lake City, Utah, USA.

- Skyllingstad, E.D., Barbour, P., and Dorman, C.E. (2001). The dynamics of northwest summer winds over the Santa Barbara Channel. *Monthly weather review*, 129(5), 1042-1061. Doi: 10.1175/1520-0493(2001)129<1042:TDONSW>2.0.CO;2.
- Smith, C.M., Hatchett, B.J., and Kaplan, M.L. (2018a) Characteristics of sundowner winds near Santa Barbara, California, from a dynamically downscaled climatology: environment and effects near the surface. *J. Appl. Meteorol. Clim.*, 57, 589–606. Doi: 10.1175/JAMC-D-17-0162.1.
- Smith, C., Hatchett, B., and Kaplan, M. (2018b) Characteristics of Sundowner winds near Santa Barbara, CA, from a dynamically downscaled climatology: Environment and effects aloft and offshore. *Journal of Geophysical Research: Atmospheres*, 123(23), 13-092.
- Stull, R.B., and Ahrens, C.D. (2000). *Meteorology for scientists and engineers*. Brooks/Cole.
- Stull, R.B. (2012) *An introduction to boundary layer meteorology*. Vol. 13. Springer Science & Business Media.
- Sukup, S. (2013) Extreme northeasterly wind events in the hills above Montecito, California. Western Region Technical Attachment NWS WR-1302. National Weather Service Western Region, Salt Lake City, UT.
- Syphard, A.D., Clarke, K.C., and Franklin, J. (2007) Simulating fire frequency and urban growth in southern California coastal shrublands, USA. *Landscape Ecology*, 22, 431-445. Doi: 10.1007/s10980-006-9025-y.
- Syphard, A.D., Radeloff, V.C., Keuler, N.S., Taylor, R.S., Hawbaker, T.J., Stewart, S.I., and Clayton, M.K. (2008) Predicting spatial patterns of fire on a southern California landscape. *Int. J. Wildland Fire*, 17, 602-613. Doi: 10.1071/WF07087.

- Syphard, A.D. and Keeley, J.E. (2015) Location, timing and extent of wildfire vary by cause and ignition. *Int. J. Wildland Fire*, 24, 37-47. Doi: 10.1071/WF14024.
- Thompson, M.P., Bowden, P., Brough, A., Scott, J.H., Gilbertson-Day, J., Taylor, A., Anderson, J., and Haas, J.R. (2016). Application of wildfire risk assessment results to wildfire response planning in the southern Sierra Nevada, California, USA. *Forests*, 7(3), 64. Doi: 10.3390/f7030064.
- Zigner, K., Carvalho, L., Peterson, S., Fujioka, F., Duine, G.J., Jones, C., Roberts, D., and Moritz, M. (2020) Evaluating the Ability of FARSITE to Simulate Wildfires Influenced by Extreme, Downslope Winds in Santa Barbara, California. *Fire*, 3, 29. Doi: 10.3390/fire3030029.

### **3. Evaluating the Ability of FARSITE to Simulate Wildfires Influenced by Extreme, Downslope Winds in Santa Barbara, California**

Katelyn Zigner<sup>1</sup>, Leila M.V. Carvalho<sup>1,2</sup>, Seth Peterson<sup>1</sup>, Francis Fujioka<sup>3</sup>, Gert-Jan Duine<sup>2</sup>, Charles Jones<sup>1,2</sup>, Dar Roberts<sup>1,2</sup>, Max Moritz<sup>1,2,4</sup>

<sup>1</sup> Department of Geography, University of California, Santa Barbara, CA, USA

<sup>2</sup> Earth Research Institute, University of California, Santa Barbara, CA, USA

<sup>3</sup> CEESMO, Chapman University, Orange, CA, USA.

<sup>4</sup> University of California Cooperative Extension, Agriculture and Natural Resources Division, Oakland, CA, USA.

This work has been published in Fire:

Zigner, K., Carvalho, L.M.V., Peterson, S.H., Fujioka, F., Duine, G.J., Jones, C., Roberts, D.A., Moritz, M. (2020) Evaluating the ability of FARSITE to simulate wildfires influenced by extreme, downslope winds in Santa Barbara, California. Fire 3(3): 29. DOI: 10.3390/fire3030029

### **3.1 Abstract**

Extreme, downslope mountain winds often generate dangerous wildfire conditions. We used the wildfire spread model Fire Area Simulator (FARSITE) to simulate two wildfires influenced by strong wind events in Santa Barbara, CA. High spatial-resolution imagery for fuel maps and hourly wind downscaled to 100 m were used as model inputs, and sensitivity tests were performed to evaluate the effects of ignition timing and location on fire spread. Additionally, burn area rasters from FARSITE simulations were compared to minimum travel time rasters from FlamMap simulations, a wildfire model similar to FARSITE that holds environmental variables constant. Utilization of two case studies during strong winds revealed that FARSITE was able to successfully reconstruct the spread rate and size of wildfires when spotting was minimal. However, in situations when spotting was an important factor in rapid downslope wildfire spread, both FARSITE and FlamMap were unable to simulate realistic fire perimeters. We show that this is due to inherent limitations in the models themselves, related to the slope-orientation relative to the simulated fire spread, and the dependence of ember launch and land locations. This finding has widespread implications, given the role of spotting in fire progression during extreme wind events.

### **3.2 Introduction**

Around the world, destructive wildfires significantly disrupt lives through personal and economic losses, degraded air quality (Richardson et al. 2012), and an enhanced risk of landslides and debris flows (Parise and Cannon 2012). Understanding future climatic and anthropogenic changes that will alter wildfire season and intensity is crucial for highly-populated and at-risk locations such as southern California communities. Wet winters and

dry summers in this climate lead to a wildfire season generally between May and October, although rising temperatures associated with climate change will advance fuel drying and extend the length of the fire season (Westerling et al. 2006; Diffenbaugh et al. 2015; Abatzoglou and Williams 2016). Furthermore, projected increases of extreme meteorological events such as heat waves (Cayan et al. 2008) will affect the frequency, severity, and spatial distribution of wildfires. Combined with the expected changes in the regional climate, the probability of impactful wildfires may increase in the future in coastal Santa Barbara due to an increasing number of ignitions from expansion of the wildland-urban interface (Syphard et al. 2007, 2008; Faivre et al. 2014; Syphard and Keeley 2015).

Wildfire behavior is determined by fuels, topography, and weather (Countryman 1972), commonly called the “fire behavior triangle” or the “fire environment triangle”. In the case of extreme wind events, meteorological conditions are the leading factor that determines wildfire spread and intensity (Rothermel 1972, 1983; Catchpole et al. 1998; Moritz 2003; Keeley et al. 2009; Stratton 2009; Moritz et al. 2010). Extreme, downslope wind events in coastal Santa Barbara County are called “Sundowner winds” (or “Sundowners”) due to the onset of gusty winds around sunset (Ryan 1996; Blier 1998). Sundowners are most frequent in spring (Hatchett et al. 2018; Smith et al. 2018) when fire danger is relatively low, but they can occur year-round. These events may produce critical fire weather conditions throughout the evening, including gale-force winds and relative humidity below 15% (Sukup 2013; Cannon et al. 2017). Some of these events have been associated with abnormally high temperatures in the evening occasionally exceeding 30°C after sunset during summer (Ryan 1996; Blier 1998).

While strong wind events may create extreme fire weather conditions and cause rapid wildfire spread, no previous studies have placed emphasis on examining the sensitivity of

operationally-used wildfire models to simulate wildfires significantly influenced by downslope wind events. This is important because Sundowners have rapidly spread all major wildfires on the south side of the Santa Ynez Mountains (SYM) toward a coastal community of ~150,000 inhabitants (Murray et al. 2020) (Fig. 3.1). All abbreviations used in this paper are listed in Table A3.1, and statistics for all major wildfires are shown in Table 3.1. Among those remarkable wildfires was the Painted Cave fire (June 1990), which quickly spread through dense, flammable vegetation driven by strong (~26 m/s) winds (Ryan 1996; Cannon et al. 2017). Between 2016 and 2019, Sundowners rapidly spread three major wildfires in coastal Santa Barbara County: the Sherpa (June 2016), Thomas (December 2017), and Cave (December 2019) fires. Northwestern winds around 18 m/s rapidly spread the Sherpa Fire down the sparsely inhabited western slopes of the SYM. Driven by Sundowner winds, the Thomas Fire spread into the SYM and claimed the title of the largest southern California wildfire to date. Although wildfires have undeniably affected the inhabitants and ecosystem in this region, only one study so far (Peterson 2011) has attempted to reconstruct wildfires in coastal Santa Barbara County using wildfire models.

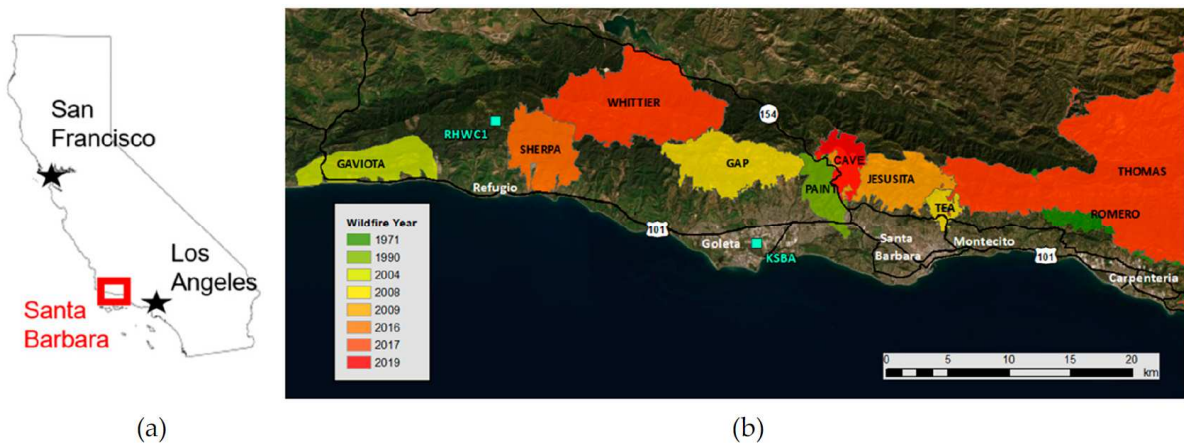


**Figure 3.1** - Region of interest (red rectangle; **a**) and perimeters of past wildfires in coastal Santa Barbara County between 1970 and 2019 (**b**), colored by the year of occurrence. The

“PAINT” Fire is the Painted Cave Fire examined in this study. The thick, black lines indicate major roads and freeways (Highway 101 and Highway 154), and the two blue squares indicate weather stations used in this analysis.

**Table 3.1** - Information on past wildfires in coastal Santa Barbara County. It should be noted that the Thomas Fire ignited to the east of Santa Barbara in Ventura County and spread west in the first two weeks after ignition. The numbers in the table are from official reports that incorporate areas in coastal Santa Barbara. Additionally, the structural impacts, injuries, and deaths associated with the Montecito debris flow caused by the Thomas Fire were not included.

Fire	Date	Acres Burned	Structural Impacts	Injuries and Deaths
Painted Cave	June 1990	2000 ha	427 destroyed	1 death
Tea	November 2008	785 ha	210 destroyed	-
Jesusita	May 2009	3500 ha	80 destroyed	-
Sherpa	June 2016	3200 ha	1 destroyed	1 injury
Thomas	December 2017	110,000 ha	1000 destroyed	2 deaths
Cave	November 2019	1265 ha	-	-

Wildland fire models such as the Fire Area Simulator (FARSITE) (Finney 1998) and FlamMap (Finney et al. 2006; Stratton 2006) are used operationally to simulate prescribed burns in the national parks in the United States (Finney and Ryan 1995; Arca et al. 2007; Papadopoulos and Pavlidou 2011), and examine model sensitivity to fuel models and fuel moisture (Phillips et al. 2006; Forghani et al. 2007). Additionally, these models provide decision support regarding appropriate responses on wildfire incidents (Scott 2006), and FARSITE is typically selected to answer questions regarding fire size, location, and timing (Stratton 2006; Scott 2006). FARSITE and FlamMap are two-dimensional semi-empirical wildfire models that describe how surface wind flow spreads fire at fire line and geographical scales. These are uncoupled wildfire models because they do not consider interactions between the fire and the atmosphere, i.e. the feedback that occurs between the fire and local wind flow. The simplicity in the treatment of fuels, topography, and weather as



independent variables is a limitation of uncoupled wildfire models, since these factors can greatly impact observed fire behavior (Coen et al. 2013). In contrast, atmospheric models, such as the Weather Research and Forecasting model (WRF) (Skamarock et al. 2008) may be combined with fire-spread models (e.g. WRF-Fire (Coen et al. 2013) and WRF-SFIRE (Kochanski et al. 2013)) to describe this coupling at fire scales (i.e. tens of meters). Although highly sophisticated, these coupled models are computationally expensive and rarely used operationally (Finney 1998; Gollner et al. 2015). Our choice to use uncoupled wildfire models is justified by the simplicity and quick simulation run time, which would be beneficial in an operational setting. The rapid simulation time is especially critical for fires in the Wildland-Urban Interface (WUI) for wildfire management and evacuation planning purposes. More information on the use, advantages, and disadvantages of FARSITE and FlamMap can be found in (Papadopoulos and Pavlidou 2011).

The ability of uncoupled fire spread models, such as FARSITE and FlamMap, to simulate downslope wildfire spread driven by extreme, downslope winds in the Santa Barbara area has not yet been assessed. Moreover, evacuation planning can become critical during wind-driven wildfires in Santa Barbara; thus, advancing research on wildfire spread and risk with operational models is essential. The overarching goal of this research is to examine the skill of FARSITE in simulating downslope fire spread under extreme conditions by focusing on two of the most rapidly spreading wildfires that have affected the southern slopes of the SYM during Sundowners. Additionally, burn area rasters from simulations in FARSITE are further compared with the minimum travel time rasters from FlamMap simulations. The successful simulation of wildfire case studies using uncoupled fire spread models such as FARSITE with focus on spatiotemporal wind variability may allow for the creation of burn probability maps for fire risk assessment during Sundowners. This research

may contribute to enhanced wildfire resource allocation and preparedness during extreme fire weather conditions. This study is organized as follows. Data sets, material, and methods are discussed in Section 3.2. Results and conclusions are presented in Section 3.3. Final conclusions are summarized in Section 3.4. A list of acronyms and the other figures are included in the Appendix.

### **3.3 Materials and Methods**

#### *3.3.1 Case studies*

Two wildfires rapidly spread by Sundowner winds were selected to test the ability of FARSITE to reconstruct fires perimeters during extreme fire weather conditions. The first case study, the Sherpa Fire, was selected because of the availability of a high-resolution fuel map from remotely sensed data taken approximately two years before the fire, and multiple fire perimeters obtained in the hours after ignition, allowing for numerous comparisons of observed and simulated fire perimeters. The fire ignited at 1515 Pacific Daylight Time (PDT) on 15th June 2016 in the slopes of western SYM along the Gaviota Coast in Santa Barbara County from embers blown off a burning log. Sundowner winds on the first night of the fire rapidly spread the fire southward down canyons. Winds were strong at the nearby Refugio station (RHCW1; see Fig. 3.1 for location), ranging 16-18 m/s on the evening of the fire. North-northwesterly winds recorded at a station downhill (south) were less than 10 m/s, illustrating the limited spatial extent of the Sundowner event (Smith et al. 2018). At the time of ignition, RHCW1 reported a temperature of 19 °C and relative humidity of 38% with no temperature ramps or sudden drops in moisture evident in the following hours. Strong,

northerly winds and gusts reaching 23 m/s continued throughout the night and rapidly spread this fire south, resulting in evacuations and the closure of Highway 101 (Fig. 3.1).

The second case study was chosen because of exceptionally fast fire spread from Sundowner winds and the significant influence on populated areas. The arson-caused Painted Cave Fire ignited on June 27th, 1990 at 1800 PDT off Highway 154, close to the SYM ridgeline (Fig. 3.1). In addition to an extended three-to-four-year drought, temperatures exceeding 38 °C and relative humidity values below 20% in the three-day heat wave preceding the fire left the dense chaparral dry and very flammable (Ryan 1996). Extreme winds and gusts launched burning branches and flaming embers ahead of the fire front and spread the fire downhill toward urban Santa Barbara, travelling 3 km in the first 20 min and 6 km to Highway 101 in 1 h (Ryan 1996; Hazard 2019). Additionally, backfiring operations spread the fire eastward across Highway 154, and an upslope (southerly) wind shift spread the fire northwest of the ignition point on the second day.

### *3.3.2 Wildland fire models*

Wildfires were simulated using the vector-based, deterministic fire model FARSITE v4 built within FlamMap6. FARSITE uses Huygen's principle of wave propagation and the Rothermel fire spread equations (Rothermel 1972) to simulate fire spread creating a series of ellipses at multiple vertices on the fire front (Finney 1998; Anderson 1982). Surface and crown fires are separated and use the Rothermel (Rothermel 1972) and Van Wagner (Van Wagner 1977) models, respectively. FARSITE uses Albini's equations (Albini 1979) for spotting from torching vegetation and calculates the maximum distance an ember can travel using wind speed, topography, and ember size, shape, and density (Finney 1998). Additionally, wind speed is considered only horizontally, and is assumed to increase

logarithmically with height above the 6.1 m (20 ft) input winds (Finney 1998). Required inputs include elevation, slope, aspect, fuel model, canopy cover, crown base height, and crown bulk density, and meteorological data, including temperature, relative humidity, horizontal wind speed and direction, and precipitation.

FlamMap is another operationally-used, uncoupled wildfire model that shares many similarities with FARSITE, including the same input data (e.g. fuel map, crown base and stand height, bulk crown density, elevation, aspect, slope, temperature, humidity, wind speed and direction, precipitation). The main difference between FARSITE and FlamMap is the absence of time-varying winds and fuel moisture conditions in FlamMap. The Minimum Travel Time (MTT) model calculates fire behavior at every grid cell and independent of one another, providing great use for comparisons of landscape treatment processes (Papadopoulos and Pavlidou 2011). More information on the differences between FARSITE and FlamMap can be found in (Andrews 2007).

### *3.3.3 Fuel and topography data*

Vegetation in southern California is primarily comprised of evergreen sclerophyllous shrubs, such as chamise and Ceanothus, as well as drought deciduous coastal sage scrub (Hanes 1965, 1973). Both are well adapted to the long, dry summers and are highly flammable (Moritz 2003; Rothermel and Philpot 1973; Countryman and Philpot 1970). In our study, canonical discriminant analysis and linear discriminant analysis were applied to an 18 m Airborne Visible/ Infrared Imaging Spectrometer (AVIRIS) image from 2014 for the Sherpa Fire (Meerdink et al. 2019), and 12 m from 2004 AVIRIS image for the Painted Cave Fire (Roth et al. 2012). The 15-year gap between the Painted Cave fire and the 2004 imagery for the Painted Cave fire is likely enough time for the recovering vegetation to

mimic the conditions at the time of the fire (Peterson and Stow 2003). The classified images were cross-walked into fuel models from Anderson's original 13 fire behavior fuel models (Anderson 1982), Scott and Burgan's fuel models (Scott and Burgan 2005), and Weise and Regelbrugge's chaparral models (Weise and Regelbrugge 1997). Fuel model specifications are shown in Table 3.2 and Figures 3.2a,c. These materials are available upon request to the corresponding author.

**Table 3.2** - Fuel model information.

Vegetation Name	Fuel Model Number	Fuel Model Source	Fuel Model Name	Fuel Model Code
Short Grass	1	Anderson	-	-
Chamise	15	Weise and Regelbrugge	-	-
Ceanothus	16	Weise and Regelbrugge	-	-
Coastal Sage Scrub	18	Weise and Regelbrugge	-	-
Suburban/WUI	23	Scott and Burgan	Moderate Load Conifer Litter	TL3
Shrubs	145	Scott and Burgan	High Load, Dry Climate Shrub	SH5
Dense Shrubs	147	Scott and Burgan	Very High Load, Dry Climate Shrub	SH7
Trees/Riparian	162	Scott and Burgan	Timber-Understory	TU2

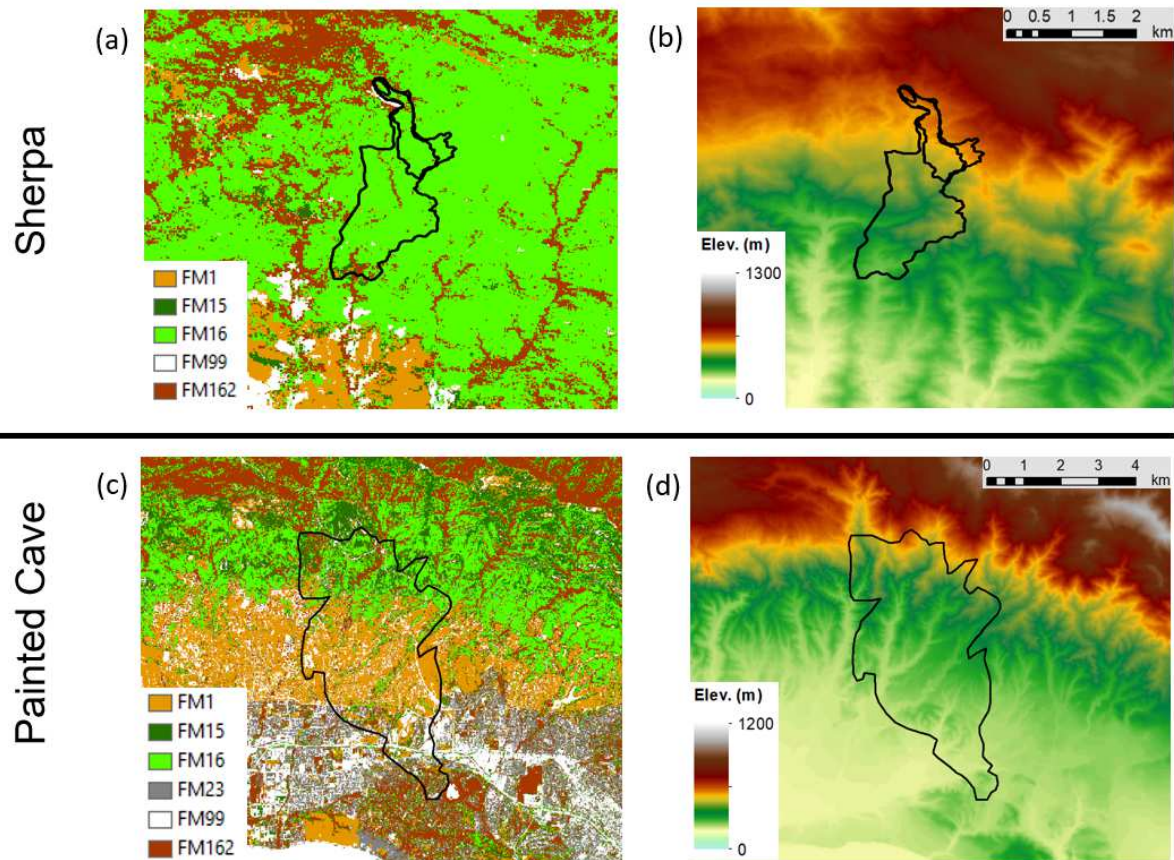


**Figure 3.2** - Fuel maps (a,c) and elevation (b,d) rasters for the Sherpa (a,b) and Painted Cave (c,d) fires. The black polygons are the fire perimeters at 1600, 1800, and 1900 PDT for the Sherpa Fire, and the final perimeter for the Painted Cave Fire. Fuel type numbers and names are indicated in Table 3.2.

Minor modifications in burnable and unburnable classifications were applied to the fuel maps for both case studies; the area south of the Sherpa Fire ignition is a campsite (Rancho La Scherpa) with a combination of sparse and irrigated vegetation. Hence, this region was classified as unburnable. The Painted Cave Fire spread southward into suburban and urban Santa Barbara, which were originally classified as unburnable, limiting the potential extent of the simulated fire spread. A dense timber-litter fuel model was chosen for suburban areas to imitate these regions with intermingled vegetation and buildings. Areas

consisting of primarily concrete roads and stucco structures considered ‘urban’ remained classified as unburnable.

Elevation data at 30 m spatial resolution acquired from the Shuttle Radar Topography Mission (Farr et al. 2007) was used for the FARSITE elevation, slope, and aspect rasters for each case study (Figs. 3.2b,d).

#### *3.3.4 Weather Data*

Given the narrow SYM (10 km) and limited availability of surface weather stations, atmospheric data were obtained with WRF simulations at 1 km grid spacing. For our case studies, hourly 1 km gridded 2 m temperature, 2 m relative humidity, and 10 m wind (east-west and north-south components) were created using the WRF with the configuration specified in Duine et al. (2019).

Hourly temperature, relative humidity, and precipitation data from a selected point were input to FARSITE through a weather stream file (Gibson and Gorski 2003) created using WRF data and applied over the entire domain. In coastal Santa Barbara County, there are significant gradients in weather conditions between the SYM slopes and areas near the coast (Duine et al. 2019; Carvalho et al. 2020). Therefore, the location used for the weather stream file data must be representative of conditions close to the fire. For these two case studies, we created weather stream files using the WRF grid cell closest to the ignition sites.

Wildfire spread is exceedingly sensitive to local winds, especially extreme winds (Rothermel 1972; Catchpole et al 1998; Carvalho et al. 2020), and the utilization of gridded wind data in wildfire modeling has improved the agreement between simulated and observed perimeters (Moritz et al. 2010; Butler and Forthofer 2004; Salis 2008). Mass-conserving meteorological wind downscalors such as WindNinja (Forthofer et al. 2009, 2014) have been

used to increase resolution of gridded winds and have produced more accurate fire perimeters in FARSITE and FlamMap in some case studies (Finney et al. 2006; Forghani et al. 2007; Butler et al. 2006; Jahdi et al. 2014; Forthofer et al. 2014). To capture the variability of winds over the complex terrain in coastal Santa Barbara County, the 1 km WRF wind output was downscaled to 100 m using WindNinja (henceforth “WN”). This software requires an elevation raster and single-point or gridded wind data, and outputs wind speed and direction in raster format. Figure 3.3 illustrates differences in winds as a consequence of different grid spacing at 1 km (WRF) compared to 100 m (WN) at the time of ignition for the Sherpa and Painted Cave fires. Smoothing effects as a consequence of the grid spacing at 1 km (WRF) and 100 m (WN) will influence simulated fire spread. It is also important to note the height differences between the 10 m agl WRF surface wind files and the 6.1 m agl WN surface wind files.



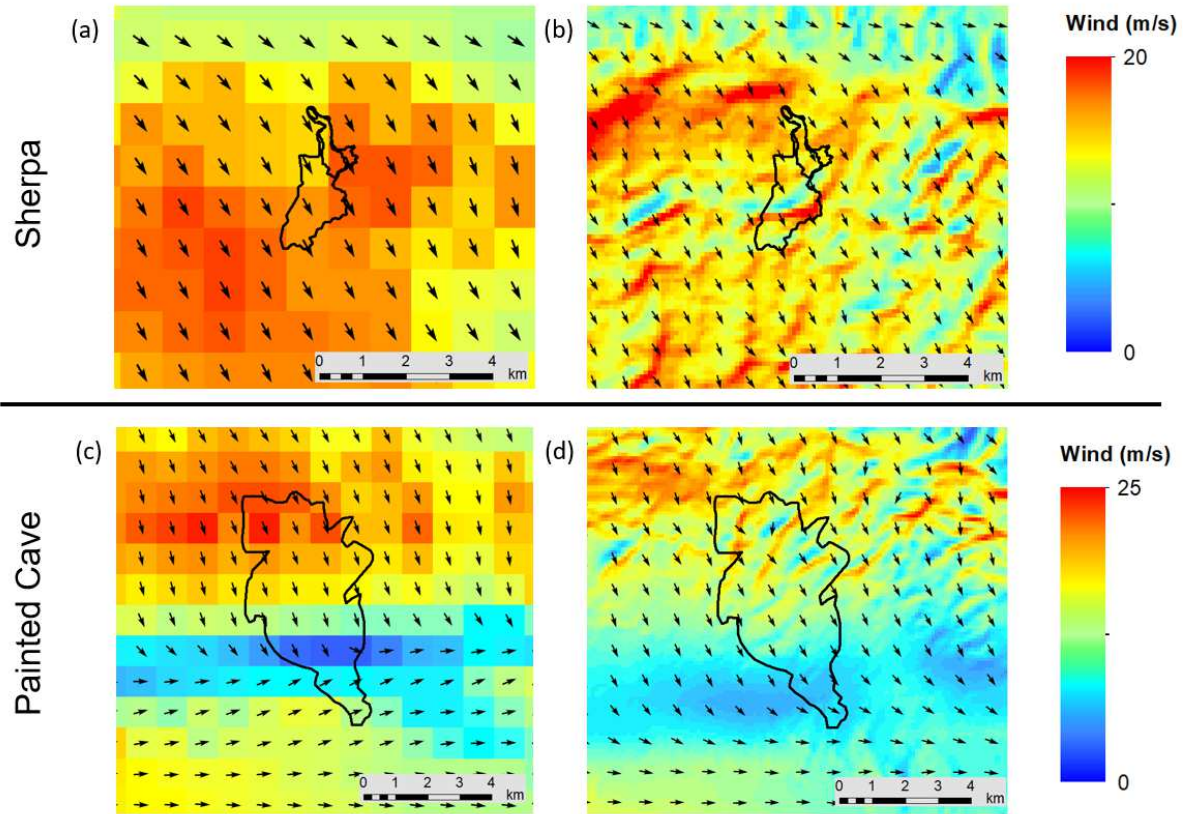


**Figure 3.3** - Examples of gridded wind data from WRF at 1 km resolution (a,c) and WN at 100 m resolution (b,d) at the time of ignition for the two wildfire case studies. It is important to note that output is at a height of 10 m (~30 ft) for the WRF surface winds and at 6.1 m (20 ft) for WN surface winds used in this analysis. The black polygons are the fire perimeters at 1600, 1800, and 1900 PDT for the Sherpa Fire, and the final perimeter for the Painted Cave Fire.

To determine potential errors associated with temperature, relative humidity, and wind speed, we compared station observations acquired from Mesowest (Horel et al. 2002) with the closest WRF and WN (for wind speed only) grid cell for each case study (Fig. 3.4). We compared model output with RHCW1 during the Sherpa Fire because of its close proximity to the fire. The Santa Barbara airport station (henceforth KSBA; see Fig. 3.1 for location) was the only weather station installed during the Painted Cave fire, and was thus used to validate meteorological variables. This station did not archive data in the early

morning hours, resulting in breaks in station data (Black lines in Figs. 3.4d–f). RHWC1 is a Remote Automatic Weather Station (RAWS) owned by the U.S. Forest Service, whereas KSBA is an Automated Surface Observing System owned by the National Weather Service. It's important to note that RHWC1 records all wind measurements at 6.1 m agl and non-wind measurements (e.g. temperature, relative humidity) at 2 m agl. KSBA measures wind at 10 m agl and measures non-wind variables at 2 m agl. WRF surface files were bilinearly interpolated to 2 m for temperature and relative humidity, and 10 m agl for wind, whereas WN produces wind rasters at 6.1 m agl.

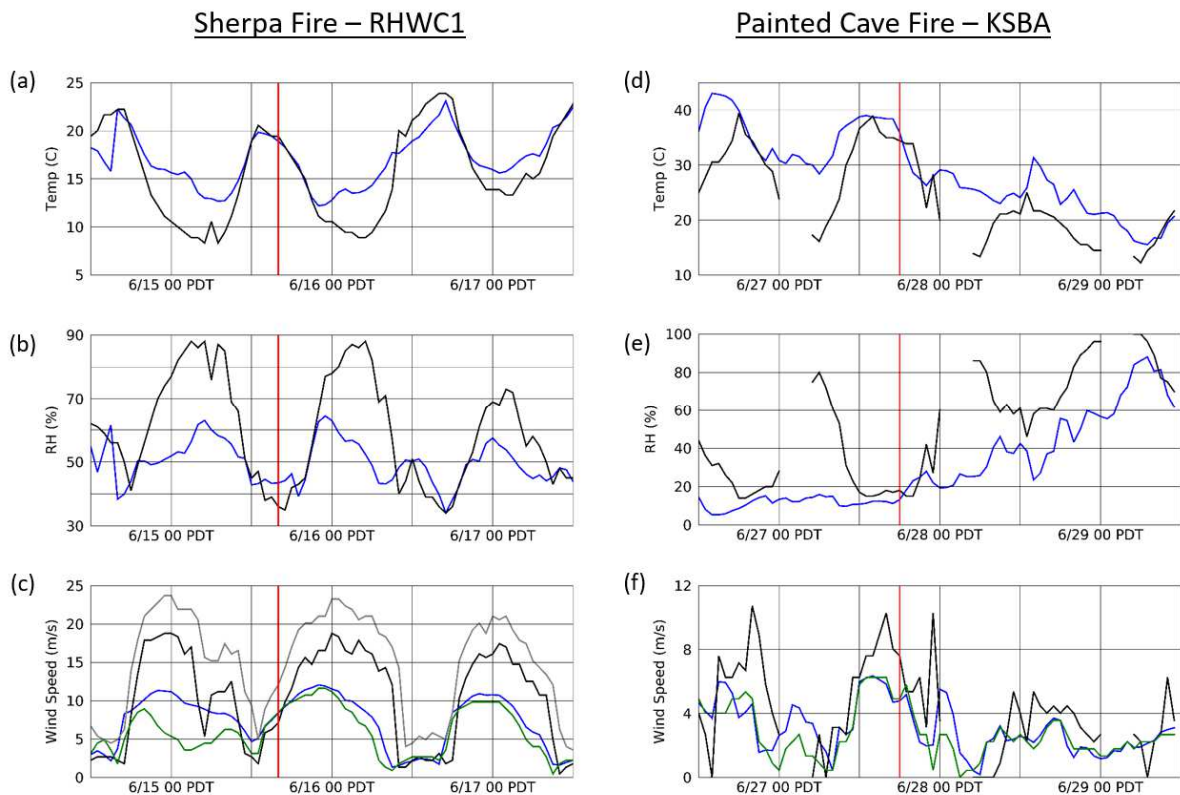


**Figure 3.4** - Observed (black) and simulated with WRF (blue) temperature (a,d), relative humidity (b,e), and wind (c,f) at the nearest weather stations for the Sherpa (RHWC1) and Painted Cave (KSBA) fires. WindNinja data was added for wind plots (green lines in (c,f)) and observed gust data was available at RHWC1 (grey line in (c)). The vertical red line indicates the time of ignition for each fire.

Although there was generally high agreement in wind speed between the WRF and WN grid cells (Fig. 3.4), we observe biases in temperature and relative humidity between WRF and stations; RAWS are usually placed in locations that are normally exposed to high wind speeds, other near canyons and passes. These topographic features are mostly smoothed in 1 km grid simulations, largely explaining differences in wind speeds between model output and station observations. Biases between WRF and KSBA have been shown in previous studies (Cannon et al. 2017; Duine et al. 2019; Carvalho et al. 2020) and are attributed to the station's proximity to the ocean, and the representation of the transition between the marine and coastal boundary layer in simulations. The choice of WRF parameterizations and implications for simulations are discussed in Duine et al. (2019).

Interestingly, the simulated temperature and relative humidity values around the ignition times were fairly close to observations during both case studies (Figs. 3.4a,b,d,e). WRF and WN underestimated wind speeds, and this difference was largest in the evening during the Sherpa Fire (Fig. 3.4c) when the observed winds were ~5 m/s higher and observed wind gusts were more than 10 m/s higher than simulated winds. During the Painted Cave fire, simulated winds typically underestimated KSBA wind speeds by less than 2 m/s (Fig. 3.4f). The underestimation of simulated winds at these grid cells may produce underestimations in simulated fire perimeters.

### *3.3.5 Gust factor*

Wind gusts play a crucial role in wildfire spread, intensity, and spotting (Rothermel 1972; Stratton 2006; Westerling et al. 2004), but are not simulated by WRF. As suggested in Mitchell (2013), gusts provide value for understanding extreme winds from an observational

and wildfire-focused standpoint based on differing calculation methods. Wind speeds reported at RAWS such as RHWC1 are the average of winds in the 10-min prior to every hour, whereas gusts are the maximum wind recorded in the previous hour. Previous studies (Mitchell 2013; Fovell and Cao 2017; Cao and Fovell 2018; Fovell and Gallagher 2018) utilized station observations to create a wind gust approximation termed the ‘gust factor’. The gust factor (GF) is calculated by dividing the gust speed by the wind speed, and varies between stations due to sampling length and frequency, averaging interval, and instrument mounting height (Fovell and Gallagher 2018).

To mimic the effect of gusts on simulated wildfire spread, we applied a GF to WN rasters. We chose to apply a gust factor to the WN gridded wind files because WRF and WN underestimated winds in both case studies (Figs. 3.4c,f). Underestimates of wind speed will result in underestimated fire spread. However, the spatiotemporal variability of wind gusts is difficult to simulate, and the application of a constant GF over the domains and at all times may lead to overestimated fire spread.

Wind gust data were not available during the Painted Cave Fire, but were available during the Sherpa Fire at RHWC1 (Fig. 3.4c). At the time of ignition for the Sherpa Fire, the GF was 1.71, although increased wind speeds and gusts later in the evening decreased the GF to 1.28 at 1800 PDT. The average GF between the time of ignition and the last observed perimeter of that first evening (1500 to 1900 PDT) was 1.38, demonstrating the variability of the GF through the use of different temporal subsets. While GFs have not been extensively analyzed in coastal Santa Barbara, studies on Santa Ana and Diablo winds calculated an average GF of 1.7 (Mitchell 2013; Fovell and Cao 2017; Cao and Fovell 2018). In this study, the Sherpa and Painted Cave fires were simulated multiple times using no gust factor, a 1.4

GF, and a 1.7 GF. We then compared the simulated and observed fire perimeters using these differing wind inputs.

### *3.3.6 Perimeter data*

Perimeter data for both fires are available from the Santa Barbara County Fire Department (<https://www.sbcfire.com>). The Sherpa Fire has observed perimeters at 1600, 1700, 1800, and 1900 PDT. Only one, the final perimeter, is available for the Painted Cave Fire, although the southward fire spread rate and parts of the fire perimeter were estimated from recollections (see Section 3.3.1).

Simulated and observed perimeters were quantitatively analyzed using the Sorensen metric (SM) (Grieg-Smith 1983; Perry et al. 1999), defined as:

$$SM = 2a / (2a + b + c)$$

where  $a$  is the area burned by both the observed and simulated fires,  $b$  is the area burned by only the observed fire, and  $c$  is the area burned by only the simulation. SM values closer to 0 indicate little agreement between observed and simulated perimeters, and values closer to 1 indicate high agreement. This metric has been used to compare wildfire perimeters in (Arca et al. 2007; Peterson et al. 2009; Salis et al. 2013, 2016).

## **3.4 Results and Discussion**

### *3.4.1 Sherpa Fire*

Figure 3.5 shows observed and simulated perimeters for the Sherpa Fire, with simulations run applying no GF (henceforth 1.0 GF), a 1.4 GF, and a 1.7 GF. All FARSITE simulations used the vegetation and spotting specifications in Table 3.3 and started at 1500

PDT. The area burned and SM values for the observed perimeters and all simulations are shown in Table 3.4. After one hour (at 1600 PDT), the 1.0 GF simulation had best agreement with observed perimeters in terms of fire shape and size, but greatly underestimated all other perimeters later in the evening (Fig. 3.5a). At 1700 PDT, the 1.4 GF simulation underestimated the perimeter (Fig. 3.5b) and the 1.7 GF simulation overestimated the perimeter (Fig. 3.5c), notably resulting in equal SM values for different reasons. At 1800 PDT, the 1.4 GF simulation had the highest SM value (0.64; see Table 3.4) and highest agreement in burned area of all simulations at this time. While the 1.4 GF simulation had the highest SM value at 1900 PDT, all GF simulations underestimated the total amount of area burned (Table 3.4). The 1.7 GF simulation had the closest amount of burned area to that observed, underestimating by less than 10 ha. The higher SM value for the 1.4 GF simulation is explained by the reduction of area burned compared to the 1.7 GF simulation.

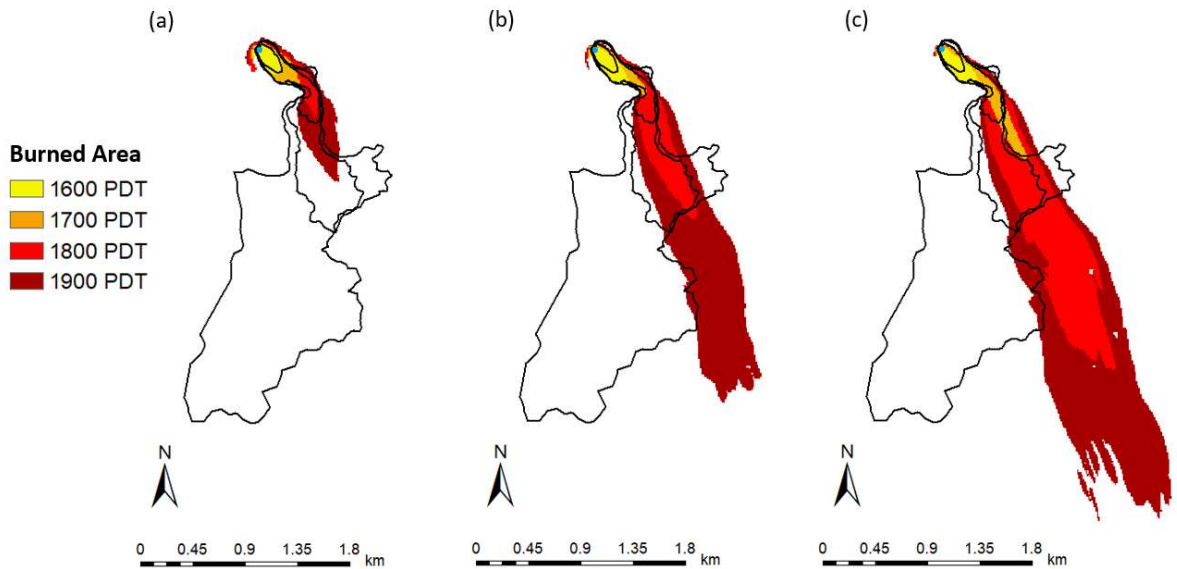


**Figure 3.5** - Sherpa fire ignition (blue dot), observed perimeters at 1600, 1700, 1800, and 1900 PDT (black polygons), and the simulated FARSITE burn areas (colored polygons) for simulations with (a) 1.0 GF, (b) 1.4 GF, and (c) 1.7 GF.

**Table 3.3** - Specifications for both wildfire case study simulations.

	Distance Resolution	30 m
<i>Fuel Properties</i>	Perimeter Resolution	30 m
	Time Step	10 min
	Canopy Cover	10%
	Stand Height	3 m
	Base Stand Height	0.1 m
<i>Spotting Settings</i>	Canopy Bulk Density	0.2 kg m <sup>-3</sup>
	Foliar Moisture Content	50%
	Spot Probability	5 %
	Spot Delay	0 min
	Min. Spot Distance	12 m
	Background Spot Grid Resolution	6 m

**Table 3.4** - Quantitative metrics for the Sherpa (top) and Painted Cave (bottom) simulations. The simulation with the burned area closest to observed and the highest SM value at each time is in bold. The all-FM1 simulation was assessed separately.

SHERPA	1600	Burned Area (ha)			SM			
		1700	1800	1900	1600	1700	1800	1900
Observed Perimeters	3.0	11.8	46.6	246.6	-	-	-	-
1.0 GF	<b>3.8</b>	8.0	13.8	33.0	<b>0.84</b>	0.66	0.37	0.17
1.4 GF	5.1	8.2	<b>32.9</b>	128.6	0.64	<b>0.68</b>	<b>0.64</b>	<b>0.25</b>
1.7 GF	5.2	<b>14.3</b>	95.2	<b>237.5</b>	0.57	<b>0.68</b>	0.40	0.21
PAINTED CAVE	1900	Burned Area (ha)			SM			
		2000	2100	2200	1900	2000	2100	2200
Observed Perimeter	1792 (final)	1792 (final)	1792 (final)	1792 (final)	-	-	-	-
1.0 GF	37	153	296	<b>407</b>	0.05	0.16	0.28	<b>0.37</b>
1.4 GF	43	162	265	351	0.04	0.17	0.26	0.33
1.7 GF	64	195	<b>298</b>	380	0.07	0.20	<b>0.29</b>	0.36
2.0 GF	<b>95</b>	<b>210</b>	247	256	<b>0.10</b>	<b>0.21</b>	0.24	0.25
1.7 GF—all FM1	156	587	1097	1720	0.16	0.49	0.71	0.76

It should be noted that the observed fire spread further west than the simulated perimeters at 1800 and 1900 PDT due to firefighting efforts limiting the eastward spread toward populated regions (Hazard, 2019). It is possible, however, that local wind shifts

and/or terrain effects may have contributed to the observed westward spread, although these were not evident in observations (from RHWC1), WRF, or WN. Additional simulations were performed in which “barriers” (unburnable areas) were applied to limit the eastward spread (not shown). Nevertheless, strong northwesterly winds drove the fire into the barriers and caused the simulated fire to extinguish rather than change direction.

We examined FARSITE sensitivity to initial conditions by running additional simulations with ignitions at 1300, 1400, 1600, and 1700 PDT, and applying a 1.7 GF (see Appendix). Including the original simulation with an ignition time at 1500 PDT, the five simulations ranged in southward extents three and four hours after ignition, where ignitions with later start times spread further south due to the presence of stronger northerly winds later in the evening (Figs. A3.1a,b). The sensitivity to ignition location was analyzed by running simulations with ignition sites approximately  $\frac{1}{2}$  km to the west, southwest, southeast, and east of the original ignition location. Simulations with the west and southwest ignition sites did not spread as far south as the east and southeast ignition sites because of the unburnable region to the south, which limited potential simulated fire spread (Figs. A3.1c,d). As expected, we observed differences in simulated fire spread perimeters when the ignition time or location varied. Nonetheless, there was less agreement between simulations when ignition time varied because of the temporal wind variability. These sensitivity tests demonstrate how relatively small changes in model input can affect FARSITE perimeter accuracy.

### *3.4.2 Painted Cave Fire*

Simulations for the Painted Cave Fire started at 1800 PDT, and all perimeters were compared to the one, final perimeter and firefighter recollections (see Section 3.3.1) to



examine southward spread. FARSITE parameterizations were the same as the Sherpa Fire (Table 3.3). The simulations using the fuel map (Fig. 3.2c) and GF values of 1.0, 1.4, and 1.7 produced perimeters that significantly underestimated firefighter observations. As previously stated, the observed fire reached San Antonio Creek Rd (~3 km) 20 min after ignition; however, it took over 3 h to reach this location in the simulations (Fig. A3.2). In an attempt to simulate faster fire spread, we applied a new fuel map with different chaparral fuels (Fig. 3.6). The new fuel models (FM), FM145 and FM147 (Scott and Burgan 2005), replaced FMs 15 and 16 (Weise and Regelbrugge 1997), respectively, and were most prominent in the region south of the ignition point (Table 3.2). The original FMs produced smaller perimeters compared to the use of Anderson's fuel models (Anderson 1982) from lower fuel loadings (Stephens et al. 2008), and the new fuel map should produce larger simulated perimeters and faster fire spread.

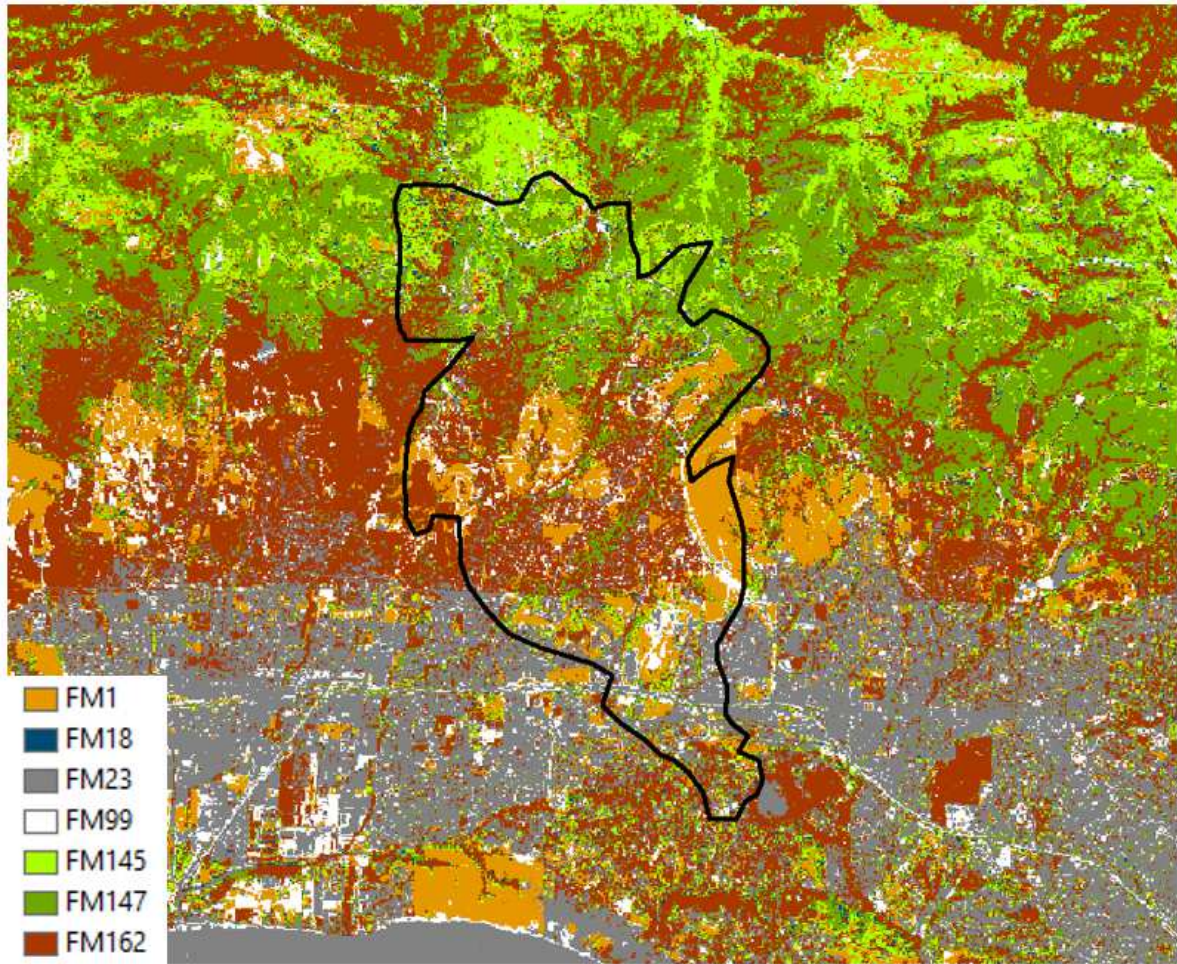


**Figure 3.6** - New fuel map for the Painted Cave fire, incorporating FM145 and FM147.

Simulations were performed using GFs of 1.0, 1.4, and 1.7 (Fig. 3.7), and the burned area and SM at each time step during each GF simulation are shown in Table 3.4. As expected, the perimeters spread south more rapidly using the new fuel map, especially one and two hours after ignition. However, the fire still did not reach San Antonio Creek Rd until three hours after ignition in the 1.7 GF simulation (Fig. 3.7c). Nonetheless, the simulated fire reached the road within two hours when a 2.0 GF was utilized (Fig. 3.7d). Regardless of the GF, all simulations vastly underestimated the time to reach San Antonio Creek Rd, and no simulations reached Highway 101 even after four hours. Furthermore, all

simulations stopped around the same location after four hours, even though there were burnable fuels downwind of the fire front. Similar to the Sherpa Fire, we examined the sensitivity to varied fire ignition time and location (see Appendix). These simulations produced marginally different fire spread perimeters, and all significantly underestimated the observed perimeter (Fig. A3.3).

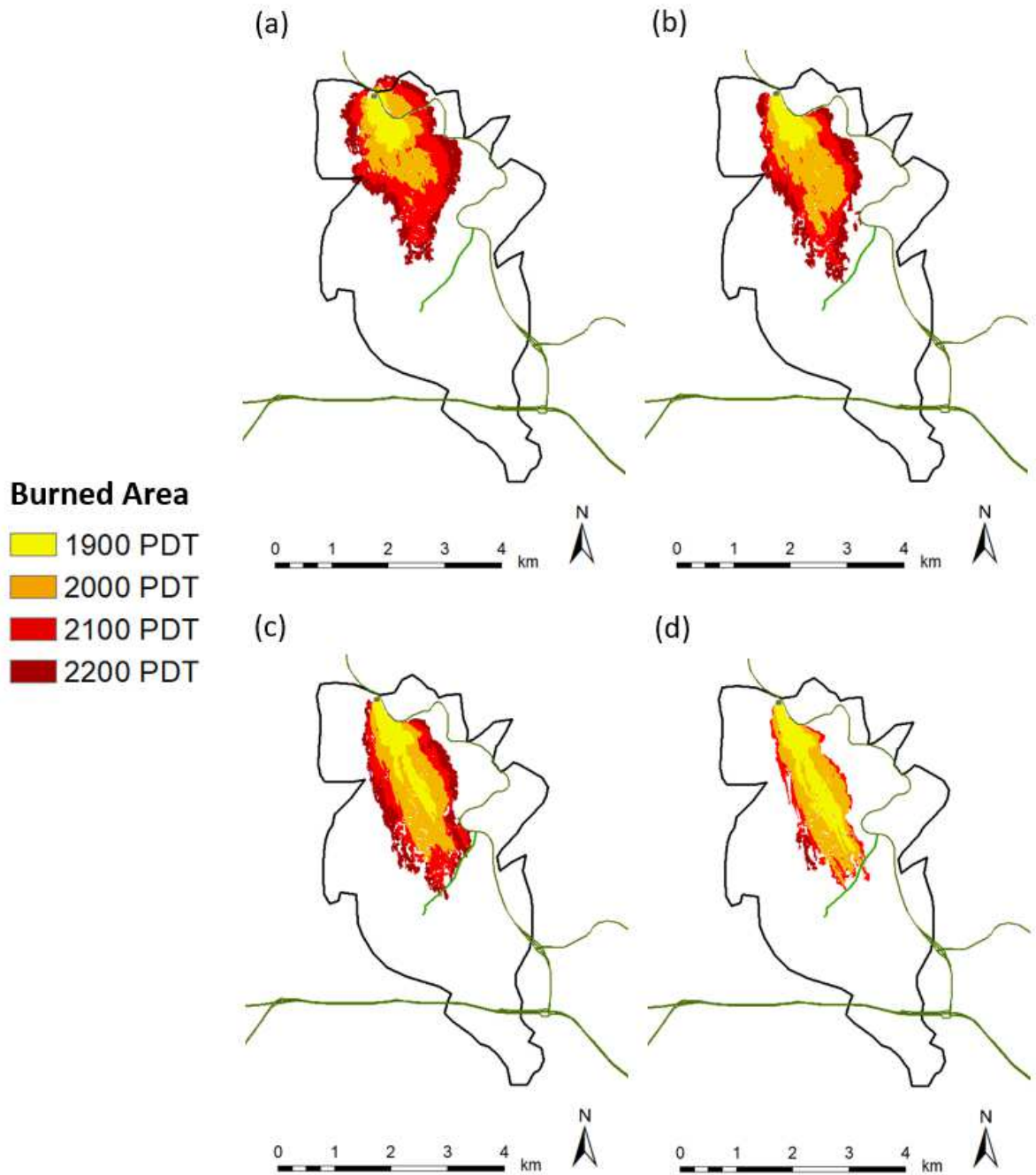


**Figure 3.7** - Painted Cave fire ignition site (light grey dot), official fire perimeter (black polygon), and simulated burn areas (colored polygons) for (a) GF 1.0, (b) GF 1.4, (c) GF 1.7, and (d) GF 2.0. The green lines indicate important reference roads; the dark green line in the southern part of the fire perimeter is Highway 101, the dark green line in the eastern part of the fire perimeter is Highway 154, and the light green line in the middle of the perimeter is San Antonio Creek Rd.



Finney (1998) suggested that FARSITE can produce reasonable fire perimeters with proper judgement and adjustments. In an attempt to simulate very rapid spread during the Painted Cave Fire, we developed an additional FARSITE sensitivity test with an all-grass (FM1) fuel map and a 1.7 GF, retaining all other inputs and parameterizations. Albeit a homogeneous fuel map is unrealistic for this region, the simulated fire spread significantly further and grew more laterally than the original run (Fig. 3.8a). The simulation reached San Antonio Creek Rd within the first two hours and Highway 101 within the first four hours. Three and four hours after ignition, the simulated areas burned were 1097 and 1720 ha and the SM values (compared to the final perimeter) were 0.71 and 0.76, respectively.

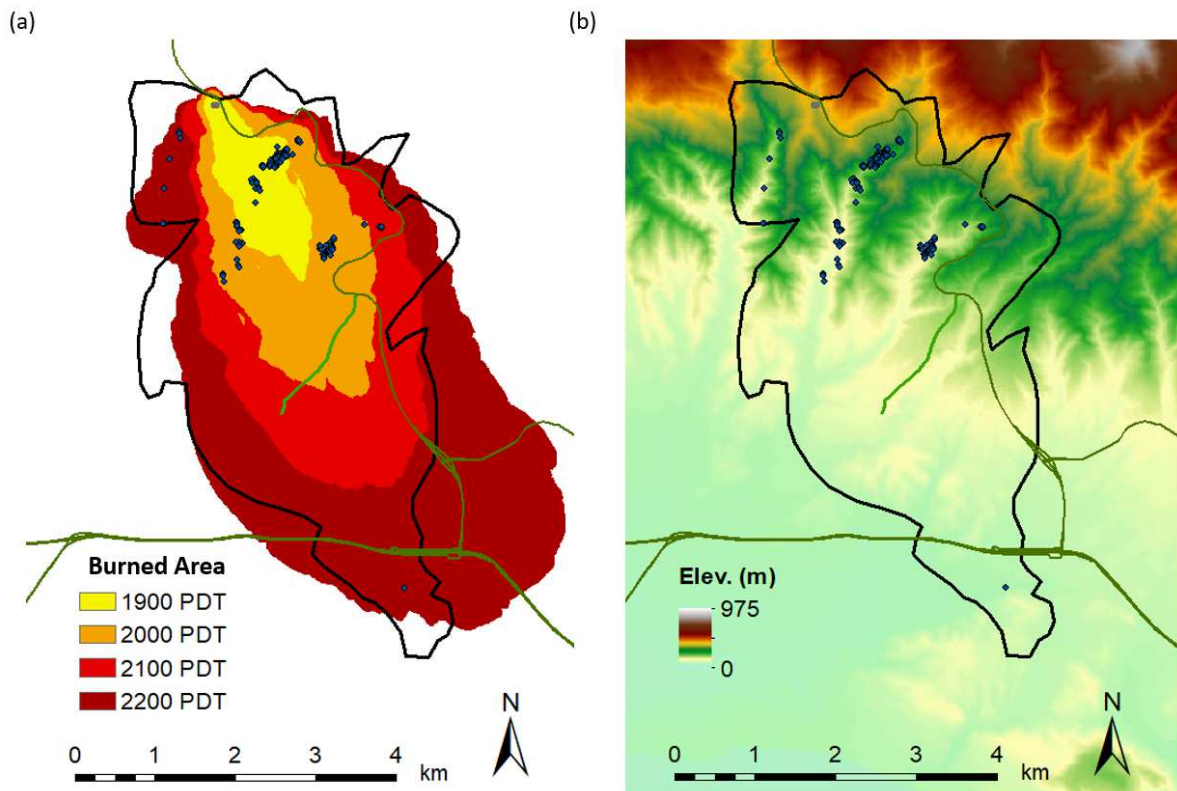


**Figure 3.8** - (a) Similar to Figure 3.7, except the simulated burn areas (colored polygons) are from the all-grass fuel map simulation. Blue dots indicate ember launch locations for spot fires. (b) Same as (a) with elevation colored.

### 3.4.3 Spotting limitations

Understanding spotting is crucial for realistically simulating wildfires in this region, and in many other mountain areas with similar fire weather regimes. Firefighters recall the significant amount of spotting that resulted in the rapid, downslope spread of the Painted Cave fire (Hazard, 2019). However, in our simulations, FARSITE produced spotting only in valleys towards uphill slopes (to the south), shown in Fig. 3.8b. Thus, if spotting was a major factor for the observed rapid spread of this fire, limitations in simulating spotting locations likely led to large underestimations in fire spread, regardless of fuel model or wind speed.

To analyze spotting in FARSITE using a simple simulation, we created east-west oriented ridges and valleys with  $10^\circ$ ,  $20^\circ$ , and  $30^\circ$  slopes. Simulations were performed using a constant fuel model (FM15) and wind (13.41 m/s from  $315^\circ$ ) over the entire domain with a 5% spot probability (same as all previous simulations). Figure 3.9 shows ember launch and landing locations for these simulations. The ridge and valley simulations with slopes less than  $10^\circ$  produced little to no spotting. In simulations with steeper slopes, the ember launch site was always lower in elevation than the landing site, and this was consistent with spotting patterns in the Sherpa and Painted Cave fire simulations (Fig. 3.8). As expected by the spotting equations used in FARSITE (Albini 1979), embers landed in the direction the wind was blowing (southeast in the idealized case). One potential explanation for the lack of upslope-landing embers is that embers were launched during downslope fire spread, but extinguished mid-air from the loss of density and volume during burning (Finney 1998). Another limitation of FARSITE is that only horizontal winds are simulated, precluding a more realistic three-dimensional structure of turbulence in spotting parameterizations. Furthermore, embers are not launched in simulated backing fires due to lower intensities

(Finney 1998), which may contribute to the lack of spotting during our downslope fire spread. To summarize, spotting and the overall simulated wildfire spread during fires driven by strong downslope winds is limited by the inability of landing embers downslope and thresholds for maximum distance or time before ember burnout in FARSITE.

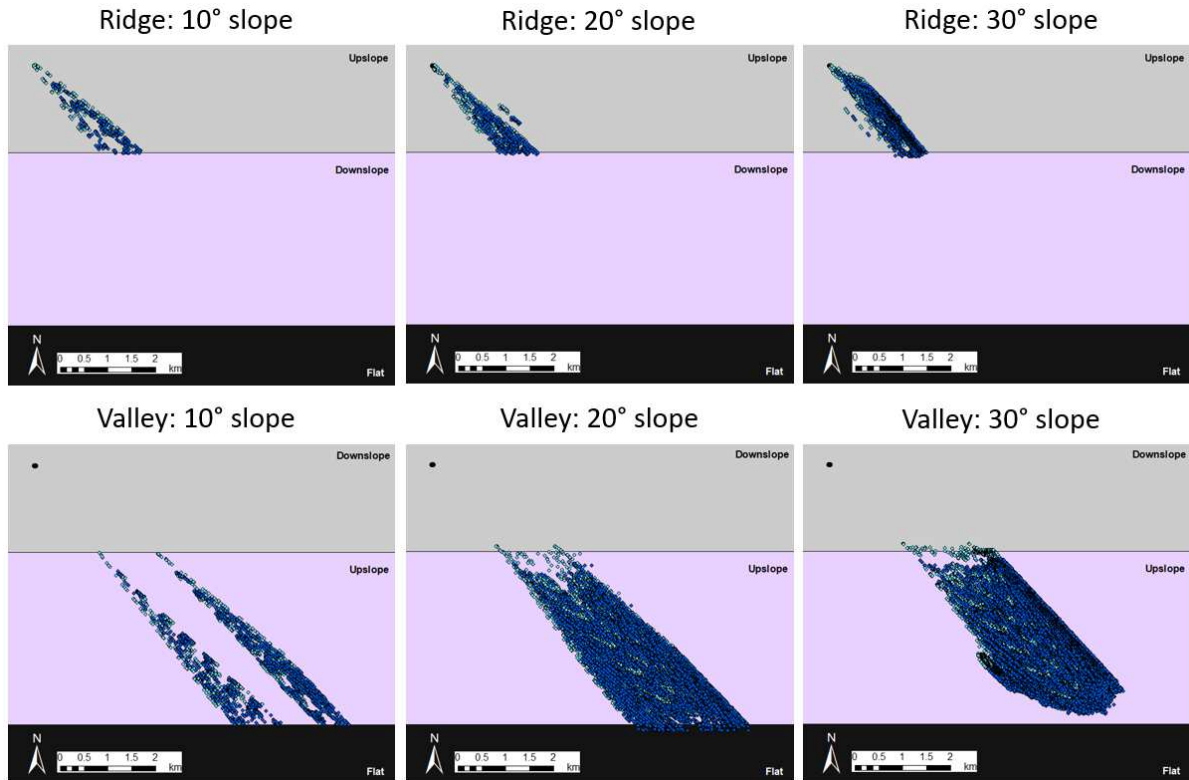


**Figure 3.9** - Spotting launch (light blue) and land (dark blue) locations on an idealized east-west oriented ridge (top) or valley (bottom) with differing slopes from the same ignition point (black dot in upper-left corner). Constant 13.41 m/s (30 mph) NW (315°) winds were applied. The fuel map used was all FM15 (chamise), although results are consistent with other fuel models tested such as FM1 (grass) and FM16 (ceanothus).

#### 3.4. 4 FlamMap comparisons

FlamMap MTT simulations were completed for the Sherpa and Painted Cave fires to examine whether FlamMap has the potential to produce more accurate fire perimeters than

FARSITE when compared to the observed perimeters. As explained in the Introduction, FlamMap and FARSITE are similar in that they use the same surface fire, crown fire, and spotting models. Therefore, the spotting limitations found in FARSITE were also present in FlamMap.

The main difference between the two models is the inability for FlamMap to use temporally-variable gridded winds. To properly compare simulations between FlamMap and FARSITE, both models were run using only the WN raster at the respective ignition times with a 1.7 GF. The Sherpa Fire simulations in both FARSITE and FlamMap underestimated the actual area burned by the fire (Fig. A3.4), primarily because winds later in the evening were stronger than those at the time of ignition, and the simulated fire was run into the unburnable area south of the ignition point, thus extinguishing. This finding highlights the importance of simulating wildfires with models that allow for spatially and temporally variable wind input during extreme winds, although the simulated fire was underestimated in both FARSITE and FlamMap potentially from underestimated wind input.

Figure 3.10 shows the observed Painted Cave Fire perimeter and the FARSITE and FlamMap local time perimeters. While FlamMap underestimated southward spread compared to the observed perimeter, it simulated fire spread further south and laterally. Interestingly, FlamMap and FARSITE produced similar perimeters in the first hour after ignition, but FlamMap spread more west, south, and east in all subsequent hours. The simulated fires grew to approximately the same southward point, near San Antonio Creek Rd, before significantly slowing spread. Upon investigation, WN produced slower winds in this region that likely decelerated southward fire spread. The differences shown in Figure 3.10 likely result from inherent differences in the model's equations; FARSITE uses Huygen's wave propagation principle to simulate wildfire spread, whereas FlamMap MTT



calculates fire behavior at each grid cell individually (Papadopoulos and Pavlidou 2011). Importantly, the same spotting limitations were evident in both models, which led to the significant underestimation in spread during the Painted Cave Fire. This is essential to understand when applying these models in operational settings for emergency management and evacuation planning, particularly in regions with complex terrain and downslope of mountains.

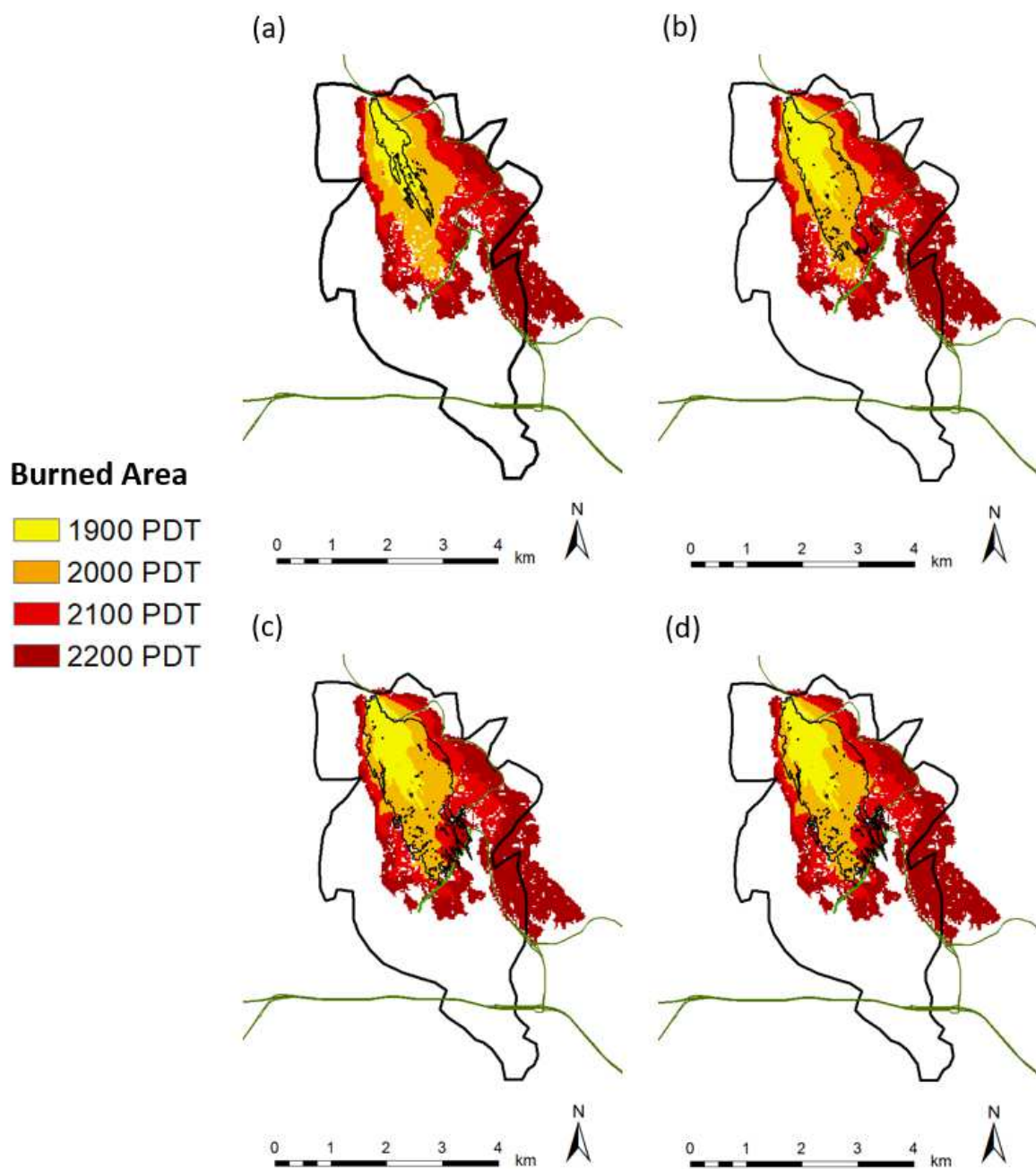


**Figure 3.10** - Same as Figure 3.7 with the FlamMap and FARSITE burn areas (thin, black polygons) at (a) 1900, (b), 2000, (c) 2100, and (d) 2200 PDT.

### 3.5 Conclusions

This study investigates the performance of FARSITE in simulating rapidly spreading wildfires on the southern slopes of the SYM in coastal Santa Barbara. Understanding wildfire risk is especially important in the wildland-urban interface in areas such as coastal Santa Barbara, where advances in evacuation planning and emergency management preparedness will increase resilience to these natural hazards. This study is also applicable to other regions where downslope windstorms are frequent. Two case studies in coastal Santa Barbara County were selected to simulate wildfires significantly influenced by extreme fire weather conditions associated with downslope winds known as Sundowners. The 2016 Sherpa Fire and the 1990 Painted Cave Fire were simulated using FARSITE by downscaling 1 km WRF output run to 100 m resolution using WN. In Sherpa Fire simulations, perimeters were generally underestimated with a 1.0 and 1.4 GF applied to WN rasters, and overestimated with a 1.7 GF except for the 1900 PDT perimeter, which underestimated the area burned by less than 10 ha. In all cases, the final simulated burned areas did not reproduce the substantial southwestward growth of the actual fire. This exposes the inability of the SM to account for directional differences of the burned areas under examination. In general, utilizing a wind downscaling software and applying a gust factor produced more accurate fire perimeters for the Sherpa Fire.

In contrast, all simulated Painted Cave Fire perimeters were underestimated, including the all-grass fuel map simulation which produced the fastest fire spread. We hypothesize that these discrepancies can be largely explained by enhanced spotting during this event, visually documented by fire fighters. The wind inputs to FARSITE and FlamMap are two-dimensional. Consequently, the simulations are unable to track embers lofted into terrain following wind fields which would likely land downslope more quickly than the

simulations allow. Understanding the spotting limitations found here in FARSITE and FlamMap is exceedingly important for operational purposes, especially for wildfires in complex terrain or during downslope fire spread. Another factor that may have caused the underestimated growth rate is the algorithm the fire model uses to assimilate the fuel characteristics of the various dead and live components, especially the different sizes. A concurrent study currently in publication review suggests that maintaining the size characteristics of the fine fuels may enhance the simulated spread rates (Fujioka 2020).

FARSITE has the potential to provide reliable perimeters for simulating wildfires in Santa Barbara influenced by Sundowner winds, although it may not capture extreme cases with large amounts of spotting downslope of the mountains. Future work should be carried out to estimate the spatiotemporal variability of the gust factor during Sundowner events and apply a methodology to gridded wind data for use in wildfire modeling. This would be particularly important in regions with complex terrain and highly variable wind and gust patterns. The authors believe inherent limitations in FARSITE are preventing downslope spotting and thus underestimating simulated fire perimeters in cases with a significant amount of spotting. This problem may be solved by examination and improvement of the spotting algorithm in the software. Additionally, FARSITE can be useful for wildfires spreading upslope, or in cases where downslope winds are not the dominant variable controlling fire spread, although this requires further testing. Advancing knowledge on weather and fire modeling in coastal Santa Barbara will increase resilience and allow for improved fire risk management and city planning.

### 3.6 Acknowledgements

This research was supported by the NSF-PREEVENTS ICER—1664173. This research was completed with the help of the National Weather Service – Los Angeles/Oxnard Office and the Montecito, Santa Barbara, and Santa Barbara County Fire Departments. Discussions on the evolution of wildfire perimeters with Chief Rob Hazard (Santa Barbara County Fire Department) and with John Benoit on FARSITE were much appreciated. The authors acknowledge the National Center for Atmospheric Research, Computational and Information Systems Laboratory, Boulder, CO.

### 3.7 Appendix

**Table A3.1** - Descriptions of all abbreviations used in the manuscript.

ABBREVIATION	DESCRIPTION
FARSITE	Fire Area Simulator
FM	Fuel model
GF	Gust factor
KSBA	Santa Barbara Airport weather station
MTT	Minimum Travel Time
RAWS	Remote Automatic Weather Station
RHWC1	Refugio weather station
SM	Sorensen Metric
SYM	Santa Ynez Mountains
WN	WindNinja
WRF	Weather Research and Forecasting model

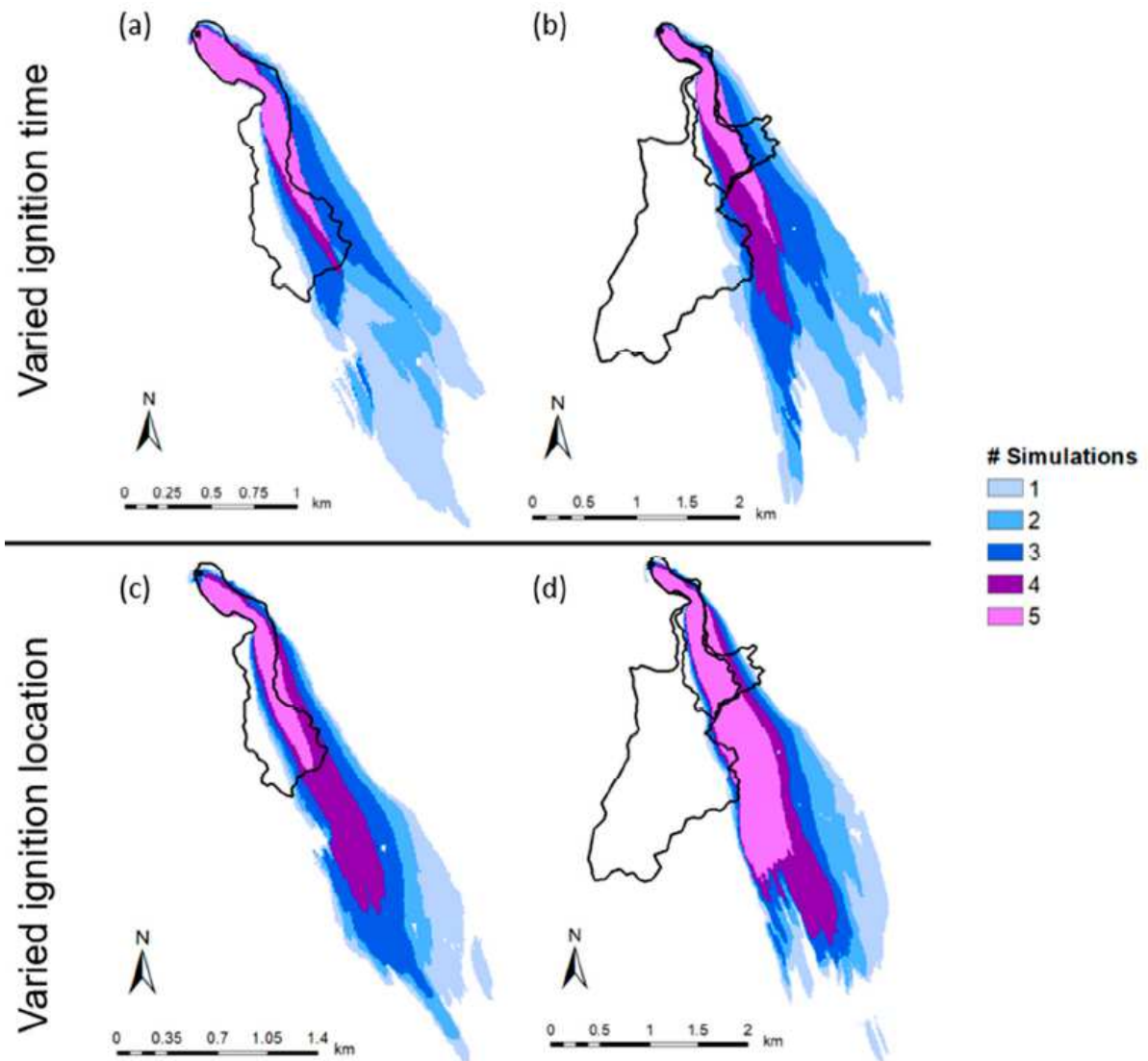


**Figure A3.1** - (a) Sherpa fire ignition site (black dot), observed perimeters (black contours) at 1800 PDT, and the count of overlapping simulations three hours after ignition in the varied ignition time simulations. (b) Same as (a) with the 1900 PDT observed perimeter added and the count of overlapping simulations four hours after ignition. (c) same as (a) with the count of overlapping simulations in the varied location simulations three hours after ignition. (d) same as (c) four hours after ignition.

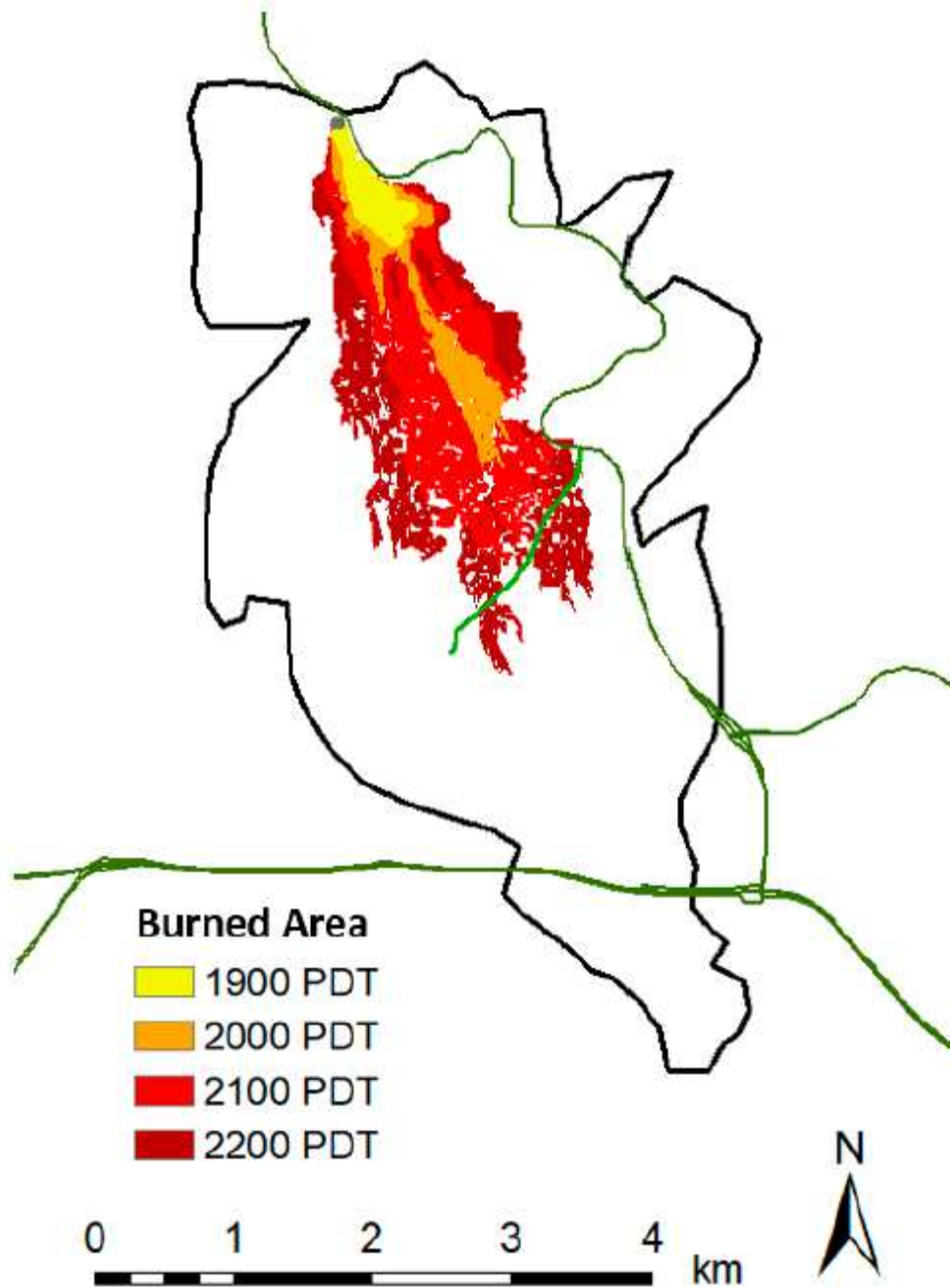


**Figure A3.2** - Same as Figure 3.7c using the original fuel map (shown in Figure 3.2c).

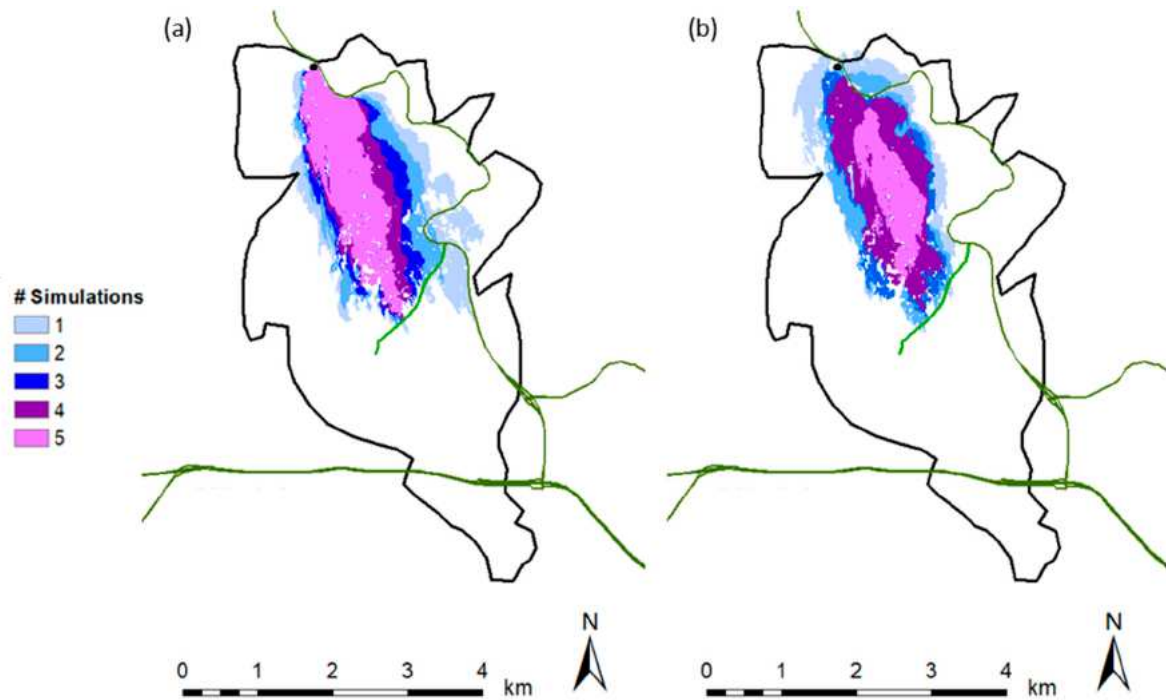


**Figure A3.3** - Painted Cave fire perimeter and reference roads (see Figure 3.7 for details). Colored polygons in (a) are the count of simulations four hours after ignition in the varied ignition time simulations. (b) The count of simulations four hours after ignition using varied ignition locations.



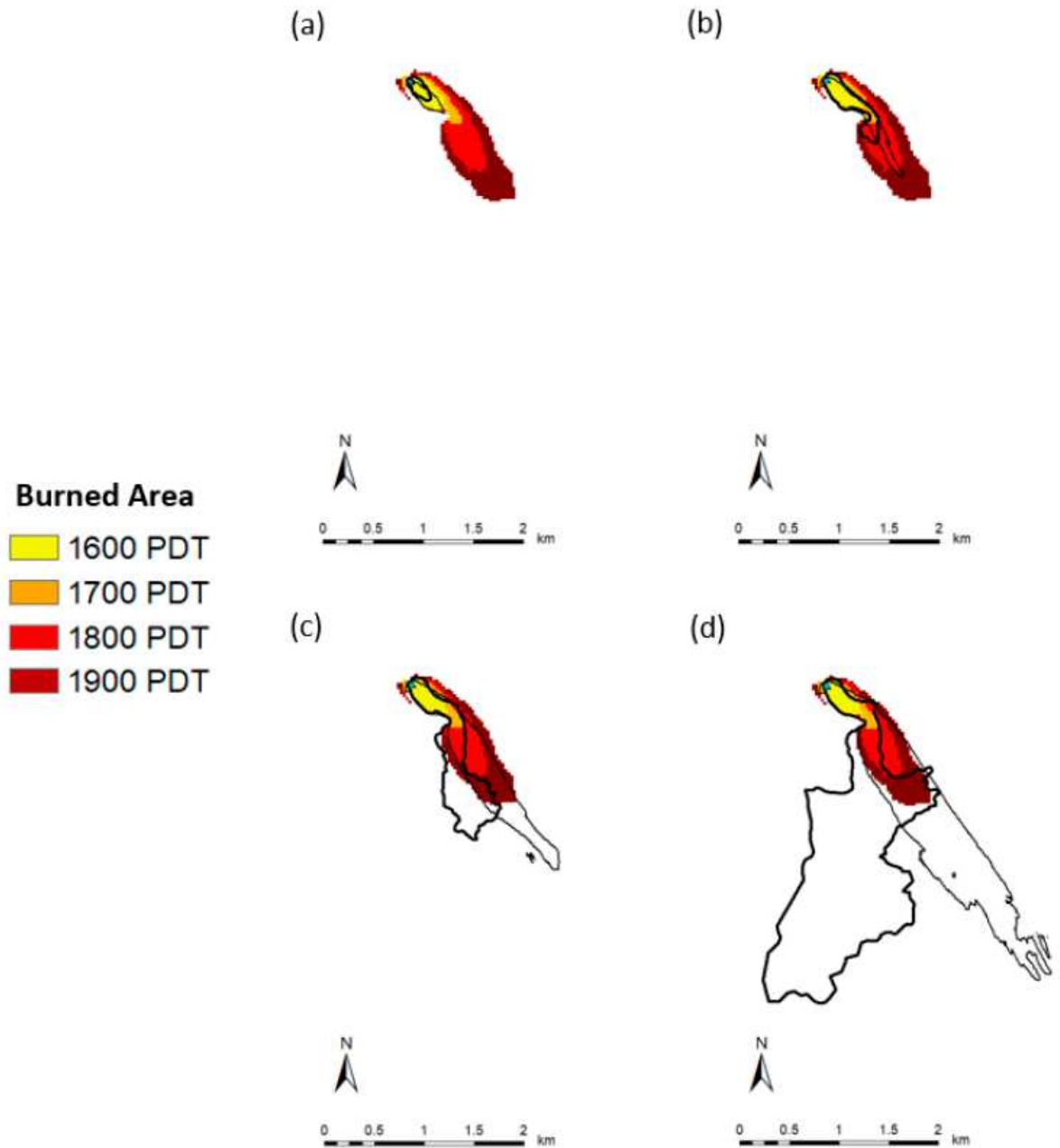


**Figure A3.4** - Sherpa fire perimeters with FlamMap local time burnt areas (colored polygons), FARSITE perimeters (thin black polygons), and observed perimeters (thick black polygons) at (a) 1600 PDT, (b) 1700 PDT, (c) 1800 PDT, and (d) 1900 PDT.

### 3.8 References

Abatzoglou, J.T., and Williams, A.P. (2016) Impact of Anthropogenic Climate Change on Wildfire across Western US Forests. *Proc. Natl. Acad. Sci. US*, 113, 11770–11775.

- Albini, F.A. (1979) Spot Fire Distance from Burning Trees: A Predictive Model; Intermountain Forest and Range Experiment Station, Forest Service, U.S. Department of Agriculture: Ogden, UT, USA; Volume 56.
- Anderson, H.E. (1982) Aids to Determining Fuel Models for Estimating Fire Behavior; General Technical Report INT-GTR-122; U.S. Department of Agriculture, Forest Service, Intermountain Forest and Range Experiment Station: Ogden, UT, USA.
- Andrews, P.L. (2007) BehavePlus Fire Modeling System: Past, Present, and Future. In Proceedings of the 7<sup>th</sup> Symposium on Fire and Forest Meteorological Society, Bar Harbor, ME, USA, 23–25.
- Arca, B., Duce, P., Laconi, M., Pellizzaro, G., Salis, M., and Spano, D. (2007) Evaluation of FARSITE Simulator in Mediterranean Maquis. *Int. J. Wildland Fire*, 16, 563.
- Blier, W. (1998) The Sundowner Winds of Santa Barbara, California. *Weather Forecast.* 13, 702–716.
- Butler, B.W., and Forthofer, J.M. (2004) Gridded Wind Data: What Is It and How Is It Used? Report on file; U.S. Department of Agriculture, Forest Service, Rocky Mountain Research Station, Fire Sciences Lab.: Missoula, MT, USA.
- Butler, B.W., Forthofer, J.M., Finney, M., McHugh, C., Stratton, R., and Bradshaw, L. (2006) The impact of high resolution wind field simulations on the accuracy of fire growth predictions. *For. Ecol. Manag.* 234, S85.
- Cannon, F., Carvalho, L.M.V., Jones, C., Hall, T., Gomberg, D., Dumas, and J., Jackson, M. (2017) WRF Simulation of Downslope Wind Events in Coastal Santa Barbara County. *Atmos. Res.* 191, 57–73.
- Cao, Y., and Fovell, R.G. (2018) Downslope Windstorms of San Diego County. Part II: Physics Ensemble Analyses and Gust Forecasting. *Weather Forecast.* 33, 539–559.

- Carvalho, L., Duine, G.-J., Jones, C., Zigner, K., Clements, C., Kane, H., Gore, C., Bell, G., Gamelin, B., Gomberg, D., et al. (2020) The Sundowner Winds Experiment (SWEX) Pilot Study: Understanding Downslope Windstorms in the Santa Ynez Mountains, Santa Barbara, California. *Mon. Wea. Rev.* 148, 1519–1539.
- Catchpole, W., Bradstock, R., Choate, J., Fogarty, L., Gellie, N., McCarthy, G., McCaw, W., Marsden-Smedley, and J., Pearce, G. (1998) Co-operative Development of Equations for Heathland Fire Behaviour. In *Proceedings of the 3<sup>rd</sup> International Conference of Forest Fire Research*, Luso, Portugal, 16–20.
- Cayan, D.R., Maurer, E.P., Dettinger, M.D., Tyree, M., and Hayhoe, K. (2008) Climate Change Scenarios for the California Region. *Clim. Chang.* 87 (Suppl. 1), 21–42.
- Coen, J.L., Cameron, M., Michalakes, J., Patton, E.G., Riggan, P.J., and Yedinak, K.M. (2013) WRF Fire: Coupled Weather–Wildland Fire Modeling with the Weather Research and Forecasting Model. *J. Appl. Meteor. Climatol.* 52, 16–38.
- Countryman, C.M., and Philpot, C.W. (1970) Physical Characteristics of Chamise as a Wildland Fuel; Res. Pap. PSW-66; U.S. Department of Agriculture Forest Service: Berkeley, CA, USA.
- Countryman, C.M. (1972) The Fire Environment Concept; USDA Forest Service: Berkeley, CA, USA; p. 15.
- Diffenbaugh, N.S., Swain, D.L., and Touma, D. (2015) Anthropogenic Warming Has Increased Drought Risk in California. *Proc. Natl. Acad. Sci. USA*, 112, 3931–3936.
- Duine, G.J., Jones, C., Carvalho, L., and Fovell, R. (2019) Simulating Sundowner Winds in Coastal Santa Barbara: Model Validation and Sensitivity. *Atmosphere*, 10, 155.
- Faivre, N., Jin, Y., Goulden, M.L., and Randerson, J.T. (2014) Controls on the Spatial Pattern of Wildfire Ignitions in Southern California. *Int. J. Wildland Fire*, 23, 799.

- Farr, T.G., Rosen, P.A., Caro, E., Crippen, R., Duren, R., Hensley, S., Kobrick, M., Paller, M., Rodriguez, E., Roth, L., et al. (2007) The Shuttle Radar Topography Mission. *Rev. Geophys.* 45.
- Finney, M.A., and Ryan, K.C. (1995) Use of the FARSITE Fire Growth Model for Fire Prediction in U.S. National Parks. In *Proceedings of the International Emergency Management and Engineering Conference*, San Diego, CA, USA, 9–12, 183–189.
- Finney, M.A. (1998) FARSITE: Fire Area Simulator-Model Development and Evaluation; Research Paper RMRS-RP-4; U.S. Department of Agriculture, Forest Service, Rocky Mountain Research Station: Fort Collins, CO, USA,.
- Finney, M.A. (1998) Efforts at Comparing Simulated and Observed Fire Growth Patterns; Final Report INT-95066-RJVA; Systems for Environmental Management: Missoula, MT, USA.
- Finney, M.A., Bradshaw, L., and Butler, B.W. (2006) Modeling Surface Winds in Complex Terrain for Wildland Fire Incident Support; Final Report for JFSP Funded Project #03-2-1-04; U.S. Department of Agriculture, Forest Service: Fort Collins, CO, USA, 1–10.
- Forghani, A., Cechet, B., Radke, J., Finney, M., and Butler, B. (2007) Applying Fire Spread Simulation over Two Study Sites in California Lessons Learned and Future Plans. In *Proceedings of the 2007 IEEE International Geoscience and Remote Sensing Symposium*, Barcelona, Spain, 23–28, 3008–3013.
- Forthofer, J.M., Shannon, K., and Butler, B.W. (2009) Simulating Diurnally Driven Slope Winds with WindNinja; U.S. Department of Agriculture, Forest Service, Rocky Mountain Research Station: Missoula, MT, USA.

- Forthofer, J.M., Butler, B.W., and Wagenbrenner, N.S. (2014) A Comparison of Three Approaches for Simulating Fine-Scale Surface Winds in Support of Wildland Fire Management. Part I. Model Formulation and Comparison against Measurements. *Int. J. Wildland Fire*, 23, 969.
- Forthofer, J.M., Butler, B.W., McHugh, C.W., Finney, M.A., Bradshaw, L.S., Stratton, R.D., Shannon, K.S., and Wagenbrenner, N.S. (2014) A Comparison of Three Approaches for Simulating Fine-Scale Surface Winds in Support of Wildland Fire Management. Part II. An Exploratory Study of the Effect of Simulated Winds on Fire Growth Simulations. *Int. J. Wildland Fire*, 23, 982.
- Fovell, R.G., and Cao, Y. (2017) The Santa Ana Winds of Southern California: Winds, Gusts, and the 2007 Witch Fire. *Wind Struct.* 24, 529–564.
- Fovell, R., and Gallagher, A. (2018) Winds and Gusts during the Thomas Fire. *Fire*, 1, 47.
- Fujioka, F.; Chapman University, Orange, CA, USA. Personal communication, 2020.
- Gibson, C., and Gorski, C. (2003) FARSITE Weather Streams from the NWS IFPS System. In *Proceedings of the 5<sup>th</sup> Symposium on Fire and Forest Meteorology*, 1-4. Available online:  
[https://gacc.nifc.gov/nwcc/content/products/intelligence/FARSITE\\_Wx\\_DataGenerator.pdf](https://gacc.nifc.gov/nwcc/content/products/intelligence/FARSITE_Wx_DataGenerator.pdf) (accessed on 9 July 2020).
- Gollner, M., Trouv'e, A., Altintas, I., Block, J., De Callafon, R., Clements, C., Cortes, A., Ellicott, E., Filippi, J.B., Finney, M., et al. (2015) Towards data-driven operational wildfire spread modeling. In *Report of the NSF-Funded Wildfire Workshop*; University of Maryland: College Park, MD, USA.
- Greig-Smith, P. (1983) *Quantitative Plant. Ecology*; University of California Press: Berkeley, CA, USA, Volume 9.

- Hanes, T.L. (1965) Ecological Studies on Two Closely Related Chaparral Shrubs in Southern California. *Ecol. Monogr.* 35, 213–235.
- Hanes, T.L. (1973) The Vegetation Called Chaparral. In *Proceedings of the Symposium on Living with the Chaparral*, Sierra Club, San Francisco, CA, USA, 30–31, 1–5.
- Hatchett, B.J., Smith, C.M., Nauslar, N.J., and Kaplan, M.L. (2018) Brief Communication: Synoptic-Scale Differences between Sundowner and Santa Ana Wind Regimes in the Santa Ynez Mountains, California. *Nat. Hazards Earth Syst. Sci.*, 18, 419–427.
- Hazard, R. Chief of Santa Barbara County Fire Department, Santa Barbara, CA, USA. Personal communication, 2019.
- Horel, J., Splitt, M., Dunn, L., Pechmann, J., White, B., Ciliberti, C., Lazarus, S., Slemmer, J., Zaff, D., and Burks, J. (2002) Mesowest: Cooperative Mesonets in the Western United States. *Bull. Am. Meteorol. Soc.*, 83, 211–226.
- Jahdi, R., Darvishsefat, A.A., Etemad, V., and Mostafavi, M.A. (2014) Wind Effect on Wildfire and Simulation of Its Spread (Case Study: Siahkal Forest in Northern Iran). *J. Agric. Sci. Technol.*, 16, 1109–1121.
- Keeley, J.E., Safford, H., Fotheringham, C.J., Franklin, J., and Moritz, M. (2009) The 2007 southern California wildfires: Lessons in complexity. *J. For.*, 107, 287–296.
- Kochanski, A.K., Jenkins, M.A., Mandel, J., Beezley, J.D., Krueger, S.K. (2013) Real Time Simulation of 2007 Santa Ana Fires. *For. Ecol. Manag.*, 294, 136–149.
- Meerdink, S.K., Roberts, D.A., Roth, K.L., King, J.Y., Gader, P.D., and Koltunov, A. (2019) Classifying California plant species temporally using airborne hyperspectral imagery. *Remote Sens. Environ.*, 232, 111308.
- Mitchell, J.W. (2013) Power Line Failures and Catastrophic Wildfires under Extreme Weather Conditions. *Eng. Fail. Anal.*, 35, 726–735.

- Moritz, M.A. (2003) Spatiotemporal Analysis of Controls on Shrubland Fire Regimes: Age Dependency and Fire Hazard. *Ecology*, 84, 351–361.
- Moritz, M.A., Moody, T.J., Krawchuk, M.A., Hughes, M., and Hall, A. (2010) Spatial Variation in Extreme Winds Predicts Large Wildfire Locations in Chaparral Ecosystems: Extreme Winds and Large Wildfires. *Geophys. Res. Lett.*, 37.
- Murray, A., Carvalho, L.M.V., Church R.L., Jones, C., Roberts, D., Xu, J., Zigner, K., and Nash, D. (2020) Coastal vulnerability under extreme weather. *Applied Spatial Analysis and Policy*.
- Papadopoulos, G.D., and Pavlidou, F.-N. A (2011) Comparative Review on Wildfire Simulators. *IEEE Syst. J.*, 5, 233–243.
- Parise, M., and Cannon, S.H. (2012) Wildfire Impacts on the Processes That Generate Debris Flows in Burned Watersheds. *Nat. Hazards*, 61, 217–227.
- Perry, G.L.W., Sparrow, A.D., and Owens, I.F. (1999) A GIS-Supported Model for the Simulation of the Spatial Structure of Wildland Fire, Cass Basin, New Zealand. *J. Appl. Ecol.*, 36, 502–518.
- Peterson, S.H., and Stow, D.A. (2003) Using Multiple Image Endmember Spectral Mixture Analysis to Study Chaparral Regrowth in Southern California. *Int. J. Remote Sens.*, 24, 4481–4504.
- Peterson, S.H., Morais, M.E., Carlson, J.M., Dennison, P.E., Roberts, D.A., Moritz, M.A., and Weise, D.R. (2009) Using HFire for Spatial Modeling of Fire in Shrublands; Research Paper PSW-RP-259; U.S. Department of Agriculture, Forest Service, Pacific Southwest Research Station: Albany, CA, USA.
- Peterson, S.H. (2011) Fire Risk in California. Ph.D. Thesis, University of California, Santa Barbara, CA, USA.

- Phillips, D.R., Waldrop, T.A., and Simon, D.M. (2006) Assessment of the FARSTE model for predicting fire behavior in the Southern Appalachian Mountains. General Technical Report SRS-92. In Proceedings of the 13th Biennial Southern Silvicultural Research Conference; U.S. Department of Agriculture, Forest Service: Asheville, NC, USA, 521–525.
- Richardson, L.A., Champ, P.A., and Loomis, J.B. (2012) The Hidden Cost of Wildfires: Economic Valuation of Health Effects of Wildfire Smoke Exposure in Southern California. *JFE*, 18, 14–35.
- Roth, K.L., Dennison, P.E., and aRoberts, D.A. (2012) Comparing Endmember Selection Techniques for Accurate Mapping of Plant Species and Land Cover Using Imaging Spectrometer Data. *Remote Sens. Environ.*, 127, 139–152.
- Rothermel, R.C. (1972) A Mathematical Model. for Predicting Fire Spread in Wildland Fuels; Research Paper INT-115; U.S. Department of Agriculture, Forest Service, Intermountain Forest and Range Experiment Station: Ogden, UT, USA, 40.
- Rothermel, R.C., and Philpot, C.W. (1973) Predicting Changes in Chaparral Flammability. *J. For.*, 71, 640–643.
- Rothermel, R.C. (1983) How to Predict the Spread and Intensity of Forest and Range Fires; Research Paper INT-GTR-143; U.S. Department of Agriculture, Forest Service, Intermountain Forest and Range Experiment Station: Ogden, UT, USA.
- Ryan, G. (1996) Downslope Winds of Santa Barbara, California; NOAA Technical Memorandum NWSWR-240; Scientific Services Division, Western Region: Salt Lake City, UT, USA.
- Salis, M. (2008) Fire Behavior Simulation in Mediterranean Marquis using FARSITE. Ph.D. Thesis, University of Sassari, Sassari, Italy.



- Salis, M., Ager, A.A., Arca, B., Finney, M.A., Bacciu, V., Duce, P., and Spano, D. (2013) Assessing Exposure of Human and Ecological Values to Wildfire in Sardinia, Italy. *Int. J. Wildland Fire*, 22, 549.
- Salis, M., Arca, B., Alcasena, F., Arianoutsou, M., Bacciu, V., Duce, P., Duguay, B., Koutsias, N., Mallinis, G., Mitsopoulos, I., et al. (2016) Predicting Wildfire Spread and Behaviour in Mediterranean Landscapes. *Int. J. Wildland Fire*, 25, 1015–1032.
- Santa Barbara County Fire Department. Available online: <https://www.sbcfire.com> (accessed on 10 June 2020).
- Scott, J.H., and Burgan, R.E. (2005) Standard Fire Behavior Fuel Models: A Comprehensive Set for Use with Rothermel's Surface Fire Spread Model; General Technical Report RMRS-GTR-153; U.S. Department of Agriculture, Forest Service, Rocky Mountain Research Station: Ft. Collins, CO, USA.
- Scott, J.H. (2006) Comparison of Crown Fire Modeling Systems Used in Three Fire Management Applications; RMRS-RP-58; U.S. Department of Agriculture, Forest Service, Rocky Mountain Research Station: Ft. Collins, CO, USA.
- Skamarock, W.C., and Klemp, J.B. (2008) A Time-Split Nonhydrostatic Atmospheric Model for Weather Research and Forecasting Applications. *J. Comput. Phys.*, 227, 3465–3485.
- Smith, C.M., Hatchett, B.J., and Kaplan, M.L. (2018) Characteristics of Sundowner Winds near Santa Barbara, California, from a Dynamically Downscaled Climatology: Environment and Effects near the Surface. *J. Appl. Meteor. Climatol.*, 57, 589–606.
- Stephens, S.L., Weise, D.R., Fry, D.L., Keiffer, R.J., Dawson, J., Koo, E., Potts, J., and Pagni, P.J. (2008) Measuring the Rate of Spread of Chaparral Prescribed Fires in Northern California. *Fire Ecol.*, 4, 74–86.

- Stratton, R.D. (2006) Guidance on Spatial Wildland Fire Analysis: Models, Tools, and Techniques; General Technical Report RMRS-GTR-183; U.S. Department of Agriculture, Forest Service, Rocky Mountain Research Station: Ft. Collins, CO, USA.
- Stratton, R.D. (2009) Guidebook on LANDFIRE Fuels Data Acquisition, Critique, Modification, Maintenance, and Model Calibration; Technical Report Np. RMRS-GTR-220; U.S. Department of Agriculture, Forest Service, Rocky Mountain Research Station: Fort Collins, CO, USA, 1–54.
- Sukup, S. (2013) Extreme Northeasterly Wind Events in the Hills above Montecito, California; Western Region Technical Attachment NWS WR-1302; NWS Western Region: Salt Lake City, UT, USA, 21.
- Syphard, A.D., Clarke, K.C., and Franklin, J. (2007) Simulating Fire Frequency and Urban Growth in Southern California Coastal Shrublands, USA. *Landsc. Ecol.*, 22, 431–445.
- Syphard, A.D., Radeloff, V.C., Keuler, N.S., Taylor, R.S., Hawbaker, T.J., Stewart, S.I., and Clayton, M.K. (2008) Predicting Spatial Patterns of Fire on a Southern California Landscape. *Int. J. Wildland Fire*, 17, 602.
- Syphard, A.D., and Keeley, J.E. (2015) Location, Timing and Extent of Wildfire Vary by Cause of Ignition. *Int. J. Wildland Fire*, 24, 37.
- Van Wagner, C.E. (1977) Conditions for the start and spread of crown fire. *Can. J. For. Res.*, 7, 23–34.
- Weise, D.R., and Regelbrugge, J. (1997) Recent Chaparral Fuel Modeling Efforts. In Chaparral Fuel Modeling Workshop, 11–12. Available online:

<http://web.physics.ucsb.edu/~complex/research/hfire/fuels/refs/weiseregel1997.pdf>  
(accessed on 9 July 2020).

Westerling, A.L., Cayan, D.R., Brown, T.J., Hall, B.L., and Riddle, L.G. (2004) Climate, Santa Ana Winds and Autumn Wildfires in Southern California. *Eostransactions Am. Geophys. Union*, 85, 289–296.

Westerling, A.L., Hidalgo, H.G., Cayan, D.R., and Swetnam, T.W. (2006) Warming and Earlier Spring Increase Western U.S. Forest Wildfire Activity. *Science*, 313, 940–943.

## **4. Wildfire Risk in Complex Terrain and in the Coastal Santa Barbara Wildland-Urban Interface during Extreme Winds**

### **4.1 Abstract**

Each year, wildfires ravage the western U.S. and change the lives of millions of inhabitants. Situated in southern California, coastal Santa Barbara has witnessed devastating wildfires in the past decade, with nearly all ignitions started by humans. Therefore, estimating the risk imposed by accidental ignitions in this fire-prone region will further increase resilience toward wildfires. The main objective of this study is to provide a spatial analysis of regions at high risk of fast wildfire spread, particularly in the first two hours, considering varying scenarios of ignition locations and atmospheric conditions. To achieve this goal, multiple wildfire simulations were conducted using the Fire Area Simulator (FARSITE) with three ignition modeling methods and three wind scenarios. The first ignition method considers ignitions randomly distributed in 500 m buffers around previously observed ignition sites. Since these ignitions are mainly clustered around roads and trails, the second method considers a 50 m buffer around this built infrastructure, with ignition points randomly sampled from within this buffer. The third method assumes a Euclidean distance decay around roads and trails up to 1000 m, where the probability of selection linearly decreases further from the transportation paths. The ignition modeling methods were then employed in wildfire simulations with varying wind scenarios during climatological winds and during strong, downslope winds. Under climatological conditions, the simulated fire areas were smaller and the wildfires did not spread far from the ignition locations. In contrast, wildfires ignited during strong, northerly winds quickly spread into the wildland-urban interface (WUI) toward urban areas. The major exit road (HWY 154) was intersected

multiple times in all ignition and wind method combinations, which could impact evacuation route planning and resource allocation.

## **4.2 Introduction**

Destructive wildfires in the western U.S., and especially in California, occur every year greatly impacting the lives of millions of inhabitants. Some of the most impactful wildfires occur in the rapidly-growing wildland-urban interface (WUI), which is the area where communities are intermixed with the surrounding natural environment (Radeloff et al. 2005, 2018, Hammer et al. 2009). More specifically, regions may be divided into smaller classes such as urban, WUI interface, WUI intermix, and rural (Moritz et al. 2014, Kramer et al. 2019). The majority of fatalities, home losses, and fire suppression costs occur in the WUI under critical weather conditions (Moritz et al. 2014), and WUI expansion has increased the probability of ignition and the general wildfire risk (Keeley et al. 2004, Syphard et al. 2007, Faivre et al. 2014, Bryant and Westerling 2014).

Most wildfires are started by humans in southern California (Balch et al. 2017), and in Santa Barbara County, approximately 99% of historical wildfire ignitions are due to humans (Keeley and Syphard 2018). Human expansion into rural areas leads to greater housing developments and increased wildfire risk (Moritz and Knowles 2016, Nauslar et al. 2018, Radeloff et al. 2018). Human-ignited fires occur year-round (Bartlein et al. 2008), and those occurring in the absence of strong winds are relatively easy to control and contain (Jin et al. 2014). According to Balch et al. (2017), human-ignited wildfires account for 84% of all wildfires ignited and 44% of the area burned in the U.S. In Mediterranean California specifically, most anthropogenically-caused wildfires occur in summer and spring, with less

in fall and winter (Balch et al. 2017). Ignition patterns in southern California are related to distance to roads, trails, and human development, as well as slope and fuel type (Syphard et al. 2008, 2012, Faivre et al. 2014). In fact, the distance to road explained about 40% of the ignitions in the Santa Monica Mountains and San Diego County (Syphard and Keeley 2015). Maximum fire frequency occurs in areas with an intermediate level of human activity, though the area burned is less related to this factor (Syphard et al. 2007). Areas with a high probability of ignition and that are prone to extreme winds are of greatest fire risk and attention (Syphard and Keeley 2015).

Three factors, known as the ‘fire triangle,’ control wildfire behavior (Countryman 1972): fuels, topography, and weather. During critical fire weather conditions, wind is the dominant factor in determining fire spread (Moritz 2003, Abatzoglou et al. 2018). In coastal Santa Barbara County, the most critical fire weather is often associated with downslope windstorms on the slopes of the Santa Ynez Mountains (SYM), known as Sundowner winds or Sundowners (Blier 1998, Jones et al. 2020). Sundowners occur year-round and may create critical fire weather conditions as the strong, northerly, and dry winds rapidly spread fires southward toward highly populated areas (Fig. 4.1a). Sundowners have enhanced fire spread in all seasons, particularly in the summer and fall, when the strong winds and dry fuels create large, impactful wildfires (Blier 1998, Cannon et al. 2017, Jones et al. 2020). In fact, more hectares are burned during extreme wind conditions than non-extreme wind conditions (Kolden and Abatzoglou 2018).

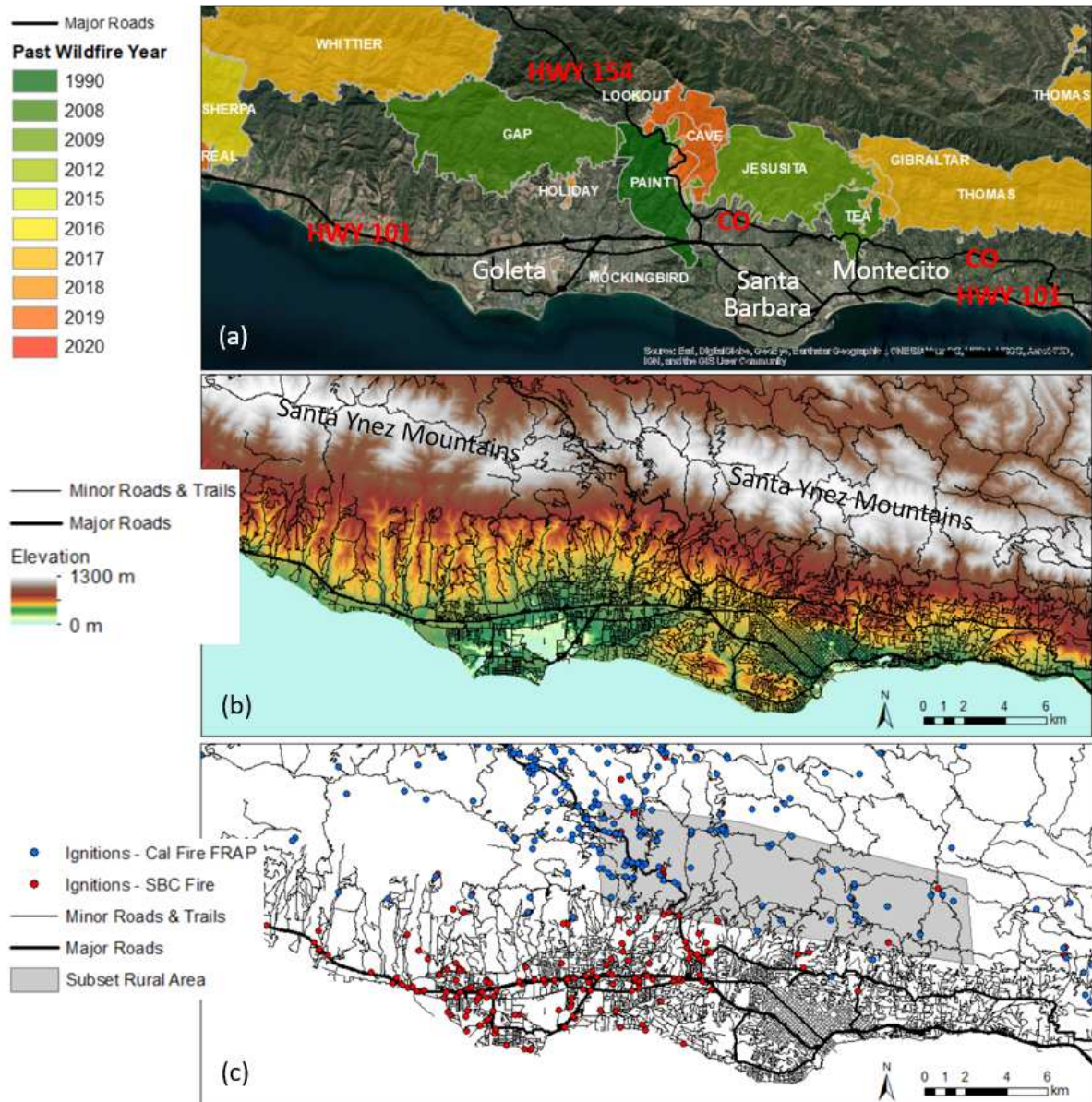


**Figure 4.1** - The area of interest: Coastal Santa Barbara County, CA. (a) Satellite imagery overlaid with previous wildfires (colored polygons), and major roads (thick, black lines and uppercase red text). The label “CO” stands for “Cathedral Oaks Road”. The names of previous wildfire are smaller and in uppercase text, and cities are in larger, sentence-case text. (b) Elevation (colored) and all roads and trails. Major roads are shown as thick lines and minor roads are shown as thinner lines. The mountain range to the north of the cities is labeled. (c) Roads and trails (lines) with previous ignitions overlaid. Color indicates the source of the ignition. The area subset for ignition modeling to the north of the cities is shaded gray.

While a decrease in relative humidity and temperature ramps are seasonally dependent (Blier 1998, Carvalho et al. 2020, Zigner et al. 2021), Sundowners often create critical fire weather conditions due to gusty winds and the depletion of dew point (Zigner et al. 2020, Cannon et al. 2017). The strongest winds are observed in the middle of the SYM mountain slopes, though strong winds may extend into the foothills and onto the coastal plain (Jones et al. 2020, Zigner et al. 2021, Carvalho et al. 2020). Jones et al. (2020) found evidence of three Sundowner regimes: Western, Eastern, and Santa Barbara (a combination of Western and Eastern). The majority of coastal Santa Barbara inhabitants live in a region that is often affected by the “Eastern” or “Santa Barbara” Sundowner, with winds typically exhibiting north-to-northeast direction. Also, few major roads serve the relatively dense population living in the foothills and urban centers. The main east-west road running through coastal Santa Barbara is HWY 101, and the only route heading north from the city of Santa Barbara is HWY 154 (Fig. 4.1a), which has been closed due to multiple wildfires in the past. Another important road is Cathedral Oaks Road (labeled “CO” in Fig. 4.1a), which is the only road that allows access to and from homes in the foothills north of the cities. Some of these wildfires have crossed these major routes, such as the Painted Cave (1990), Tea (2008), Jesusita (2009), and Sherpa (2016) fires, and the Thomas (2017) and Cave (2019) fires have come close (Fig. 4.1a).

Wildfire spread models such as the Fire Area Simulation (FARSITE) (Finney 1998) are commonly used operationally to determine wildfire size, location, and timing in operations for wildfire incidents (Stratton 2006, Scott, 2006, Finney and Ryan 1995, Papadopoulos and Pavlidou 2011). This uncoupled model uses Huygen’s principle of wave propagation and the Rothermel fire spread equations to propagate fires using elliptical shapes at vertices on the fire front based on fuels, topography, and wind (Rothermel 1972).



Zigner et al. (2020) used FARSITE to simulate two significant wildfires in the region: the Sherpa (June 2016) and Painted Cave (1990) fires. They found that FARSITE could simulate wildfires that had a small amount of spotting fairly well (i.e. the Sherpa fire), though the spotting algorithm in FARSITE does not allow for spotting during downslope fire spread and thus underestimated the burned area of fires that had large amounts of spotting (i.e. Painted Cave fire). Despite this limitation, the study demonstrated the utility of simple, uncoupled models like FARSITE in simulating the general behavior of wildfires on the SYM slopes in the first 1-2 hours after ignition, which is useful for the purposes of fast and efficient evacuation.

A handful of previous studies have analyzed fire risk by creating wildfire maps using statistical models (Preisler et al. 2004, Peterson et al. 2011, Moritz et al. 2010, Parisien et al. 2012, Bryant and Westerling 2014). However, no studies have focused on local scales ( $< 1$  km grid spacing) and none have studied Sundowners specifically. The primary goal of this study is to identify areas at the highest wildfire risk under various ignition modeling methods and wind scenarios in the fire-prone coastal Santa Barbara. Given that the majority of wildfires are ignited by humans in Santa Barbara, the following specific questions are investigated: how do the simulated wildfire spread frequency and rate of spread vary with respect to previously observed ignitions and distance to roads and trails? What are the areas at highest risk in Santa Barbara during non-Sundowner conditions and during Sundowner conditions? To answer these questions, we examine three methods of wildfire ignition modeling and perform FARSITE simulations with distinct initial conditions. Wildfire risk maps are assessed based on the frequency of burned areas and minimum time of arrival of the wildfires under various ignition and wind conditions. The paper is organized as follows. Section 4.2 explains the data and methods. Section 4.3 investigates differences in ignition

modeling methods and the resulting variability in risk maps with varying ignition locations and wind scenarios. The discussion and conclusions are provided in Section 4.4.

### ***4.3 Data and Methods***

#### ***4.3.1 Study area***

Situated on the California coast between Los Angeles and San Francisco, picturesque coastal Santa Barbara County is located between the Santa Barbara Channel (part of the Pacific Ocean) to the south and the east-west oriented Santa Ynez Mountains to the north (Fig. 4.1b). Spanning approximately 100 km, the Santa Ynez Mountains (SYM) exhibit a width around 10 km and peaks around 1.2 km, with generally decreasing ridgeline height toward the west. The numerous canyons on the south side of the mountains channel winds, creating localized gusty areas and increasing fire danger especially during Sundowners.

From west to east, the populated cities in coastal Santa Barbara include Goleta, Santa Barbara, and Montecito, totaling approximately 150,000 people. Many inhabitants live in the SYM foothills or on the mountains, generally within or near the WUI (Murray et al. 2020). Few narrow and winding roads serve these regions, increasing danger in this wildfire-prone region (Fig. 4.1).

#### ***4.3.2 Road and Trail, Ignition, and Historical Wildfire Data***

To complete wildfire ignition modeling, both transportation and ignition data are required. Vectorized road and trail data were provided from the U.S. Forest Service with the

feature class subtype indicated for each segment, allowing for differentiation between major roads, minor roads, and trails (Figs. 4.1b,c).

Ignition data were pulled from two sources. The first ignition data source is from the Santa Barbara County (SBC) Fire Department, which recorded ignitions in Santa Barbara County outside of the Los Padres National Forest (north of the city) since 2007 (data acquired upon request). Until 2016, the U.S. Forest Service (USFS) was not required to report ignitions to the county fire department, hence the sparse ignitions recorded by the SB County Fire Department in rural locations (Matthew Marsh USFS, per. comm.) (Fig. 4.1c). This ignition database ends in 2019 when it was requested by the authors. The second source of ignition data is from the U.S. Forest Service FIRESTAT fire Occurrence database and extends from 1986-2019 (<https://data.fs.usda.gov/geodata/edw/datasets.php>). All ignition points are located within the Los Padres National Forest, filling in the gaps from the SB County dataset (Fig. 4.1c). In both datasets, each ignition point contains data on the ignition date and time, cause, location, containment date and time, incident number, agency, and number of acres burned. While duplicate ignition points were not found within either database, we did determine some duplicates between the two datasets, as determined by matching coordinates and dates. When this occurred, only one data point was used in the statistical analysis. Wildfire perimeter data were pulled from the State of California Fire and Resource Assessment Program (FRAP) fire history database in shapefile format (<https://frap.fire.ca.gov/frap-projects/fire-perimeters>).

#### *4.3.3 Ignition Modeling Methods*

In this study, three ignition modeling methods were used for modeling ignitions in the WUI and in rural parts of the SYM slopes and foothills above the city of Santa Barbara

and Montecito (see gray box in Fig. 4.1c). This region was selected because of the increased risk that wildfires may rapidly spread toward highly populated regions during Sundowner winds. Between the SBC Fire dataset (2007-2019) and FIRESTAT dataset (1986-2019) described in the previous section, eighty-five ignition points have been reported in this area, including the ignition locations of devastating wildfires influenced by Sundowner winds such as the Painted Cave (1990), Tea (2008), Jesusita (2009), and Cave (2019) fires.

For this analysis, we considered 100 ignition sites according to the following methods. In the first method, 500 m buffers were created around previous ignition locations, and new ignition points were randomly sampled from within these buffers (Fig. 4.2a). Since observations show that ignitions tend to be clustered around roads and trails, the second method uses buffers of 50 m around this built infrastructure with ignition points randomly sampled from within this buffer (Fig. 4.2b). The third method assumed a Euclidean distance decay around roads and trails up to 1000 m, where the probability of selection linearly decreased further from the transportation paths (Fig. 4.2c). New ignition points were then quasi-randomly sampled using the spatial weights. A similar method using a linear piecewise function was utilized in Peterson et al. (2011), where the probability of selection from 0-100 m from a road bed was 1 and probability decreased to 0.1 at a distance of 1 km.

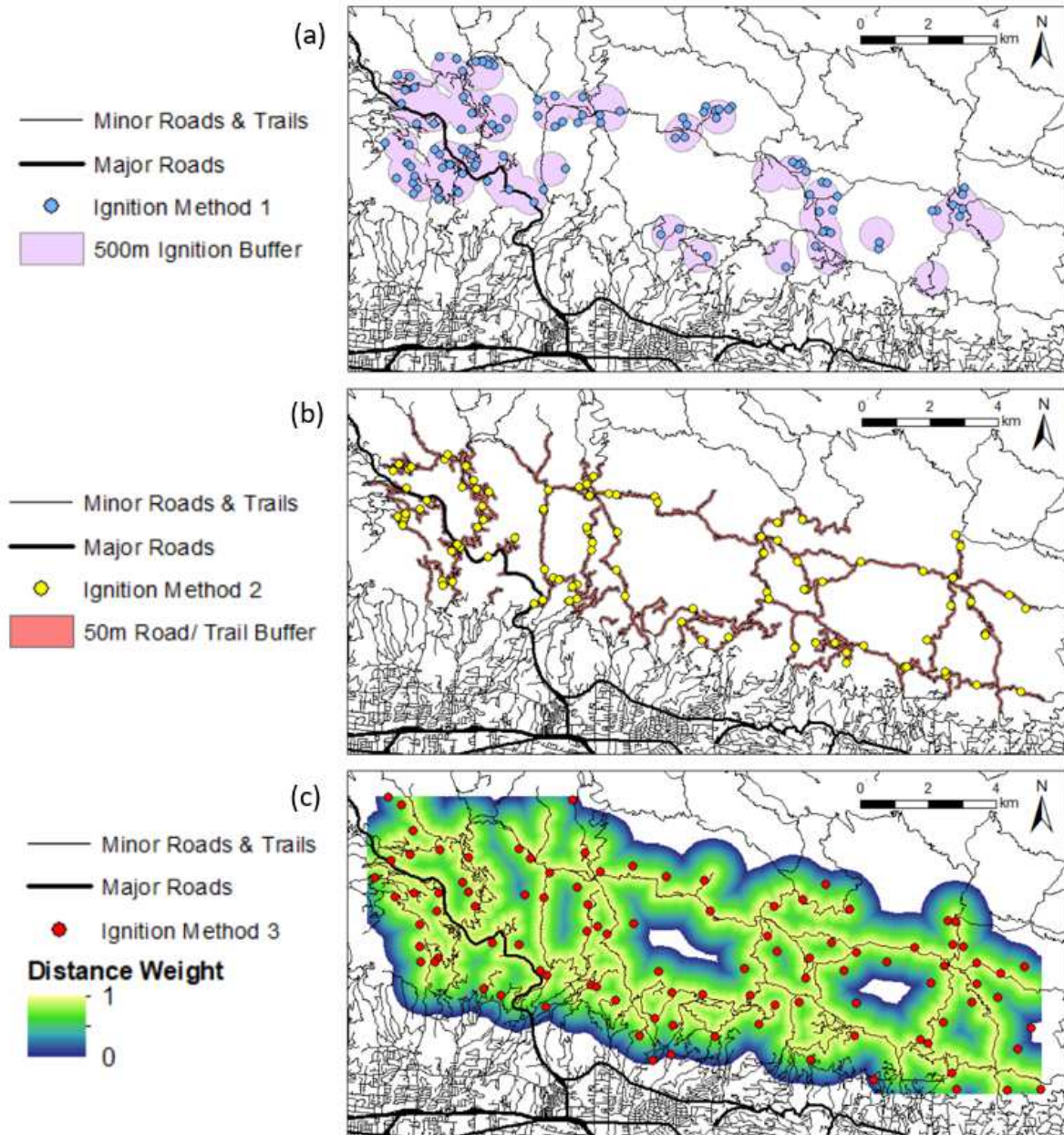


**Figure 4.2** - Results of the three ignition modeling methods overlaid on major (thick lines) and minor (thin lines) roads and trails. (a) Ignition modeling method 1: 500m buffer (purple polygons) around previous ignition points with the modeled ignition points (blue dots). (b) Ignition modeling method 2: 50m buffer (pink polygon) around roads and trails with the modeled ignition points (yellow dots). (c) Ignition modeling method 3: Distance-weight up to 1km (colored) from roads and trails with modeled ignition points (red dots).

#### 4.3.4 FARSITE and Model Input

To determine areas at high wildfire risk and create wildfire risk maps, simulations were performed using the Fire Area simulator (FARSITE) (Finney 1998). The spotting algorithm was disabled due to limitations (Zigner et al. 2020). The fuel map was created by applying canonical discriminant analysis and linear discriminant analysis to 2004 imagery with 12 m spatial resolution from the Airborne Visible/ Infrared Imaging Spectrometer (AVIRIS) (Roth et al. 2012). This imagery was selected because of the high resolution and the lack of burn scars, which may be considered an unburnable fuel. The classified imagery was cross-walked into six fuel models: Short grass, coastal sage scrub, shrubs, dense shrubs, trees/ riparian, suburban/ WUI, and urban/ unburnable (see Zigner et al. 2020 for fuel model details). Fuel moistures in all simulations were the values estimated for the 1990 Painted Cave fire because southern California had been in a drought for years and some of the lowest fuel moistures in this region were recorded in 1990 (Zigner et al. 2020).

To create wildfire risk maps, we performed numerous simulations using FARSITE with gridded wind data for three scenarios: non-Sundowner conditions (climatological), Sundowner conditions, and a Sundowner case study, chosen to represent a case with extreme winds (Fig. 4.3). Jones et al. (2020) created a 30-yr Sundowner climatology (1987-2017) based on simulations at 1 km grid spacing with the Weather Research and Forecasting (WRF) model (Skamarock et al. 2008). Sundowner cases were defined according to the first two eigenmodes of the zonal and meridional wind components from this dataset. In our study, gridded composite (mean) wind rasters during non-Sundowner (climatological) and Sundowner conditions, defined as the Eastern Sundowner regime in Jones et al. (2020), were calculated and created for use in FARSITE (Figs. 4.3a,b). During the Eastern Sundowner regime, downslope winds (with predominant north-northeast direction) are typically stronger

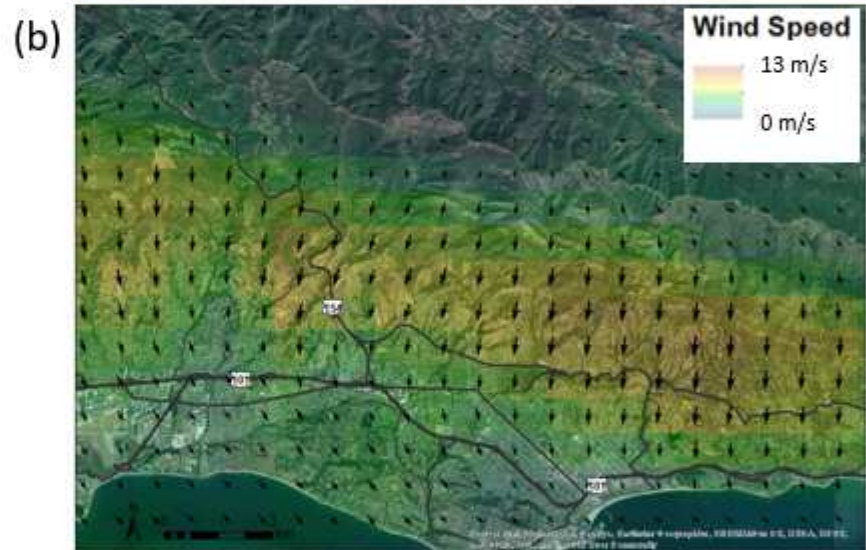
over the eastern portion of the SYM, and affect populated areas in Santa Barbara and Montecito. Wildfires such as the Jesusita and Tea fires rapidly spread during significant Eastern Sundowner regimes (Jones et al. 2020). Since composites may smooth the strongest winds, to investigate a scenario with extreme winds, an additional gridded wind raster was created using a case study of a Sundowner with winds exceeding 13 m/s (or 30 mph) at many grid cells in Goleta, Santa Barbara, and Montecito on April 14th, 2005 (Fig. 4.3c). All other atmospheric variables utilized in FARSITE (i.e. temperature and relative humidity for fuel drying purposes) were maintained constant among simulations and are the same as modeled at the ignition point of the 1990 Painted Cave fire on June 27. Details can be found in Zigner et al. (2020).



Non-Sundowner  
Composite



Sundowner  
Composite



Sundowner  
Case Study

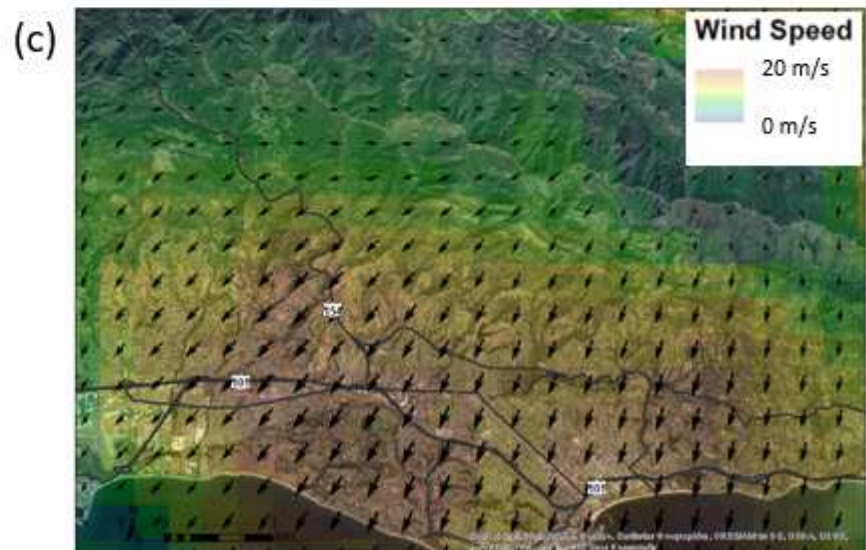




**Figure 4.3** - Gridded wind rasters using WRF data for (a) non-Sundowner composite, (b), Sundowner composite, and (c) Sundowner case study.

Wildfire risk maps were created for the three ignition modeling methods and the three gridded wind scenarios. Fires were ignited at every ignition point for the respective method. The ignition time was set to 2000 PST, aligning with typical Sundowner onset in the central and eastern parts of the SYM (Jones et al. 2020). Fires were simulated using FARSITE for two hours after ignition.

#### **4.4 Impacts of Varied Ignition Modeling Methods on Wildfire Spread**

##### *4.4.1 Ignitions in the WUI: Observations and Modeling*

Generally, the observed ignitions are not uniform throughout the area of study. Rather, they are clustered in the eastern and western parts of the area of interest, around roads and trails on the SYM slopes and foothills (Fig. A4.1). Therefore, the absence of ignitions in the middle of the area of interest in ignition methods 1 and 2 is explained by the lack of previously observed ignitions, and the distribution of roads and trails that were used in the modeling. Modeled ignitions are more dispersed in method 3, resulting in more ignitions to the north (toward the SYM ridgeline) and south (in the WUI and near the city). It is important to note that many ignitions surround HWY 154 (Figs. 4.2,A4.1), which serves as an important evacuation route for the community. This has implications for resource planning and allocation, in addition to evacuation planning.

Figure 4.4 further illustrates the differences among methods by showing the distribution of distances between modeled ignitions with respect to the nearest observed

ignition (Fig. 4.4a), as well as the distances between ignitions and roads and trails (Fig. 4.4b). As expected, the modeled ignitions in method 1 are the closest to the observed ignition locations. Nonetheless, the model value of distance is between 200-300 m and very few are less than 100m away (Fig. 4.4a). The observed ignitions are farthest from the modeled ones in ignition method 3, which is explained by the larger expanse of potential ignition locations allowed by the method (Fig. 4.2c). Concerning the distance between ignitions and the nearest road or trail, the observed ignitions are generally within 100m of a road or trail, but there are a few that are over 500 m away (Fig. 4.4b). Ignition methods 1 and 3 appear similar, with between 10-25% of the ignitions with distances between 0-300 m from roads and trails, and less than 10% of ignitions with distances exceeding 300 m. In contrast, due to the constraints placed on ignition modeling method 2 (50m buffer around roads and trails), all ignitions in that method are much closer and within a 50 m distance.

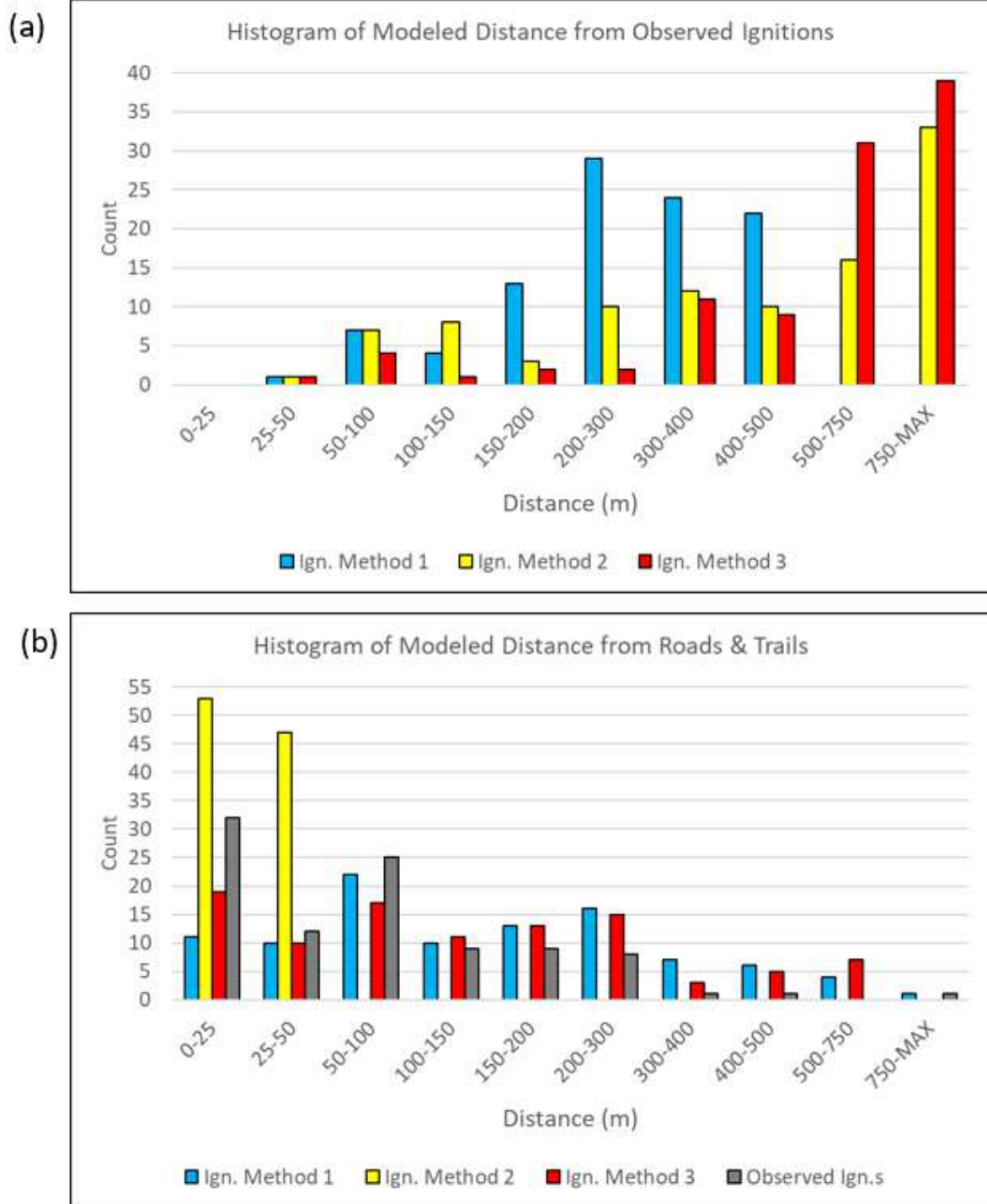


**Figure 4.4** - Bar plots showing the distance of each modeled ignition to the nearest observed observation (a) and road or trail (b). The observed ignition distance to the nearest road or trail is included in (b).

#### *4.4.2 Wildfire spread risk in the WUI using varied ignition methods and wind scenarios*

Here we assess the wildfire risk in the WUI of Santa Barbara using the three proposed ignition methods, focusing on two main aspects: 1) the spatial pattern of ‘hits’, or regions that have been hit by a simulated wildfire within the first three hours of simulations; 2) the time of arrival (TOA) of a wildfire. The analysis of TOA is a metric to evaluate the rapid spread of a wildfire given the ignition point, the set of meteorological and fuel conditions, and the topography.

##### *a) Climatological (non-Sundowner) conditions*

First, we examine differences in ignition methods with mean winds simulated during non-Sundowner conditions (as defined in Section 4.3.4) during all seasons (Fig. 4.5). Relatively weak winds less than 5 m/s were present throughout most of the domain (Fig. 4.3a). For ignition method 1 (buffer around observed ignition locations), some areas near HWY 154 were hit by over 10 simulations and many areas were hit by at least 4 simulations, partially resulting from the cluster of ignitions in this region (Fig. 4.5a). Interestingly, multiple previous wildfires have occurred in this area (Fig. 4.1a), putting this location at high risk of being hit by a wildfire. Two other relatively smaller areas in the eastern part of the region of interest were hit up to 6 times, and very few simulations hit areas the middle. Results were similar for ignition method 2 (buffer around roads and trails); a few areas in the west and east had over 6 hits (Fig. 4.5c). The simulated fires in ignition method 3 covered the most area of all ignition methods because of the greater spread of the ignitions compared to the other two methods. Therefore, this method represents a more random approach to ignitions, while typically maintaining a close distance to roads and trails. Few grid cells were hit by more than 5 simulations, although more areas had at least 1 hit (Fig. 4.5e).

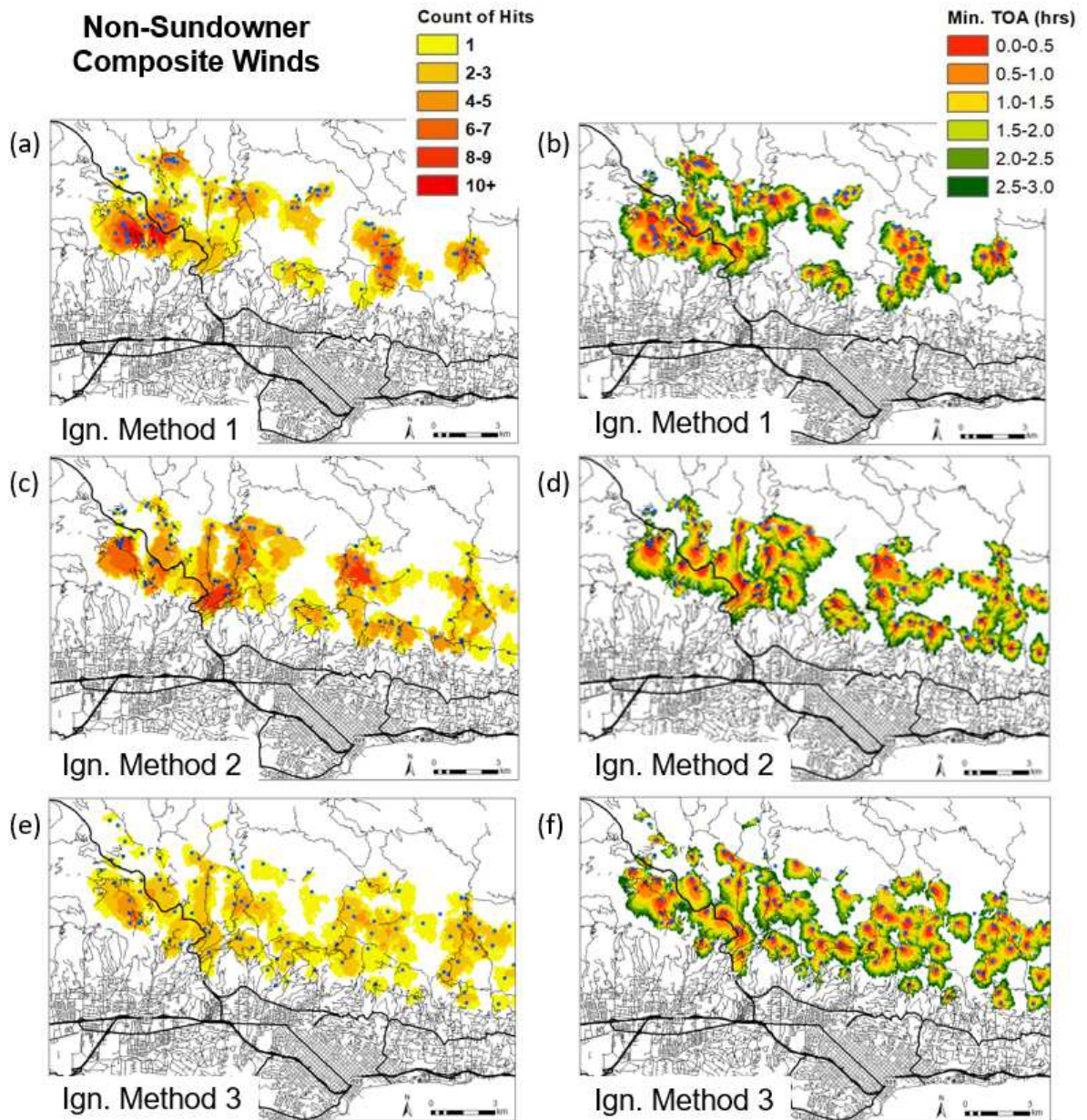


**Figure 4.5** - Maps showing the total number of hits by the 100 simulations at each grid cell (a,c,e) and the earliest time of arrival (TOA) at each grid cell in any of the simulations (b,d,f). Simulations were run using the non-Sundowner composite. Maps (a) and (b) show results from ignition method 1, (c) and (d) show results from ignition method 2, and (e) and (f) show results from ignition method 3. The lines are roads and trails and the blue dots indicate the ignition locations for the specified ignition modeling method.



When considering all 300 simulations that used the climatological winds, regardless of ignition method, an area in the western part of the region of interest and to the west of HWY 154 was hit the most, by up to 25 simulations (~8% of all simulations) (Fig. 4.6a). Multiple areas around HWY 154 and some areas in the west part of the region were hit by at least 13 (~4%) of the simulations. It's important to note that none of these simulations reached the evacuation route Cathedral Oaks road and few spread into the WUI, explained by the absence of strong winds steering the fires in a particular direction.

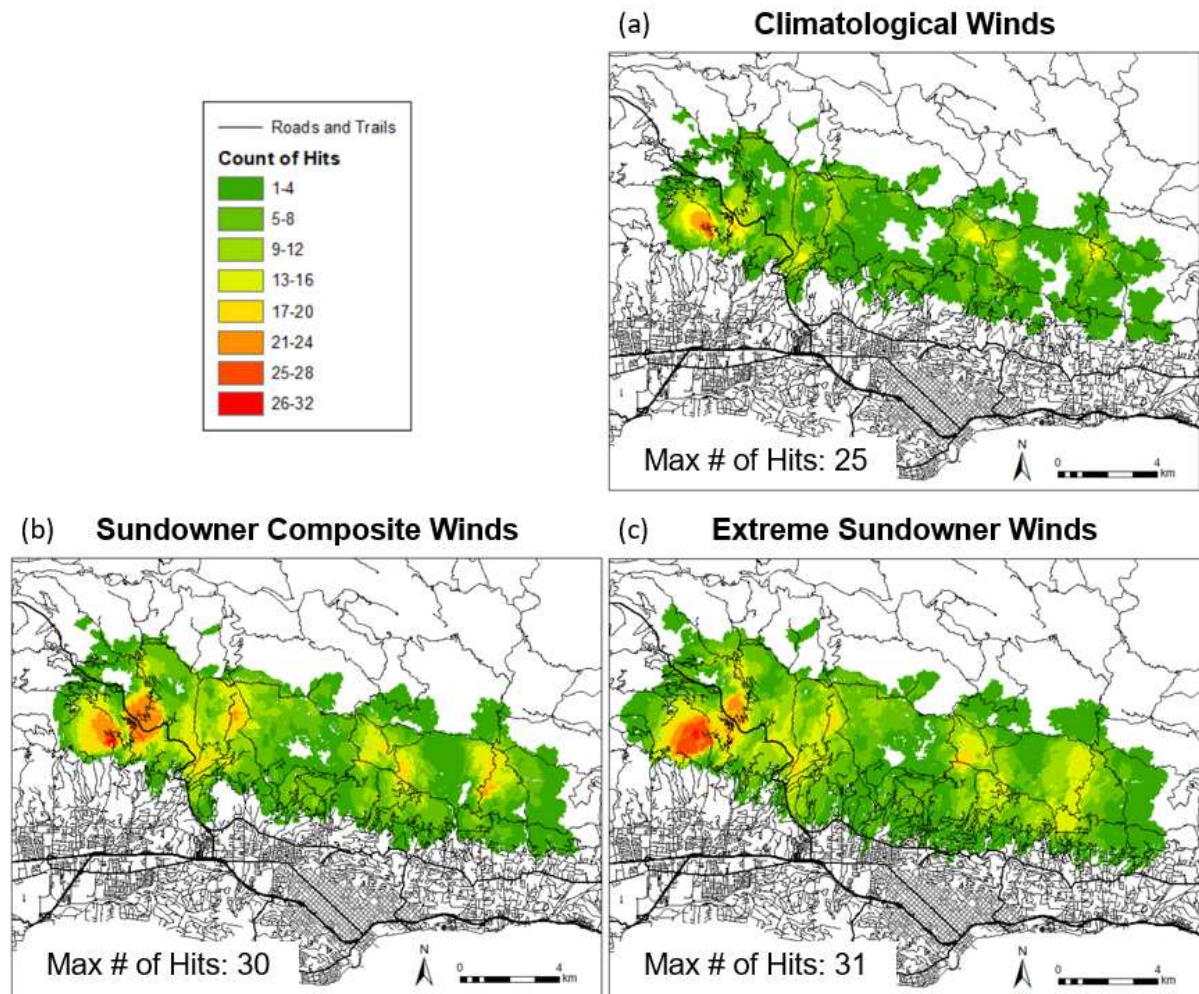


**Figure 4.6** - Similar to the subplots in Figure 4.5 showing the total number of hits at each grid cell, but all ignition methods were combined for (a) climatological wind input, (b) Sundowner composite wind input, and (c) extreme Sundowner case study wind input.

The simulated fires generally did not travel far from the ignition location and spread radially (Fig. 4.5), given the relatively weak winds ( $< 5$  m/s) throughout the domain (Fig. 4.3a). These results imply that during climatological mean wind conditions, fires are less likely to spread quickly toward highly populated areas to the south, assuming that temperatures, relative humidity, fuels, and fuel moistures are comparable.

Boxplots of simulated wildfire sizes separated by the meteorological condition and ignition method at half-hour intervals (from 0.5 h to 3 h after ignition) are shown in Fig. 4.7. Simulated fires were the smallest during climatological conditions, usually growing to less than 30 ha in the first hour and less than 200 ha three hours after ignition (three left boxplots in Fig. 4.7b,f). The largest wildfires were around 300 ha three hours after ignition. Notice that some wildfires were close to 0 ha due to unburnable fuels near the ignition location, which extinguished the fire early after ignition.

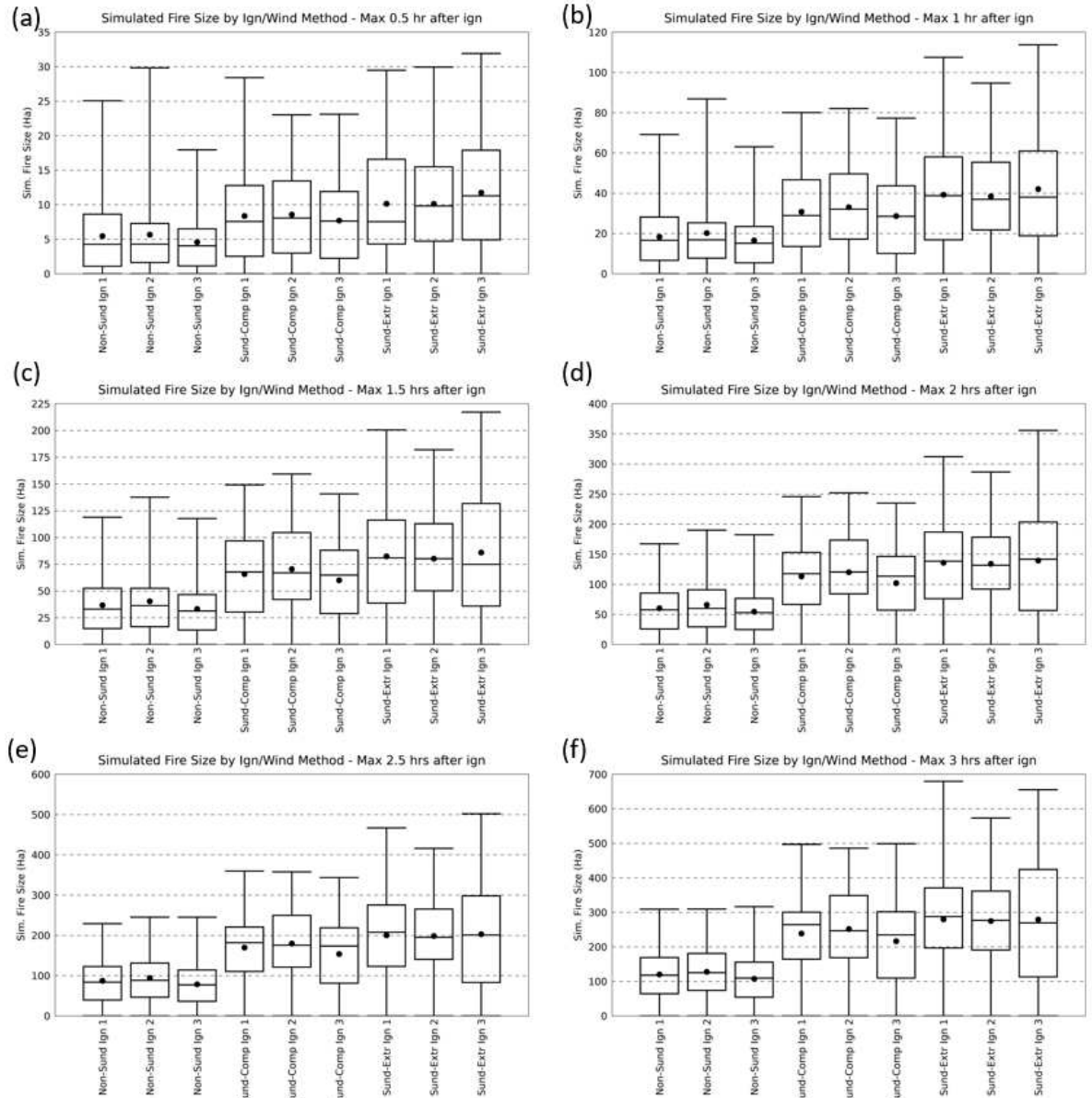


**Figure 4.7** - Boxplots showing the distribution of wildfire sizes for each ignition method and wind scenario combination every half an hour. The whiskers identify the minimum and maximum values and the box includes the lower quartile, median, and upper quartile. No outliers were identified, and the dot indicates the mean. Note the different y-axis values on each histogram.

Figure 4.8 shows the percentage of the total number of grid cells burned in the region of interest (columns) separated according to the number of times a simulation hit a cell in that domain (“# of Hits”, rows) for each ignition method and wind scenario analyzed in this



study. Notice that the sum of each column is  $\sim 100\%$  since only grid cells that were hit by at least one simulation for each ignition method and wind scenario combination were used in these statistics. For instance, during non-Sundowner conditions, simulations indicate that approximately 73%, 81% and 95% of the cells hit in at least 1 of the 100 simulations were hit between 1-3 times for ignition methods 1, 2, and 3, respectively. This means that method 1, which considers buffers around previous ignitions (probability of ignitions is highly non-uniform in the area, see Figs. 1c,2a), resulted in a relatively higher fraction of grid points that were hit more than 6 times, compared to the other 2 methods. In particular, the proximity of ignitions to HWY 154 in method 1 resulted in  $\sim 1.5\%$  of grid cells being hit more than 10 times (Fig. 4.8), whereas ignition methods 2 and 3 had no grid cells hit more than 7 times. Conversely, ignition method 3 assumes the most dispersed ignition locations, and about 56% of the grid cells were only hit once. While the number of hits should change with the number of simulations, the relative percentage of hits separated according to the ignition methods should follow similar pattern. Since methods 1 and 2 have high weight on the previously observed sites of ignitions, these results indicate that the probability of burn is not homogeneous in the region, and there are areas of relatively high risk of being hit by a wildfire, even during relatively calm winds.

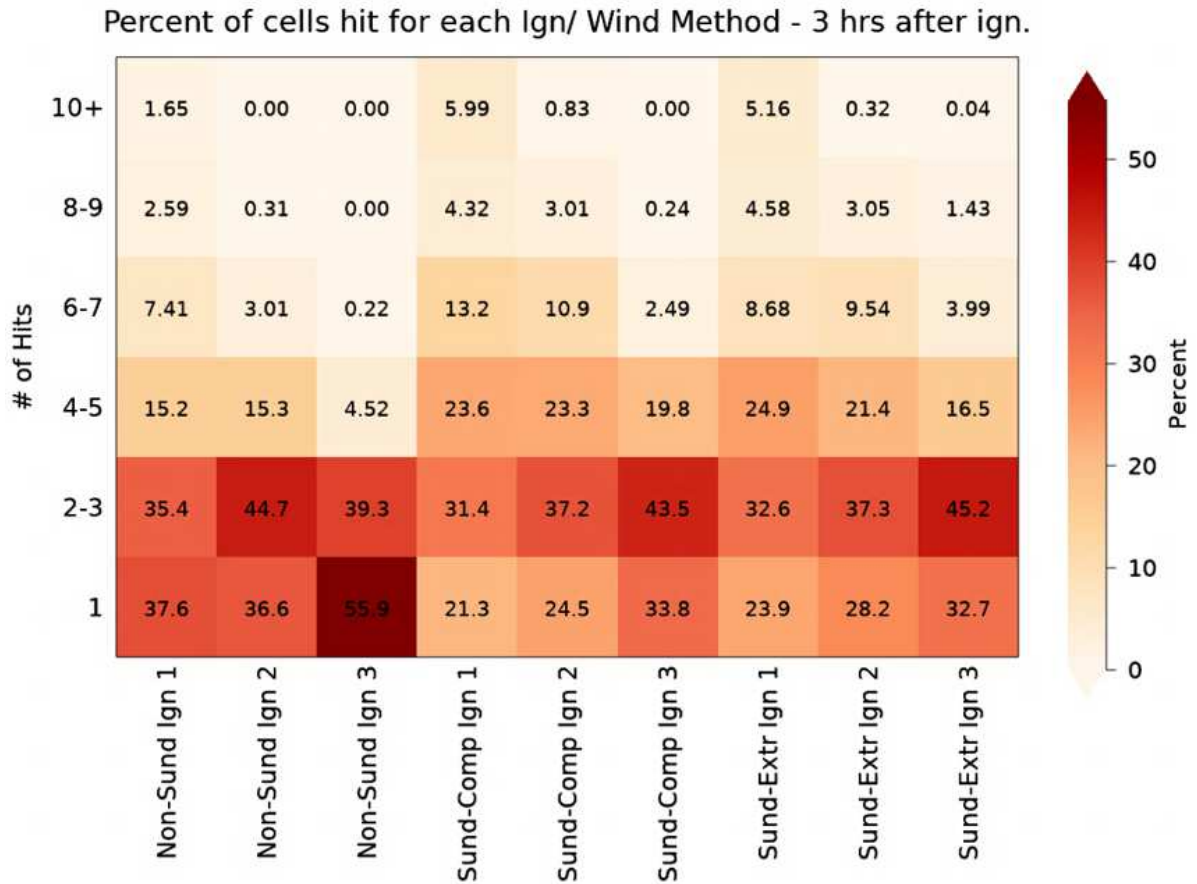


**Figure 4.8** - The percent of grid cells hit out for each “# of Hits” range considering the total number of grid cells hit for a particular ignition method/ wind scenario combination.

*b) Mean Sundowner conditions*

The composite of winds during Sundowners shows strong (~13 m/s) northerly winds present on the southern SYM slopes and in the foothills above Santa Barbara and Montecito (Fig. 4.3b). For all ignition methods, the simulated wildfires grew larger than when the climatological winds were used (Figs. 4.7,4.9) as a result of more southerly spread. In the runs using ignition method 1, the area around HWY 154 is hit more than 10 times for approximately 6% of the entire area burned (Figs. 4.8,4.9). While the middle of the subset area on the SYM slopes was not hit, there were two other clusters in the eastern part that

were hit over 8 times (Fig. 4.9a). For simulations run using ignition methods 2 and 3, there were some area that were hit over 8 times, but generally the fires were more spread out, resulting in a larger area of the entire region of interest hit in at least 1 simulation. Additionally, the east-west running Cathedral Oaks Road was hit by one simulation for ignition method 3, and multiple fires reached relatively close in all ignition modeling methods.

Similar to simulations run using the climatological winds, locations near HWY 154 were hit by the most simulations, up to 30 times when considering all ignition methods (Fig. 4.6b). One differentiation from the climatological simulations is that an additional region of high risk is evident right next to and east of HWY 154. This implies that the stronger winds spread fires that ignited to the northeast of this region further south than when weak winds were present. Furthermore, simulated fires spread more south toward the WUI and highly populated areas. In fact, most of the fires that reached the WUI slowed significantly around 2 hours after ignition (greens in Figs. 4.9b,d,f). This may be due to the fuel model used in the WUI, which is difficult to burn and will slow or stop the fire in the model. It's important to note that FARSITE is generalizing the WUI materials and fuels, and thus these results indicate this region may be at higher risk, but that cannot be proven given the fuel and model limitations.

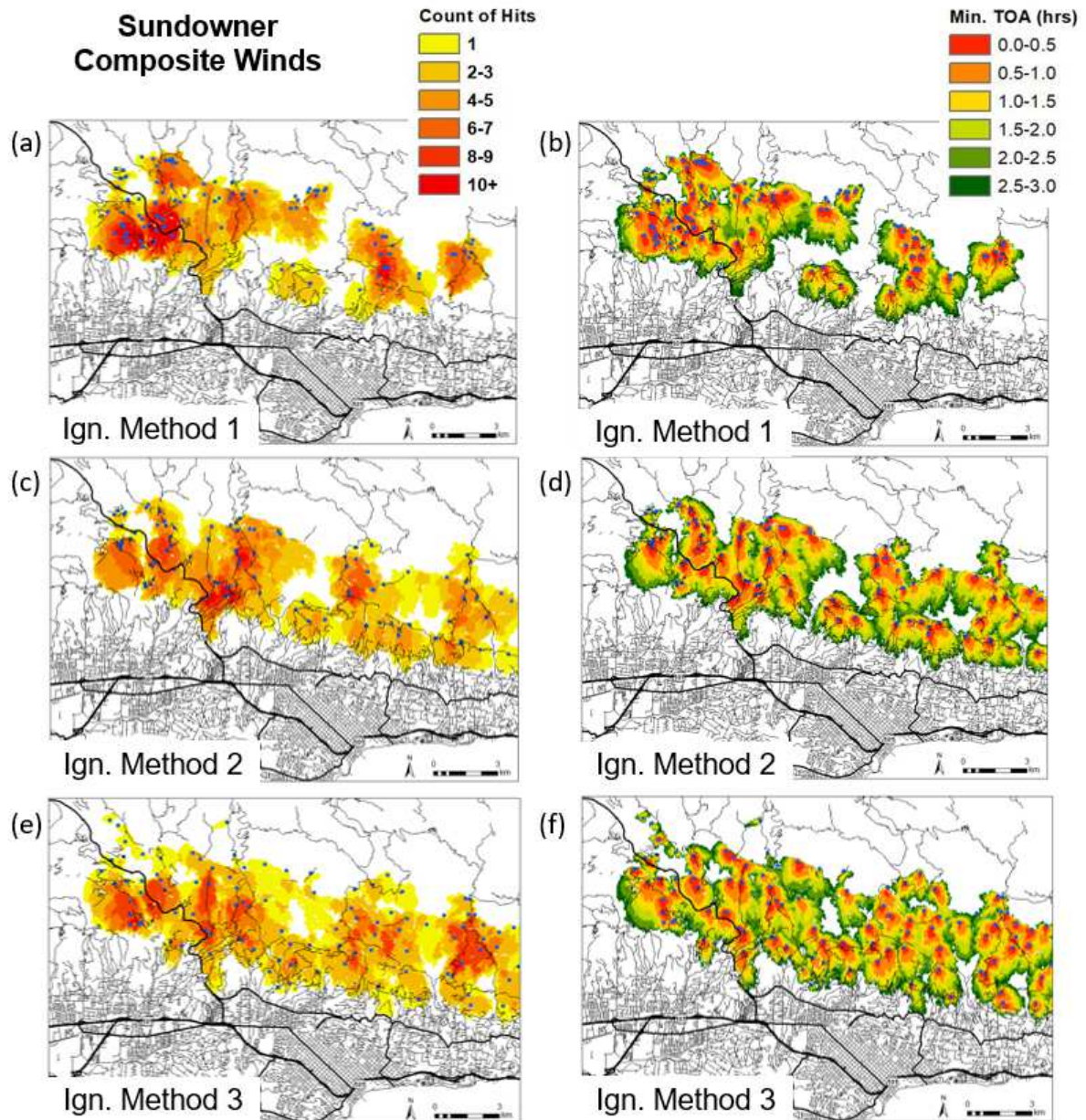


**Figure 4.9** - Same as Figure 4.5, but with wildfire simulations using the Sundowner composite winds.

Overall, most simulated fires that used the Sundowner composite grew larger than those run using the climatological winds (Fig. 4.7), which is expected since strong winds propagated the fires further southward. By 1 hour after ignition, the mean and median fire size were around 30 ha, which grew to over 100 ha by 2 hours after ignition, and the largest

fires were around 500 ha only 3 hours after ignition (Fig. 4.7f). Interestingly, the majority of grid cells burned were hit 2-3 times regardless of ignition method, and ignition method 3 had over 75% of burned grid cells hit 1-3 times and none hit over 9 times (Fig. 4.8).

*c) Extreme Sundowner winds: April 14th, 2005 case study*

During the extreme Sundowner case study, northeasterly winds exceeding 20 m/s were present across the southern SYM slopes and over the coastal cities (Fig. 4.3c). These strong winds rapidly spread the simulated wildfires southwest toward urban areas (Fig. 4.10). Similar to the previous runs using ignition method 1, HWY 154 was a hot spot for wildfire activity since many ignitions were nearby, and there was an area in the east that was hit many times as well. Cathedral Oaks Road, which is a significant evacuation route for many communities in the WUI, was reached by 5 simulations in ignition method 1 (Fig. 4.10a), and these fires spread quickly into the city, particularly within the first 1.5 hours (red, orange, and yellow in Fig. 4.10b). For ignition methods 2 and 3, the majority of the southern SYM slopes was hit in at least one simulation (Fig. 4.10c,e). For ignition method 2, Cathedral Oaks Road was hit by 5 simulations, and it was hit by over 10 simulations in ignition method 3, in part due to the closer proximity of ignition points to urban areas. It is important to note that with ignition method 3, 2 simulations reached Cathedral Oaks Road within half an hour after ignition (Fig. 4.10f). This implies that during Sundowners with strong winds over the WUI, wildfires ignited in the foothills near the city may reach urban areas exceptionally fast, and it may be best to have firefighting crews and resources ready to act.



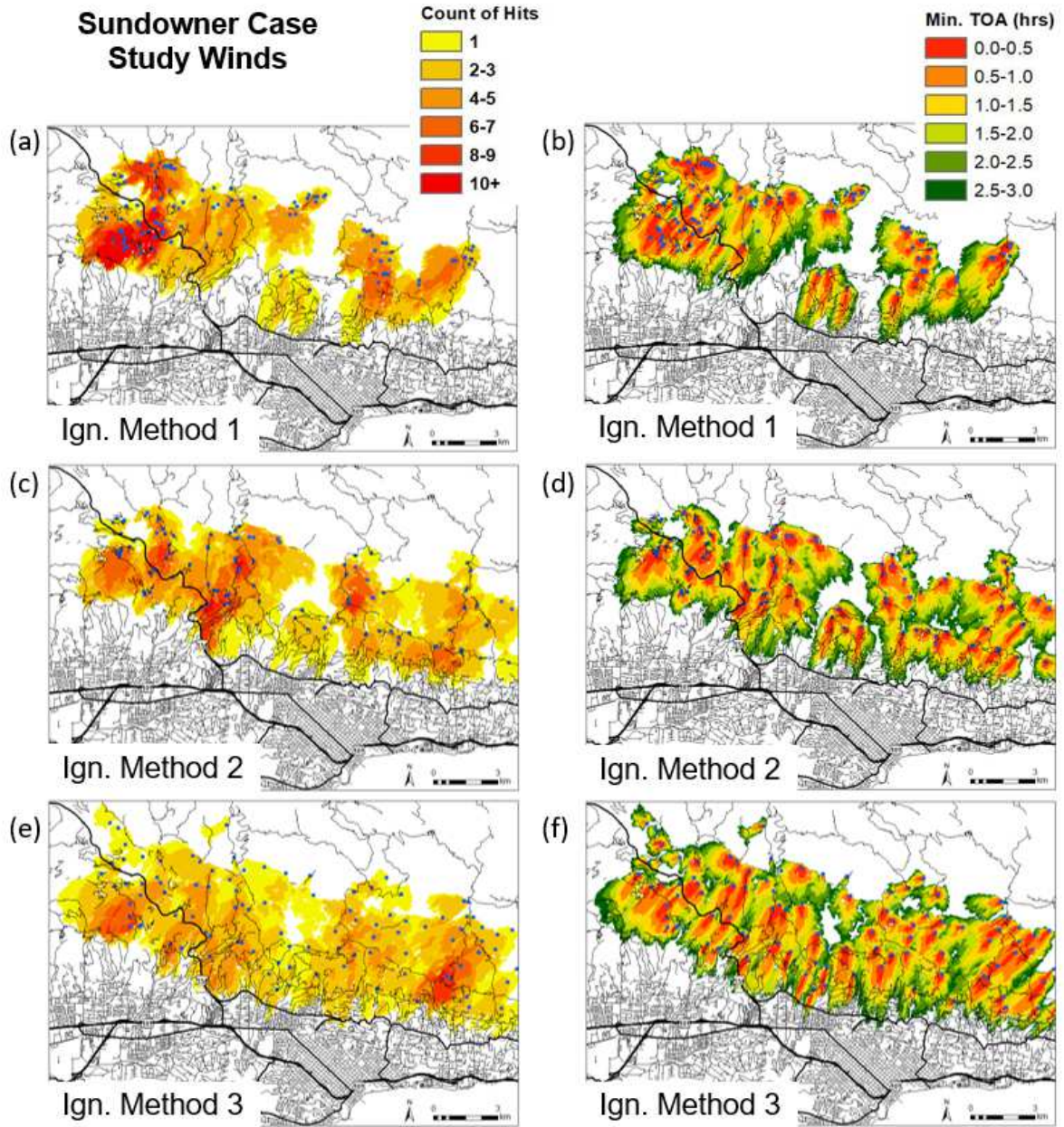


**Figure 4.10** - Same as Figure 4.5, but with wildfire simulations using the extreme Sundowner winds.

When all ignition methods are combined and extreme Sundowner winds are used, over 10% of simulations (31 hits) occur near HWY 154 (Fig. 4.6c). The use of these strong winds led to the simulated wildfires reaching more areas in the domain than when other wind scenarios were used, explained by the strong winds spreading fires further south.

Additionally, the east part of the region exhibits areas where over 13 simulations hit (~4% of the total amount of simulations), and these areas are larger and further south than in the other wind scenarios. Perhaps the most important feature to note is that a large portion of both HWY 154 and Cathedral Oaks Rd were hit by at least 1 simulation when extreme winds were used (Fig. 4.6c). Recall that spotting was disabled for these runs due to limitations found in Zigner et al. (2020), and historical wildfires such as the 1990 Painted Cave fire spread rapidly into urban areas driven by downstream spotting. Therefore, these simulations are likely underestimating how rapidly a fire may spread southward. A more sophisticated fire and ember model would be required to adequately identify the potential effects of spotting.

The size of wildfires simulated using extreme Sundowner winds were comparable and to those from the Sundowner composite simulations (Fig. 4.7). However, at all times after ignition analyzed, the largest fires were produced from the Sundowner case study wind simulations. Similar to the Sundowner composite simulations, the majority of cells burned were hit by 1-3 simulations (Fig. 4.8). Notice that the simulations using ignition method 1 for this extreme case resulted in the largest number of cells hit by wildfires. Overall, all ignition methods hit HWY 154 repeatedly and the Sundowner composite and Sundowner case study winds spread fires more rapidly to the south toward populated areas, with some reaching Cathedral Oaks Road.

#### *d) Analysis of all simulations*

Figure 4.11 shows the count of hits for all 900 simulations, regardless of ignition method and wind scenario. Nearly all grid cells on the entire SYM slopes were hit in at least one simulation, and a few areas stand out as higher wildfire risk according to our

simulations. On the SYM slopes to the west of HWY 154 and north of the city of Goleta, some grid cells were hit by 80 simulations, or 8.9% of the total simulations run. Slightly to the east of this maximum, over 50 simulations hit the regions directly next to the major route HWY 154, the main road running north from coastal Santa Barbara. This region has been hit by a handful of wildfires in the past, including the 1990 Painted Cave, 2009 Jesusita, and 2020 Cave fires, making this a high-risk area for wildfires.

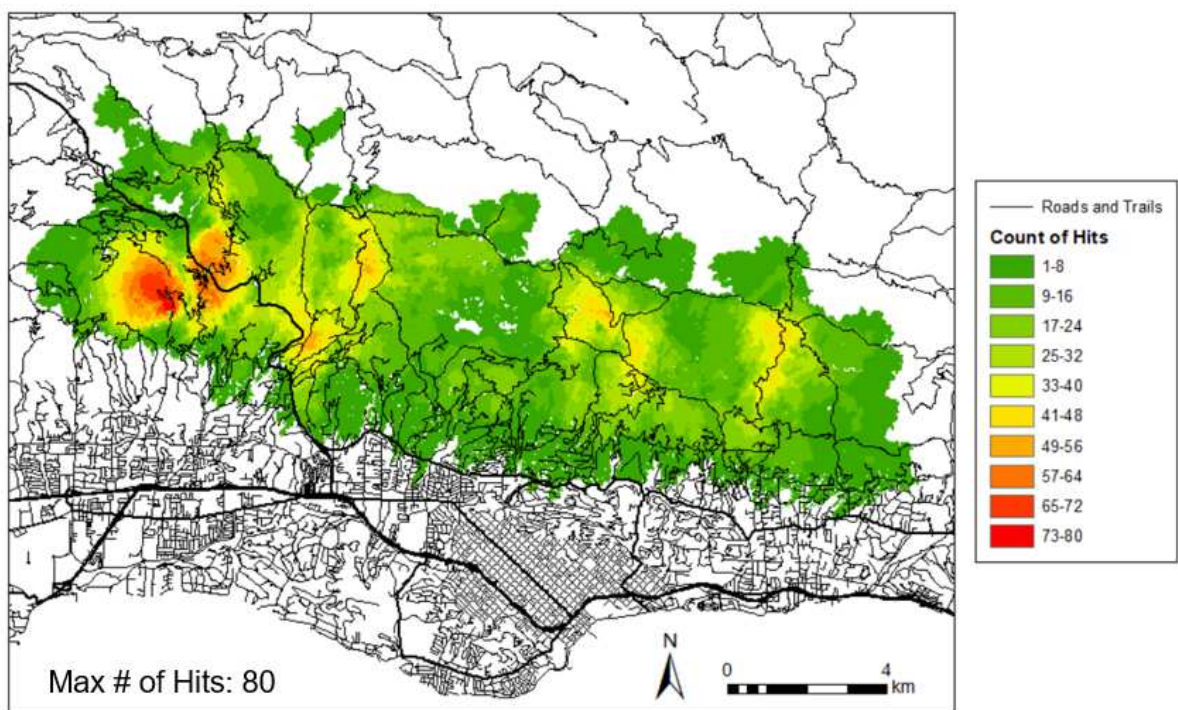


**Figure 4.11** - Similar to Figure 4.6, but using all simulations, regardless of ignition modeling method and wind scenario input.

Other grid cells in areas to the east (on the SYM slopes overlooking Santa Barbara and Montecito) have clusters with over 40 simulation hits (yellow in Fig. 4.11). This is mainly around roads and trails, where the number of ignitions is higher based on the ignition modeling methods. Finally, similar to the results from the simulations run using the extreme



Sundowner wind scenario, a large portion of Cathedral Oaks Rd was hit by at least one simulation. Many roads in the WUI depend on this road daily, as it is the only entrance and exit to some homes and businesses on the mountain slopes. The fact that it was hit in multiple locations highlights the importance of increasing wildfire resilience through understanding high-risk regions and improving firefighting and evacuation strategies.

#### **4.5 Discussion and Conclusions**

With an increasing trend of communities living in the WUI and roads and trails built further into the wilderness, identifying regions at high ignition risk is the first step toward improving wildfire prevention and enhancing strategies to protect the community. This is particularly imperative during critical fire weather conditions such as Sundowner wind events. This study examined wildfire risk in the Santa Barbara WUI on the south-facing slopes of the Santa Ynez Mountains. This region, located in southern California, has experienced numerous wildfires that rapidly spread toward populated areas to the south, driven by strong Sundowner winds. While impactful wildfires have affected the whole extent of the southern SYM slopes, for computation reasons this study focuses on a domain north of the cities of Santa Barbara and Montecito, where the community is bounded by the mountains and the coast (Fig. 4.1).

Observational datasets from the last few decades show a pattern of ignitions strongly linked to the proximity from roads and trails, clearly suggesting an anthropogenic connection with wildfires in the region. However, the observed ignitions were not uniformly distributed throughout the area of interest on the southern SYM slopes. For instance, the density of ignitions is higher in the western part near the main north-south route, HWY 154, and more

generally around roads near the mountain ridge. Nonetheless, while the pattern of ignitions may be linked to the density of homes in the WUI, road traffic, and trails in this regions, the persistent drought conditions and other unforeseen natural and/or anthropogenic changes may increase ignition probability in other regions that had previously observed relatively few ignitions. To account for these possible additional scenarios, we propose three ignition modeling methods and three distinct wind scenarios to investigate fire risk in this region, maintaining other meteorological variables, which are related to fuel moisture, reflective of the extreme conditions from the 1990 Painted Cave fire.

The majority of ignition modeling studies have examined the relationship between observed ignitions and other variables such as human development and infrastructure (Syphard et al. 2007, 2008, 2012, Syphard and Keeley 2015, Abatzoglou et al. 2018, Faivre et al. 2014). Previous simulation studies have utilized a single ignition modeling method (Peterson et al. 2011, Scott et al. 2013) or relied on previous ignitions (Finney et al. 2011) for runs. Furthermore, almost all previous research on ignitions and simulations in southern California is focused in a different area, such as the Santa Monica Mountains (Syphard and Keeley 2015, Peterson et al. 2011). This novel study analyzed a new location highly impacted by wildfires, coastal Santa Barbara, and compared various ignition modeling methods and the resulting simulations.

Modeled ignitions were created in ignition method 1 by randomly sampling from buffers up to 500 m from previous ignition locations. This had the most clustered ignition points, with an absence of ignitions in the middle part of the area of interest due to a lack of previously observed ignitions. A large amount of the modeled ignitions were in the western part of the domain near HWY 154 (Fig. 4.2a), which is a major road and evacuation route running north-south from the city. Regardless of the wind scenario, the area by HWY 154

was continuously hit the most in simulations due to the higher density of ignition points in this region (Figs. 4.5, 4.9, 4.10).

When ignitions were randomly sampled from a 50 m buffer around all roads and trails on the south SYM slopes (Fig. 4.2b), similar to a methodology used in Peterson et al. (2011), the ignitions were more spread out, though gaps were still evident where no roads or trails are present. Similar to ignition method 1, the regions with the most simulation hits were near HWY 154 and in a few regions in the eastern part. More ignitions were closer to the WUI and urban areas in the south, thus more simulations spread into the WUI closer to the coastal communities in Santa Barbara.

When ignitions were sampled using a distance decay function around roads and trails up to 1000 m with the probability of ignition selection linearly decreasing with increasing distance from the road or trail (Fig. 4.2c), the spatial distribution of ignitions was the most expansive in the area of interest because ignitions were not restricted by a harsh buffer around previous ignitions or roads and trails; the ignitions were the furthest north and south points out of all methods (Fig. A4.1). When simulations were run, there were very few grid cells that were not hit by any simulations on the mountain slopes (Figs. 4.5, 4.9, 4.10). Furthermore, many fires reached Cathedral Oaks Road, and some simulations spread south of the road as well (Fig. 4.10).

In addition to the different ignition methods, varying the wind scenario greatly changed the shape and size of the simulations, and varied the regions that were considered at risk, especially in the WUI. During climatological conditions, the simulated fires did not travel far from the ignition source and spread in a radial pattern (Fig. 4.5), resulting in the smallest fires of all wind methods (Fig. 4.7). This indicates that during climatological conditions, wildfires may be less likely to spread rapidly and cause large, destructive

wildfires in this region. However, fires spread further south and grew larger when the Sundowner composite and extreme Sundowner case study winds were used in the simulations. During the Sundowner composite and Sundowner case study conditions, simulated wildfires reached heavily trafficked areas due to the strong north and northeasterly winds (Figs. 4.6b,c). When the Sundowner case study winds were used with ignition method 3, some simulations reached Cathedral Oaks Road and the surrounding WUI within the first half an hour (Fig. 4.10f).

Limitations are inherent in this work. Wildfires ignited via powerlines were not considered in this work, though they were found as a major ignition source in Keeley et al. (2012). As explained in the Introduction, FARSITE does not model spotting when fires spread downslope and thus was enabled in our simulations. It's known that spotting can be an important factor in the rapid spread of wildfires (Zigner et al. 2020), so the maps produced in this study are likely more conservative. A different model with more computational expenses would be required to model how enabling spotting would influence fire risk in this region. Also, the fuel map used in simulations had no burn scars and the live fuel moisture values used were the lowest possible observed for the vegetation in this region. The lack of burn scars may highlight regions as high risk when a recent fire in that location may lessen the potential risk. Thus, these findings must be taken with consideration to recent events and fuel moisture at that time. As far as the wind scenarios, by their nature, composites may smooth out more extreme conditions, as shown by the differences in winds between the Sundowner composite wind raster and the Sundowner case study raster (Figs. 4.3b,c). While we only looked at simulations for one extreme Sundowner case study, each Sundowner has individual characteristics and spatial extents.

Future work may include creating additional ignition points in this region of interest and running simulations to more thoroughly cover the southern SYM slope. Other extreme case studies may be used as wind scenarios and input in FARSITE to more accurately highlight areas at highest risk during extreme fire weather. Another idea is to examine the ability to identify a region of potential ignition locations for a specific point by reversing topography and winds. It may be beneficial to understand whether an ignition at a given location is probable to impact a specific point on a major evacuation route, such as HWY 154 or Cathedral Oaks Rd. Nevertheless, the findings from this study may assist wildfire planners and city officials by providing guidance for resource and staffing allocations on days with weak to strong winds. In addition, this may help focus locations for improvements in evacuation planning, road and trail design, and other public policies to prevent and mitigate the effects of wildfires.

#### **4.6 Acknowledgements**

This research was supported by the NSF-PREEVENTS ICER-1664173. This research was completed with the help of the Montecito, Santa Barbara, and Santa Barbara County Fire Departments and the National Weather Service - Los Angeles/Oxnard Office. Discussions on the evolution of wildfire perimeters with Chief Rob Hazard (Santa Barbara County Fire Department) were much appreciated.

## 4.7 Appendix

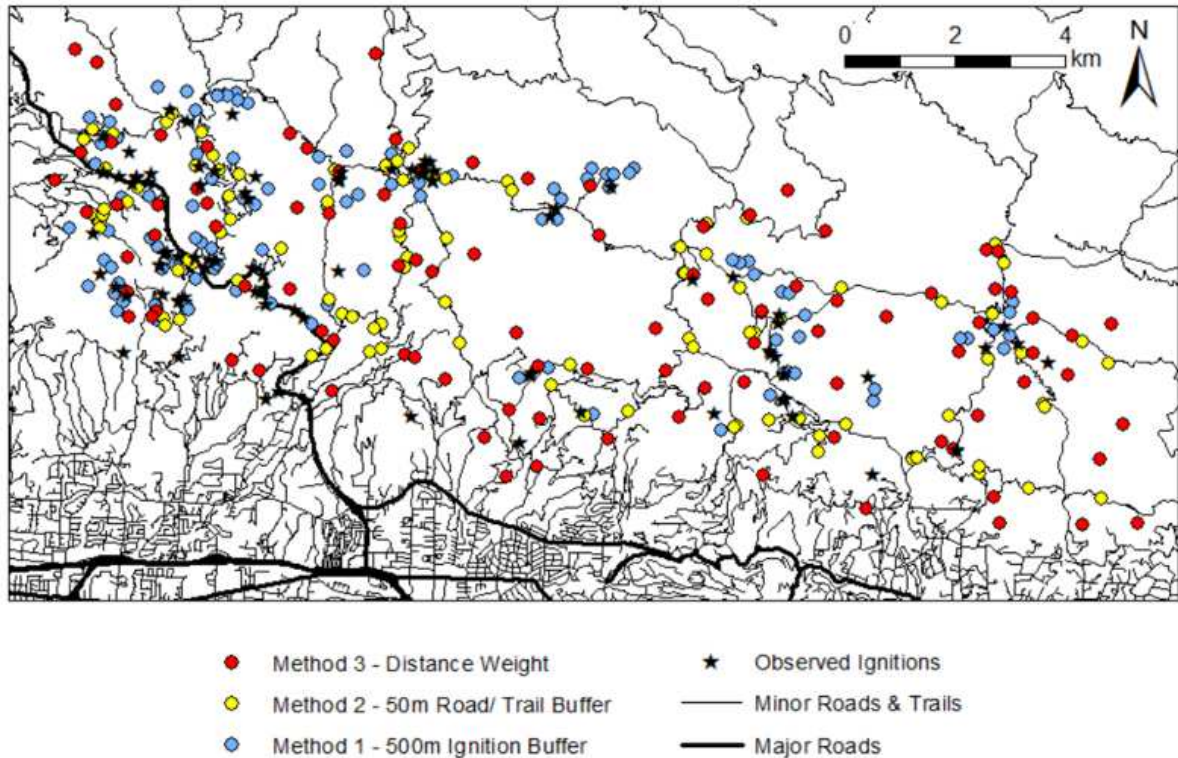


**Figure A1** - Ignition points from the three ignition modeling methods (colored dots) and previous ignition locations (black stars) overlaid on roads and trails (black lines).

## 4.8 References

- Abatzoglou, J. T., Balch, J. K., Bradley, B. A., and Kolden, C. A. (2018) Human-related ignitions concurrent with high winds promote large wildfires across the USA. *International journal of wildland fire*, 27(6), 377-386.
- Balch, J. K., Bradley, B. A., Abatzoglou, J. T., Nagy, R. C., Fusco, E. J., and Mahood, A. L. (2017). Human-started wildfires expand the fire niche across the United States. *Proceedings of the National Academy of Sciences*, 114(11), 2946-2951.

- Bartlein, P.J., Hostetler, S.W., Shafer, S.L., Holman, J.O., and Solomon, A.M. (2008) Temporal and spatial structure in a daily wildfire-start data set from the western United States (1986–96). *International Journal of Wildland Fire*, 17(1), 8-17.
- Blier, W. (1998) The sundowner winds of Santa Barbara, California. *Weather and Forecasting*, 13, 702-716. Doi: 10.1175/1520-0434(1998)013<0702:TSWOSB>2.0.CO;2.
- Bryant, B. P., and Westerling, A. L. (2014) Scenarios for future wildfire risk in California: links between changing demography, land use, climate, and wildfire. *Environmetrics*, 25(6), 454-471.
- Cannon, F., Carvalho, L., Jones, C., Hall, T., Gomberg, D., Dumas, J., and Jackson, M. (2017) WRF Simulation of Downslope Wind Events in Coastal Santa Barbara County. *Atmospheric Research*, 191, 57–73. Doi: 10.1016/j.atmosres.2017.03.010.
- Carvalho, L., Duine, G.J., Jones, C., Zigner, K., Clements, C., Kane, H., Gore, G., Bell, G., Gamelin, B., Gomberg, D., Hall, T., Johnson, M., Dumas, J., Boldt, E., Hazard, R., and Enos, W. (2020) The Sundowner Winds Experiment (SWEX) Pilot Study: Understanding Downslope Windstorms in the Santa Ynez Mountains, Santa Barbara, CA. *Monthly Weather Review*, 148, 1519-1539. Doi: 10.1175/MWR-D-19-0207.1.
- Countryman, C.M. (1972) *The Fire Environment Concept*; USDA Forest Service: Berkeley, CA, USA; p. 15.
- Faivre, N., Jin, Y., Goulden, M. L., and Randerson, J. T. (2014) Controls on the spatial pattern of wildfire ignitions in Southern California. *International Journal of Wildland Fire*, 23(6), 799-811.

- Finney, M.A., and Ryan, K.C. (1995) Use of the FARSITE Fire Growth Model for Fire Prediction in U.S. National Parks. In Proceedings of the International Emergency Management and Engineering Conference, San Diego, CA, USA, 9–12. pp. 183–189.
- Finney, M.A. (1998) FARSITE: Fire Area Simulator-Model Development and Evaluation; Research Paper RMRS-RP-4; U.S. Department of Agriculture, Forest Service, Rocky Mountain Research Station: Fort Collins, CO, USA.
- Finney, M. A., McHugh, C. W., Grenfell, I. C., Riley, K. L., and Short, K. C. (2011) A simulation of probabilistic wildfire risk components for the continental United States. *Stochastic Environmental Research and Risk Assessment*, 25(7), 973-1000.
- Hammer, R.B., Stewart, S.I., and Radeloff, V.C. (2009) Demographic trends, the wildland–urban interface, and wildfire management. *Soc. Nat. Resour.*, 22, 777–782.
- Jin, Y., Randerson, J. T., Faivre, N., Capps, S., Hall, A., and Goulden, M. L. (2014) Contrasting controls on wildland fires in Southern California during periods with and without Santa Ana winds. *Journal of Geophysical Research: Biogeosciences*, 119(3), 432-450.
- Jones, C., Carvalho, L., Duine, G.J., and Zigner, K. (2021) A New Climatology of Sundowner Winds in Coastal Santa Barbara, California, Based on 30-yr High Resolution WRF Downscaling. Submitted to *Atmospheric Research*. Doi: 10.1175/2010MWR3406.1.
- Keeley, J.E., Fotheringham, C.J., and Moritz, M.A. (2004) Lessons from the october 2003. Wildfires in Southern California. *Journal of Forestry*, 102(7), 26-31.
- Keeley, J.E., Safford, H., Fotheringham, C.J., Franklin, J., and Moritz, M. (2009) The 2007 southern California wildfires: lessons in complexity. *Journal of Forestry*, 107(6), 287-296.



- Keeley, J. E., and Syphard, A. D. (2018) Historical patterns of wildfire ignition sources in California ecosystems. *International journal of wildland fire*, 27(12), 781-799.
- Kolden, C.A., and Abatzoglou, J.T. (2018) Spatial distribution of wildfires ignited under katabatic versus non-katabatic winds in mediterranean Southern California USA. *Fire*, 1(2), 19.
- Kramer, H. A., Mockrin, M. H., Alexandre, P. M., and Radeloff, V. C. (2019) High wildfire damage in interface communities in California. *International journal of wildland fire*, 28(9), 641-650.
- Nauslar, N.J., Abatzoglou, J.T., and Marsh, P.T. (2018) The 2017 North Bay and Southern California fires: a case study. *Fire*, 1(1), 18.
- Moritz, M. A. (2003). Spatiotemporal analysis of controls on shrubland fire regimes: age dependency and fire hazard. *Ecology*, 84(2), 351-361.
- Moritz, M. A., Moody, T. J., Krawchuk, M. A., Hughes, M., and Hall, A. (2010) Spatial variation in extreme winds predicts large wildfire locations in chaparral ecosystems. *Geophysical Research Letters*, 37(4).
- Moritz, M.A., Batllori, E., Bradstock, R.A., et al. (2014) Learning to coexist with wildfire. *Nature*, 515(7525), 58-66.
- Moritz, M.A., and Knowles, S.G. (2016) Coexisting with wildfire. *American Scientist*, 104(4), 220.
- Murray, A.T., Carvalho, L., Church, R.L., Jones, C., Roberts, D., Xu, J., Zigner, K., and Nash, D. (2020) Coastal vulnerability under extreme weather. *Applied Spatial Analysis and Policy*, 1-27.
- Papadopoulos, G.D., and Pavlidou, F.-N. (2011) A Comparative Review on Wildfire Simulators. *IEEE Syst. J.*, 5, 233–243.

- Parisien, M. A., Snetsinger, S., Greenberg, J. A., Nelson, C. R., Schoennagel, T., Dobrowski, S. Z., and Moritz, M. A. (2012) Spatial variability in wildfire probability across the western United States. *International Journal of Wildland Fire*, 21(4), 313-327.
- Peterson, S. H., Moritz, M. A., Morais, M. E., Dennison, P. E., and Carlson, J. M. (2011) Modelling long-term fire regimes of southern California shrublands. *International Journal of Wildland Fire*, 20(1), 1-16.
- Preisler, H. K., Brillinger, D. R., Burgan, R. E., and Benoit, J. W. (2004) Probability based models for estimation of wildfire risk. *International Journal of wildland fire*, 13(2), 133-142.
- Radeloff, V.C., Hammer, R.B., Stewart, S.I., Fried, J.S., Holcomb, S.S., and McKeefry, J.F. (2005) The wildland–urban interface in the United States. *Ecol. Appl.*, 15, 799–805.
- Radeloff, V.C., Helmers, D.P., Kramer, H.A., Mockrin, M.H., Alexandre, P.M., Bar-Massada, A., Butsic, V., Hawbaker, T.J., Martinuzzi, S., Syphard, A.D., et al. (2018) Rapid growth of the US wildland-urban interface raises wildfire risk. *Proc. Natl. Acad. Sci. USA*.
- Rothermel, R.C. (1972) A Mathematical Model. for Predicting Fire Spread in Wildland Fuels; Research Paper INT-115; U.S. Department of Agriculture, Forest Service, Intermountain Forest and Range Experiment Station: Ogden, UT, USA; p. 40.
- Scott, J.H. (2006) Comparison of Crown Fire Modeling Systems Used in Three Fire Management Applications; RMRS-RP-58; U.S. Department of Agriculture, Forest Service, Rocky Mountain Research Station: Ft. Collins, CO, USA.

- Scott, J. H., Thompson, M. P., and Calkin, D. E. (2013) A wildfire risk assessment framework for land and resource management. Gen. Tech. Rep. RMRS-GTR-315 (US Forest Service Rocky Mountain Research Station, Fort Collins, CO).
- Skamarock, W. C., Klemp, J. B., Dudhia, J., Gill, D. O., Barker, D. M., Wang, W., and Powers, J. G. (2008) A description of the Advanced Research WRF version 3. NCAR Technical note-475+ STR.
- Stratton, R.D. (2006) Guidance on Spatial Wildland Fire Analysis: Models, Tools, and Techniques; General Technical Report RMRS-GTR-183; U.S. Department of Agriculture, Forest Service, Rocky Mountain Research Station: Ft. Collins, CO, USA.
- Syphard, A. D., Radeloff, V. C., Keeley, J. E., Hawbaker, T. J., Clayton, M. K., Stewart, S. I., and Hammer, R. B. (2007) Human influence on California fire regimes. *Ecological applications*, 17(5), 1388-1402.
- Syphard, A. D., Radeloff, V. C., Keuler, N. S., Taylor, R. S., Hawbaker, T. J., Stewart, S. I., and Clayton, M. K. (2008) Predicting spatial patterns of fire on a southern California landscape. *International Journal of Wildland Fire*, 17(5), 602-613.
- Syphard, A. D., Keeley, J. E., Massada, A. B., Brennan, T. J., and Radeloff, V. C. (2012) Housing arrangement and location determine the likelihood of housing loss due to wildfire. *PloS one*, 7(3), e33954.
- Syphard, A. D., and Keeley, J. E. (2015) Location, timing and extent of wildfire vary by cause of ignition. *International Journal of Wildland Fire*, 24(1), 37-47.
- Williams, A. P., Abatzoglou, J. T., Gershunov, A., Guzman-Morales, J., Bishop, D. A., Balch, J. K., and Lettenmaier, D. P. (2019) Observed impacts of anthropogenic climate change on wildfire in California. *Earth's Future*, 7(8), 892-910.

Zigner, K., Carvalho, L., Peterson, S., Fujioka, F., Duine, G.J., Jones, C., Roberts, D., and Moritz, M. (2020) Evaluating the Ability of FARSITE to Simulate Wildfires Influenced by Extreme, Downslope Winds in Santa Barbara, California. *Fire*, 3, 29. Doi: 10.3390/fire3030029.

## 5. Conclusion

Extreme, downslope winds and wildfires greatly influence communities in coastal Santa Barbara County. Given the effects of climate change and human expansion into previously rural regions, this trend is not expected to resolve soon. Understanding and improving the forecasting of critical fire weather and identifying the most at-risk locations in this wildfire-prone region is imperative to increase resilience and advance firefighting strategies and evacuation planning. Previously, weather stations had not been utilized to complete a comprehensive analysis of extreme weather conditions in this region, and no wildfire simulations had been run to determine high-risk regions. *This dissertation advances knowledge on fire weather in coastal Santa Barbara and identifies locations of fire risk during extreme weather conditions through three research objectives:*

- 1) Examine the spatiotemporal characteristics of wind, temperature, dew point, and fire weather in coastal Santa Barbara, and identify regions with frequent fire weather danger (Chapter 2)
- 2) Test the ability of a wildfire model to simulate previous wildfires that were rapidly spread downslope under extreme conditions, focusing on two of the most rapidly spreading wildfires that have affected the southern slopes of the SYM (Chapter 3)
- 3) Determine areas at highest wildfire risk in the wildland-urban interface of Santa Barbara by running simulations with varied ignition modeling methods and wind scenarios (Chapter 4)

Individual weather stations located throughout coastal Santa Barbara County were examined in the second Chapter. This is the first study to comprehensively analyze all

trustworthy weather stations in the Santa Ynez Valley, on the southern SYM slopes, and in the foothills and the plain to determine the seasonal and diurnal cycles of wind. Distinct wind regimes were evident between stations on the mountain slopes and stations in the foothills and on the coastal plain; the winds were typically stronger on the slopes and the daily maximum occurred later in the day, in contrast to in the afternoon as recorded at non-mountain stations. Furthermore, the analysis showed a relationship between winds recorded at buoys to the west near Point Conception and in the Santa Barbara Channel with winds at select mountain stations. Variability in temperature and dew point is evident during Sundowners at mountain stations (measured using the NWS criteria): temperatures are typically warmer (cooler) than normal at stations in the eastern (western) SYM when Sundowners occur in spring and summer, and dew points are typically lower. Critical fire weather conditions occur at all stations, though they are most frequent on the SYM slopes, which is where wildfires typically ignite, as explained in Chapters 3 and 4.

In the third chapter of this dissertation, the ability of a commonly-used wildfire model to accurately simulate two influential wildfires that were spread by Sundowner winds was explored. The 2016 Sherpa fire in western Santa Barbara was simulated relatively accurately, though there were differences in spread direction potentially due to firefighting efforts, fuels or turbulent processes that were not accounted for in the model. The addition of a gust factor to wind speeds resulted in simulated fire perimeters and burned areas more closely aligning to what was observed. The 1990 Painted Cave fire impacted Goleta and Santa Barbara, and even crossed the major evacuation route HWY 101 within the first hour due to downstream spotting. Even with a gust factor applied, the simulations underestimated the spread, however patterns in spotting revealed a larger issue. A key finding of this work was that the spotting algorithm used in FARSITE does not produce spot fires, or fires ahead

of the main fire front, when the landing site of an ember is modeled lower in elevation than the launch site of the ember. In the case of Sundowners, embers can be transported far distances by mountain waves and wave breaking in the atmosphere. Since uncoupled models such as FARSITE cannot simulate these 3-dimensional processes, ember transport may not accurately be resolved when wildfires occur during Sundowners. Nevertheless, not all wildfires are significantly influenced by spotting, and the selection of a case study, such as the Painted Cave fire which had a large magnitude of spotting, highlights some deficiencies of this relatively simple fire model.

The main goal of the fourth chapter of this dissertation was to identify high-risk wildfire regions in coastal Santa Barbara, focusing on the wildland-urban interface and areas around major evacuation routes. Three ignition models were proposed, which utilize distances from previous ignitions and from roads and trails to sample new ignition points. Three wind scenarios were created and input to FARSITE, including gridded winds during climatological (non-Sundowner) conditions, the mean Sundowner composite, and an extreme Sundowner case study. Simulated fires were smallest and spread fairly radially when climatological winds were input, whereas fires spread into the wildland-urban interface in the first couple hours when the Sundowner composite or extreme Sundowner wind scenarios were used. The largest fires simulated using the non-Sundowner composite winds were approximately 300 Ha after three hours, whereas some simulated fires grew to over 650 Ha burned after three hours when the extreme Sundowner case study winds were utilized. This demonstrates the large influence of winds on rapid wildfire spread. Partially due to ignition point placement, locations around the major north-south route from coastal Santa Barbara were hit the most, with a maximum of 80 hits (~9%) on the SYM slopes to the west of HWY 154 considering all 900 simulations. Moreover, multiple simulations hit

the main east-west evacuation route used for homes and businesses on the SYM foothills; over 10% of simulations using the distance decay ignition method and extreme Sundowner case study combination reached this road.

The novel research presented in this dissertation provides insight on the atmospheric circulations in coastal Santa Barbara, including Sundowner winds, and advances the understanding of risks in the WUI of a fire-prone zone of Southern California. When wildfire ignitions coincide with Sundowners, the resulting wildfire spread can be rapid, in part due to spotting ahead of the fire front. Albeit some wildfire spread models lack the ability to accurately reconstruct some historical wildfires driven by strong downslope winds, simulations demonstrated to be useful in providing important statistics for decision making, particularly shortly after ignition. Determining locations of highest wildfire risk in this fire-prone region will assist firefighters and evacuation planners in creating appropriate and updated techniques and plans to increase safety and resilience to wildfires.

#### *Suggestions for future work*

The research presented in this dissertation highlights the importance of improving the forecasting of Sundowners and critical fire weather conditions in coastal Santa Barbara. To accomplish this, future research regarding Sundowner mechanisms could be completed, with focus on the differences between Sundowner regimes (Jones et al. 2020). This may be done through utilizing atmospheric models and collecting additional observations upstream during different Sundowner types. For example, western Sundowners may be more heavily influenced by oceanic influences whereas the San Rafael Mountains may impact characteristics of eastern Sundowners. Furthermore, the influence of upstream conditions in



the Santa Ynez Valley may be of importance in differentiating the regimes, which could be revealed through further analysis using observational and modeled data.

Future work regarding the simulation of wildfires in Santa Barbara, especially those rapidly spread by extreme winds, could benefit greatly from closely examining and improving the spotting algorithm used in the model FARSITE. This could be compared to other widely-used models to simulate spotting when fire spread is downslope or in regions with complex terrain. Other uncoupled wildfire models, such as Prometheus (Barber et al. 2007), or coupled models, such as WRF-Fire (Coen et al. 2013), could be used to simulate wildfires that were influenced by Sundowner winds. Those results could then be compared to the findings from this research to determine if another model could better reconstruct wildfires in this region. Work could also be completed on the utilization of different gust factors in wildfire simulations when the ignition occurs during a Sundowner. Additional historical wildfire case studies could be examined and simulated to more accurately test the ability of FARSITE to reconstruct previous fires.

Incorporating more ignition locations and wind scenarios in the wildfire risk map creation could improve the map by filling in gaps and ensuring the locations at highest risk were hit in simulations. This is especially important to examine during Sundowners when fire spread could be rapid, so other case studies could be used as wind input for the risk maps. In addition to roads and trails, an ignition method involving above-ground powerlines could be included. Another way to think about fire risk is to consider locations where an ignition may reach a specific location, such as a busy evacuation route or heavily trafficked region. This may be done by reversing elevation and wind direction to create a region of potential ignition locations. Future work may determine whether other uncoupled or coupled wildfire models can reconstruct historical wildfires influenced by Sundowners more

accurately, and thus provide an improved wildfire risk map. Nevertheless, this work provides an estimate of areas where ignitions and wildfire threat may be maximized in this populous region. Ultimately, this work aims to improve the forecasting and understanding of critical fire weather and increase resilience to wildfires in coastal Santa Barbara.

### *References*

- Barber, J., Bose, C., Bourlioux, A., Braun, J., Brunelle, E., Bryce, R., Garcia, T., Hillen, T., Lam, C., Ong, B., Poschl, C., and Tymstra, C. (2007) PROMETHEUS-Canada's wildfire growth simulator.
- Coen, J.L., Cameron, M., Michalakes, J., Patton, E.G., Riggan, P.J., and Yedinak, K.M. (2013) WRF-Fire: Coupled Weather–Wildland Fire Modeling with the Weather Research and Forecasting Model. *J. Appl. Meteor. Climatol.* 52, 16–38.
- Jones, C., Carvalho, L., Duine, G.J., and Zigner, K. (2021) A New Climatology of Sundowner Winds in Coastal Santa Barbara, California, Based on 30-yr High Resolution WRF Downscaling. Submitted to *Atmospheric Research*. Doi: 10.1175/2010MWR3406.1.